Comprehensive Framework Based on Dynamic and Steady State Analysis to Evaluate

Power System Resilience Against Natural Calamities

by

Giritharan Vijay Iswaran

A Thesis Presented in Partial Fulfilment
of the Requirements for the Degree
Master of Science

Approved July 2022 by the
Graduate Supervisory Committee

Mojdeh Hedman, Chair
Vijay Vittal
Raja Ayyanar

ARIZONA STATE UNIVERSITY

August 2022

ABSTRACT

Power system robustness against high impact low probability events is becoming a major concern. About 90% of US power outages reported in the last three decades are due to Hurricanes and tropical storms. Various works of literature are focused on modelling the resilience framework against hurricanes. To depict distinct phases of a system response during these disturbances, an aggregated trapezoid model is derived from the conventional trapezoid model and proposed in this work. The model is analytically investigated for transmission system performance, based on which resiliency metrics are developed for the same.

A probabilistic-based Monte Carlo Simulations (MCS) approach has been proposed in this work to incorporate the stochastic nature of the power system and hurricane uncertainty. Furthermore, the system's resilience to hurricanes is evaluated on the modified reliability test system (RTS), which is provided in this work, by performing steady-state and dynamic security assessment incorporating protection modelling and corrective action schemes using the Siemens Power System Simulator for Engineering (PSS®E) software. Based on the results of steady-state (both deterministic and stochastic approach) and dynamic (both deterministic and stochastic approach) analysis, resilience metrics are quantified. Finally, this work highlights the interdependency of operational and infrastructure resilience as they cannot be considered discrete characteristics of the system.

The objective of this work is to incorporate dynamic analysis and stochasticity in the resilience evaluation for a wind penetrated power system.

ACKNOWLEDGMENTS

TABLE OF CONTENTS

LIST OF TABLES

LIST OF FIGURES

LIST OF ABBREVIATIONS AND SYMBOLS

Abbreviations

AC	Alternating Current
CAISO	California Independent System Operator
DFIG	Doubly fed induction generator
DSA	Dynamic security assessment
EPRI	Electric Power Research Institute
GSC	Grid side converter
HILE	High impact low frequency event
IORA	Infrastructure & operational resilience assessment
MCS	Monte Carlo Simulation
NERC	National Electric Reliability Council
NHC	National Hurricane Center
NIAC	National Infrastructure Advisory Council
OPF	Optimal power flow
PPD	Presidential Policy Directive
PSLF	Positive Sequence Load Flow
PSS®E	Power System Simulator for Engineering

RoCoF	Rate of Change of Frequency
RTS	Reliability Test System
STTDS	Short-term time domain simulations
UC	Unit commitment
UFLS	Under-frequency load shedding
UFGT	Under-frequency generator trip
UFOGT	Under/over-frequency generator trip
UVFLS	Under-voltage/frequency load shedding
UVLS	Under-voltage load shedding
WECC	Western Electric Coordinating Council
WTG	Wind turbine generator
pu	per unit

Symbols

B_{ij}	Imaginary part of transmission line admittance
B_k	Susceptance of the transmission line
C_g	Power generation cost in \$/MWh
C_g^{NL}	No-load cost of generator in \$/h

C_g^{SU}	Startup/shutdown generator cost in \$/h
E_{FD}	Synchronous machine stator voltage corresponding to field voltage
E_d', E_q'	d and q-axis component of transient voltage
G_{ij}	Real part of transmission line admittance
H	Synchronous machine inertia
P_g^t	Active power generation of generator in MW
P_k^A	Continuous rating of transmission line
P_L^0	Initial real power bus load in MW
$P_{L,t}$	Hourly net busload
$P_{L,t}^{sched}$	Scheduled hourly busload
P_t^{var}	Uncertain load due to hurricane stochasticity
P_r	Rated active power output of WTG
$P_t(v)$	Active power output for current wind speed in MW
$Q_g^{(t)}$	Reactive power output of generator in MVAR
R_g^H	Hourly ramping capacity of the generator
R_g^{shut}	Shutdown ramping capacity of the generator

R_g^{start}	Startup ramping capacity of the generator
S_{ij}^A	Continuous thermal rating of line in MVA
S_{ij}^B	Long-term emergency thermal rating of line in MVA
$S_L^{(t)}$	Effective bus load in MVA
S_L^0	Initial bus load in MVA
$V_n^{(t)}$	Bus voltage in volts
Z_R	Relay impedance
d_n^t	Net load demand
f_{nadir}	Frequency nadir
g	Set of generators
i_d, i_q	d and q-axis component of current
k	Set of transmission lines
n	Set of buses
t_0	Event initiation time
t_d	Subordinate time
t_{ee}	Event end time
t_{sr}	Recovery initiation time

t_{ir}	Infrastructure recovery initiation time
t_{nadir}	Time taken to reach f_{nadir}
t_{qr}	Operational recovery end time
u_g^t	Commitment status of the generator
v	Wind speed in m/s
v_{br}	Breakdown wind speed in m/s
v_{cr}	Critical wind speed in m/s
v_g^t	Startup status of generator
w_g^t	Shutdown status of generator
w_i	Cut-in wind speed in m/s
w_0	Cut-out wind speed in m/s
w_r	Rated wind speed in m/s
x_l	leakage reactance
x_d, x_q	d and q-axis component of stator reactance
x_d', x_q'	d and q-axis component of transient reactance
x_d'', x_q''	d and q-axis component of subtransient reactance
Λ_t	Area under the curve

$\mathfrak{D}_r$	Disruption rate
$\mathfrak{R}_r$	Recovery rate
$\mathcal{R}$	Resilience Indicator
$\mathcal{T}_a$	Absorption time
$\mathcal{T}_g^{down}$	Minimum downtime of the generator
$\mathcal{T}_g^{up}$	Minimum uptime of the generator
$\mathcal{T}_i$	Intact time
$\mathcal{T}_p$	Preparation time
$\mathcal{T}_r$	Recovery time
$\vartheta(v_i)$	Failure probability of the transmission network for any wind speed, v_i(m/s)
$\vartheta(v)$	Failure probability of the transmission network for wind speed, v (m/s)
ℓ_k^t	Status of the transmission line
$\psi_n^{(t)}$	Busload multiplier
θ	Voltage angle of a bus
λ_D, λ_Q	d and q-axis component of flux linkage

τ'_{d0}, τ'_{q0}	d and q-axis open circuit transient time constant
τ''_{d0}, τ''_{q0}	d and q-axis open circuit subtransient time constant
ω, δ	Rotor speed and angle of synchronous machine
Δf	Frequency change

CHAPTER 1

INTRODUCTION

1.1   Power System Influence by Disasters

History of various events reported a major impact on the power system's operational flexibility and reliability. Such events which are low probable in the past decades are known as high impact low-frequency events (HILEs). Examples of HILEs include extreme weather conditions, natural disasters, man-made disasters, and operator negligence (or inaction). In response to such events, the power system experiences either a short-term or a long-term electricity outage based on the event severity. These events are constantly being reported to have a major impact on the social and economic statuses of the country. Various studies have been conducted to quantify the prior assertion. According to the Fourth National Climate Assessment, the greenhouse gases can lead to major cascading scenarios such as increasing temperature causing infrastructure damage (due to heatwaves, especially in arid regions), insufficient generation resources and increasing load creating huge stress on the electric grid [1]-[2]. Secondly, Texas incurred a huge loss of 125 billion USD due to Hurricane Harvey's damage in the year 2012 [3]. These socio-economic threats to the country due to HILEs are unavoidable with existing operational standards and regulations.

The influence of extreme events on conventional grids can be lessened with the updated frame of North American Electric Reliability Corporation (NERC) reliability standards and regulations for which various research works are being carried out. As the grids are undergoing modernization at the transmission and distribution level, predicting

and preventing the grid threats require adverse regulatory amendments. With high penetration of inverter-based resources (IBRs) such as solar farms (SFs), wind farms (WFs) and battery energy storages (BESs), the transition in power system characteristics are inevitable and are highly different from the conventional electric grid. Current research is focused on performing resilience studies based on steady-state analysis.

1.2   Power System Resilience: Definitions and Attributes

The power system resilience can be defined in different aspects with respect to the scenario or the type of disturbance influencing the overall characteristics of the power system. In general, resilience can be defined as the capability of the system to absorb and adapt to the scenario without any permanent rupture, quickly bouncing back to its nominal state and learning based on the history of the network's past experiences. Some of the grid resilience definitions used by various power system operating councils and authorities are briefly explored in this section.

According to the National Infrastructure Advisory Council (NIAC) [4], infrastructure resiliency can be defined as "...the ability to reduce the magnitude and/or duration of disruptive events. The effectiveness of a resilient infrastructure or enterprise depends upon its ability to anticipate, absorb, adapt to, and/or rapidly recover from a potentially disruptive event." Based on the Presidential Policy Directive/PPD-221, the term "resilience" means the ability to prepare for and adapt to changing conditions and withstand and recover rapidly from disruptions. Resilience includes the ability to withstand and recover from deliberate attacks, accidents, or naturally occurring threats or incidents [5]. According to Electric Power Research Institute's (EPRI)

Electric Power System Resilience: Challenges and Opportunities (February 2016) [6], "In the context of the power system, resilience includes the ability to harden the system against—and quickly recover from—high-impact, low-frequency events." In the context of the National Academies of Sciences, Engineering, and Medicine's Enhancing the Resilience of the Nation's Electricity System, "Resilience is not just about lessening the likelihood that these outages will occur. It is also about limiting the scope and impact of outages when they do occur, restoring power rapidly afterwards, and learning from these experiences to better deal with the events in the future" [7].

	Robustness	Resourcefulness	Rapid Recovery	Adaptability
People and processes	Emergency drills for control centers	RTOs prevent cascading failures	Mutual aid agreements, critical load recovery	Revising emergency response plans and industry standards
Infrastructure and Assets	Interconnected connected grid for absorptive caapcity	State estimators monitor real-time transmission, system transfer to N-1 failure	Spare transmission tower and shared inventory of EHV transformers	Substation placed on stilts after flooding

Figure 1.1 Attributes of Power System Resilience [4]

Based on NIAC, the four attributes of power system resilience such as robustness, resourcefulness, rapid recovery and adaptability [4] are depicted in Figure 1.1. Robustness measures the system's ability to carry out critical operations during the event and withstanding the same. For instance, the building system hardness can be improved by incorporating redundancy and substitutions (such as AMI technologies, and transportation). Resourcefulness measures how much the system is prepared to effectively manage its operation while the event unfolds. This attribute of resilience contributes to planning and training-based preparedness. Rapid recovery reflects the ability of the system

to efficiently bounce back to its per-contingency state as quickly as possible after the disruption period. The ability of the system to learn new lessons from the event and the introduction of new procedures for grid resilience enhancement by improving the co-attributes such as robustness, resourcefulness and rapid recovery.

Grid resilience (or) power system resilience can be classified based on its characteristics and quantification. Based on the characteristics, it can be classified as operational, infrastructure, coordination, and system resilience. The operational and infrastructure resilience indulge in portraying the system's capability to adapt to the event without compromising its characteristics (such as blackouts, uncontrolled islanding causing cascading outages, availability of generation fuels for unit support) and recover to its original state as quickly as possible. More resilient grids can roll with the strikes and adjust to adversity without long-term trouble. The quantification of infrastructure resilience can be governed by the availability of operational transmission corridors, substations, generation units, and active workforces during the recovery period. Contemporarily, the operational resilience is expressed based on load deliverability, transmission flexibility (to avoid congestion), and controlled islanding capacity such as microgrids. Community (or) coordination resilience is the sustained ability of the neighbourhood grid to effectively contribute to the system's disruption, adaptability, and recovery. This new resilience classification introduced in this work enhances the approach to achieving targeted system operation.

Infrastructure and operational resilience are highly interdependent. In order to support the assertion proposed, the following reasoning can be justified. Losing power

system components (such as transmission corridors, generation plants, and substations) can cause operational disruption (i.e., load shedding, islanding, series outages). On the other hand, misoperation can lead to the loss of operational system assets. Thus, system resilience can be defined as the overall grid resilience governed by its operation, infrastructure and community. In addition to the resilience classification, a vital factor to consider while assessing resilience is system toughness or rigidity. Thus, the system toughness has also been focused on in this work. Power system toughness can be defined as the capacity of the system to absorb the shock and operate in a pliancy region where its characteristics can be deformed and cannot be completely recovered unless a replacement is accomplished (such as generation replacement, loss of solar/wind farms). Pliancy is the characteristic of the grid to undergo disruption during shock absorption until a point of complete damage or fracture. This concept of robustness is briefly discussed in Chapter 2.

To achieve a resilient grid operation, six stages reflecting the grid characteristics such as challenge, awareness, preparation, action, adaption, and consistency are introduced in this thesis. The cyclic representation of resilience stages is depicted in Figure 1.2. One of the critical stages in resilient grid operation is that system must be prepared enough in accepting the risk and try to adapt to the event in a quicker fashion. For better adaption to the event, the system must be well prepared before the event progression which can be achieved by proper awareness of the grid operation. With the knowledge of grid operation forecast data, the power system must be well prepared before the event by formulating proper planning and operational goals to achieve an optimistic response during the event progression. With the goals set back, the planned actions must be implemented during the

crisis with the capability of learning information based on the current and previous threats. The above five actions must be consistently followed to achieve and maintain a resilient grid operation. Thus, perseverance or consistency becomes the sixth leg of the resilient grid model.
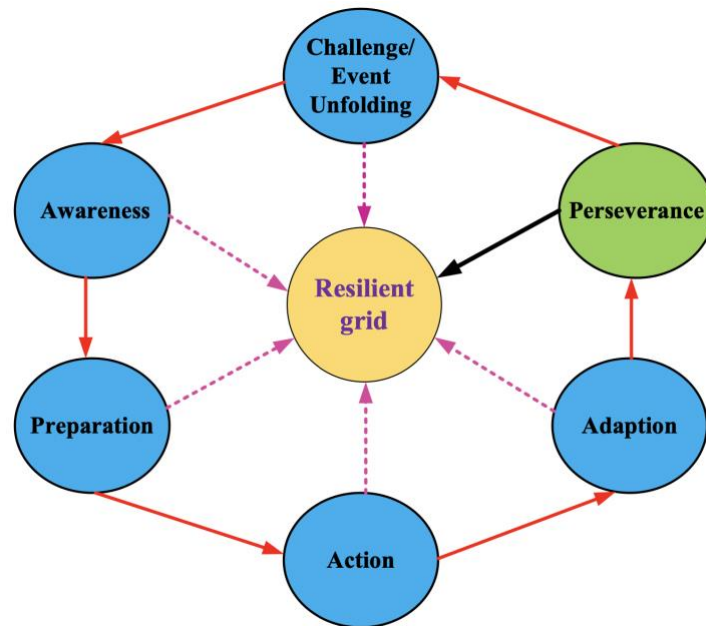
Figure 1.2 Cyclic Hexagon model for Resilience Attributes

1.3   Motivation and Goals

The vulnerabilities, outages and risks on the network are increasing with the decades as in the case of US power outages as shown in Figure 1.3 extracted from [8]. From Figure 1.3, the US power outages are reported in hours/customer during the years 2013-2020. It has also been reported that the major events causing the outages are Hurricanes. One such case was Hurricane Isaias, which caused a devastating impact on the network by knocking out 14 million customers from the grid. Thus, this work has been dedicated to discussing the Hurricane effects on the power system's operational and infrastructure characteristics.

Average duration of total annual electric power interruptions, United States (2013–2020)
hours per customer
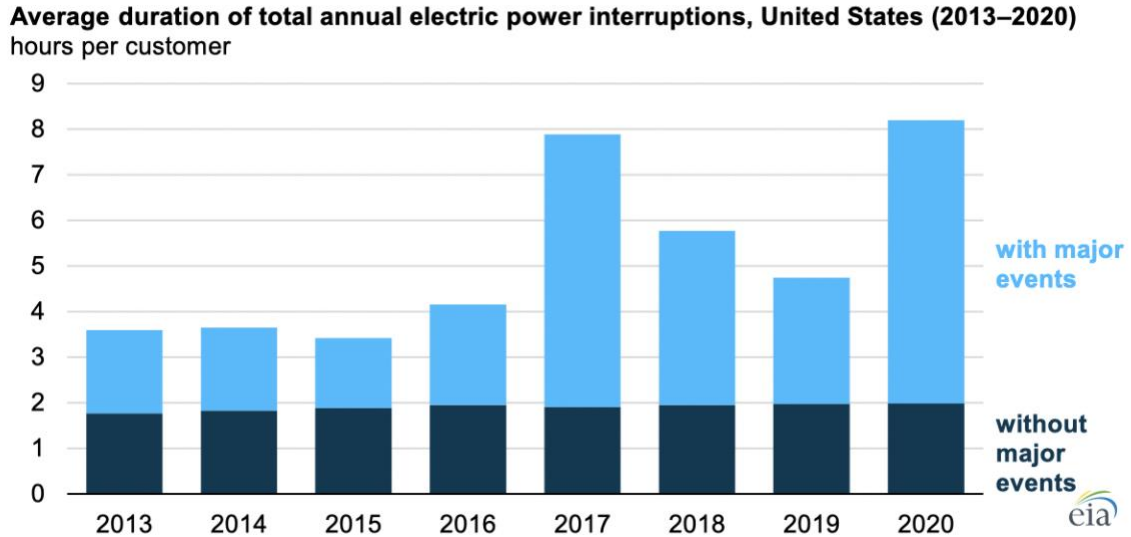
Figure 1.3 US Power Outages in the Years 2013-2020 [8]

Resilience evaluation approaches, such as triangle and trapezoid methods, are used extensively to represent infrastructure (e.g., transmission corridor status) and operational (e.g., load and generator shedding) performances in [9] and [10]. The resilience trapezoid model incorporates ramping decrement in performance indicators during an event and modifies the resilience triangle assertion of impulsive drop during the shock absorption. Moreover, prior works considered a linearized representation of resilience indicators as the event propagates and the system recovers. All these prior analyses focus only on the steady-state response of the system. However, power system security during extreme events is highly dependent on its physics of dynamics and protection systems. Such epistemic analysis is completely avoided in the previous research works while analyzing power system resilience against extreme events. In order to bridge the gap between actual system performance and estimated system performance, i.e., using steady-state analysis, this work focuses on evaluating system responses based on steady-state and dynamic analysis with protective relay modelling. The overall result obtained is coined as an aggregated result.

7

The term 'aggregated result' is used to address the combined results of steady-state and dynamic analysis in the upcoming chapters.

Based on the fragility model for the transmission assets extracted from [11], the impact of hurricanes on system performance, both in the steady-state and transient period, is analyzed and new resilience metrics are proposed in this work. The contributions of this work include:

(i)   Development of a new framework to evaluate power system resilience by assessing the transient stability of the system after critical changes in the system states during extreme weather events along with the evaluation of the steady-state condition of the system. Moreover, protection relays are included in transient stability analysis. This contribution is crucially important as the power system response during extreme events is usually governed by the dynamic response of generators, control systems, and protection system behaviour.

(ii)   Highlighting the importance of interdependence analysis of the infrastructure and operational resilience.

(iii)   Incorporating stochastic and probabilistic approaches for resilience evaluation based on Monte Carlo Simulations (MCS) with wind penetration in the system.

1.4   Bibliographic Review

An electric power system is a highly vulnerable and risk-prone network whose uninterrupted operation is of paramount importance for any modern society. Severe events can create disturbances in power systems that lead to operation interruptions and even major cascading outages and blackouts if proper preventive actions are not being considered to

8

make the system robust against such events. The power outage due to a Hurricane Ida which created a major impact on people's life [12] is an example of such outages. Such events are referred to as high impact low probability events which include natural disasters and man-made disasters.

These major disturbances can be induced externally and internally as well. Examples of external causes include extreme weather conditions, and cyber-security/malicious attacks on the power system. Texas outage, north-eastern outages in September 2013 due to Hurricane Ida, California wildfires, and Ukraine power grid hack are major examples supporting the assertion [12] – [14]. During the month of February 2021, a severe snowstorm attacked the Texas grid which caused power outages due to insufficient generation availability. There has been a shortage of fuel to the gas power plants due to frozen pipes that carry natural gas to the plant. Secondly, the wind turbine blades are locked because of high wind speeds making them idle during the event [1]. Apart from outages, it was also reported the crisis has caused a total death of around 246 people [2].

Another major event that affected the northeastern grid during the year 2013 is Hurricane Ida. The event had catastrophic changes in northeastern states such as Mississippi, Alabama, Louisiana, Massachusetts, Connecticut, New York, New Jersey and Pennsylvania causing 1.2 million electricity customers to lose power [12]. Though other states, except Louisiana, were recovered within the next 24 hours, Louisiana customers (about 0.5 million) were still experiencing power outages. The recovery and restoration of the power grid were delayed due to the event's impact. In recent years, power system

resilience has been a nascent subject attracting many scholars [15]-[17] to understand its operational and infrastructure characteristics.

Based on a study conducted in [18], among different scenarios, extreme weather events have been constantly reported causing huge impacts on system operation. With the increasing trend of power system outages that are induced by extreme weather conditions, enhancing power system resilience to such events is gaining more attention in the research community. Apart from the reliability metrics, numerous resilience metrics have been developed recently to quantify the network robustness against windstorms as detailed in [11].

Diverse quantifications are considered in the literature such as analyzing system adaption and disruption [19]-[21], and network recovery both at operational and structural levels [22]. To classify these methods, resilience planning incorporates long and short-term planning and adjustments during event progression and post-shock periods. Defensive islanding, effective remedial action design, and system hardening are among long-term planning measures, whereas short-term measures include event forecasting, accurate assessment of the availability of assets, as well as the implementation of effective preventive and corrective actions.

A defensive islanding technique is suggested in [23] for resilience enhancement in the electric power grid during extreme weather events. Besides, the authors of [23] addressed improvement in operational characteristics of the network compared to the traditionally-followed infrastructure based strategies in reducing cascading outages. This proactive measure is quantified based on the load shedding results for different time

10

snapshots and different scenarios generated by the Sequential Monte Carlo simulation. One major disadvantage the authors have not addressed is the 'problem of dimensionality'. For a small Great Britain test network, the authors need to generate 9000 scenarios. Large test systems with high penetration of renewables such as Western and Eastern networks cannot be studied based on the procedure discussed in [23] because of the increase in variability and uncertainty in the network.

Reference [24] addresses the grid planning against extreme events such as HILEs. The article highlights the importance of reframing the power engineer's idea of the reliable grid to a resilience grid by outlining the outages beyond N-2 caused by HILEs. Besides, it has been focused on the four questions namely, (i) How to incorporate resilience in power system planning? (ii) Can the weather impacts on the grid be mitigated by resilience-based planning? (iii) What is the best strategy for boosting system resilience against HILEs? (iv) How to build a robust and flexible power grid to withstand any unprecedented events in the future as well? [24].

The authors of [25] proposed a portfolio that optimizes the investments on high hedge yielding networks against the natural weather impacts. It is a two-level approach comprising network investments and risk analysis on the network with the proposed investments. This approach has been tested for the application of Earthquakes and identified the optimal portfolio for diverse simulation scenarios generated by SMCS.

The increase in windstorm intensity by 5-10% in future electric networks can increase the power grid loss and lead to 85% winter peak loss when the effect is increased

by 50% [26]. To assess the network resilience, Gaihua Fu, et.al proposed a network growth model for the future electric grid.

Reference [27] discusses the role of microgrids in enhancing power system resilience against wildfires in distribution systems. The article debates DER's involvement during microgrid operations can improve recovery time and demand satisfaction. The article further briefs the planning of DER investments and designs against wildfire events. A classic N-1 and resilient design methodology were discussed based on an illustrative case study for smart grid resilience. This article finally concludes by suggesting mandating the rules and standards for the resilient design of DERs in market studies.

Reference [28] presents a conceptual framework for understanding power system resilience, with a focus on the impact of severe weather occurrences. Because capturing the random character of weather and its impact on different system components necessitates a stochastic approach, a unique sequential Monte-Carlo-based time-series simulation model is developed to measure power system resilience. However, this approach is cursed with the problem of dimensionality, i.e., for N components, 2^N scenarios must be generated.

All these works discussed above consider a probabilistic manner for outage modelling rather than a realistic model. To bridge the gap between the realistic and intricate outage models, the approach put forth by the authors of [29] proposed a physics-based hurricane projection model to analyze the epistemic uncertainties. This work also showcased the affected customers per year exhibits huge variances.

Numerous investigations on resilience evaluation at the transmission level for climate driven changes are studied [30]-[32] whereas the resilience evaluation on distribution level against hurricane risks can cause vulnerable damages. To evaluate the importance of load, various works mentioned in [33]-[35] prioritize the load criticality by quantifying them in new resilience metrics. One such work is [34] which classifies the loads as hospital, emergency, industrial, commercial and domestic loads from high to least priorities. In the estimation of the resilience metrics, these weighted losses are incorporated accounting for the effect of load criticality.

In [36], based on the Japan Earthquake and accompanying Tsunami event, the importance of improving operational resilience by distribution side load deliverability using microgrids and community plans has been discussed.

Another way of lessening the event risk can be achieved by predicting the event and its unfolding manner. The author of the dissertation [37] implemented a neural network-based event prediction algorithm. This work compares the results of different AI techniques such as perceptron, logistic regression, support vector machine and decision tree with that of an event considered for that work. The methods have proven to be highly efficient in predicting the event unfolds based on the work's discussion.

In order to improve the system's operational resilience, the system must have enough contingency reserves, especially in the case of high renewable penetration [38]. Focusing on the demand side flexibility research works [39] and [40], load adjustments are carried out based on the frequency and voltage violation/deviations. However, this approach is a corrective model rather than a preventive measure. With emerging

13

technologies, the authors of [41] have proposed an anticipatory method of flexible loads using the Internet of Things. To overcome the actions after imbalance occurrence, this approach proposed is faster than the power system reserve contingency operation. This work first considers reconstructed power systems after the damage for generation disturbance quantification followed by anticipating the frequency deviation causing the most serve damage to the network.

1.5   Organization of the Thesis

The rest of the thesis is organized as follows. Chapter 2 discusses the trapezoid and irregular polygon model for operational and infrastructure resilience evaluation. Besides, the resilience metrics are defined in the same chapter. Chapter 3 focuses on the stochastic modelling approach and system analysis techniques. Description of the test system and power system component's dynamic models are discussed in Chapter 4. Chapter 5 focuses on discussing the deterministic and stochastic approaches for resilience evaluation and comparing their results. Conclusions and future scopes are provided in Chapter 6.

CHAPTER 2

POWER SYSTEM RESILIENCE MODEL AND ASSESSMENT

2.1   Electric Power System Resilience

Electric Power Systems is one of the highly complex, non–linear systems and highly prone to natural disasters such as extreme weather conditions, wildfires, earthquakes, and man-made errors such as operator ignorance, auxiliary power system device malfunctioning causing a huge blackout that easily propagates and collapses the entire system. One such example is the 2003 Northeast Blackout which completely caused power outages in North-eastern and midwestern parts of North America [42]. Another recent incident caused major regions of Texas to remain without electricity due to the Snowstorm in 2021 [1]-[2]. Although the system can operate without collapsing in most cases, the number of customers who are kicked off the grid is quite a considerable and high value. Besides, the system recovery to its pre-contingency state after the disaster/calamity is laborious and highly influenced by factors such as system disruption level, workforce capacity and labour availability. Current research funded by the U.S. Department of Energy involves monitoring the power system responses during the event and post-event situation along with the development of performance metrics to improve the power system response [18] in the motive of the making the system capable enough to withstand the disruption with faster adaption, highly resourceful and minimal recovery incorporation.

Unlike reliability, resilience has no unanimous definition which has been accepted worldwide since it is highly dependent on the operator's objective. The resilience is majorly classified as operational and infrastructure. The infrastructure indicator of the

system involves measuring the online status power system devices in the course of the event study. The operational performance of the system represents the quantification of demand satisfaction, generation availability, and frequency deviation. Besides, the power system is said to be resilient if its operational and infrastructure characteristics are not collapsed or highly deteriorated. Thus, the power system resilience framework is required to be effectively modelled considering different aspects of scenarios and the system's corresponding responses to those situations.

This chapter tends to briefly discuss the infrastructure and operational resilience based on linear models such as the trapezoid method discussed in [11], followed by the discussion of an irregular polygon model for measuring system resilience. This model is referred to as the aggregated model in this work. Besides, the numerical definition of performance metrics for the operational, infrastructure, and system resiliencies are elaborated.

2.2.   Resilience Model

2.2.1. Multiphase Trapezoid Model: Infrastructure and Operational Resilience

The crucial assets of the electric power systems involve generators, transmission lines, transformers, and distribution lines. Responses of these devices during the event are monitored and are collectively referred to as the power system response. During any event, the power system response framework indicating the operational and infrastructural performance with respect to time can be schematized and depicted as shown in Figure 3.1. In general, the system response can be categorized into four phases namely,

i.   Intact

ii.   Absorption

iii.   Recuperation

iv.   Recovered Operation
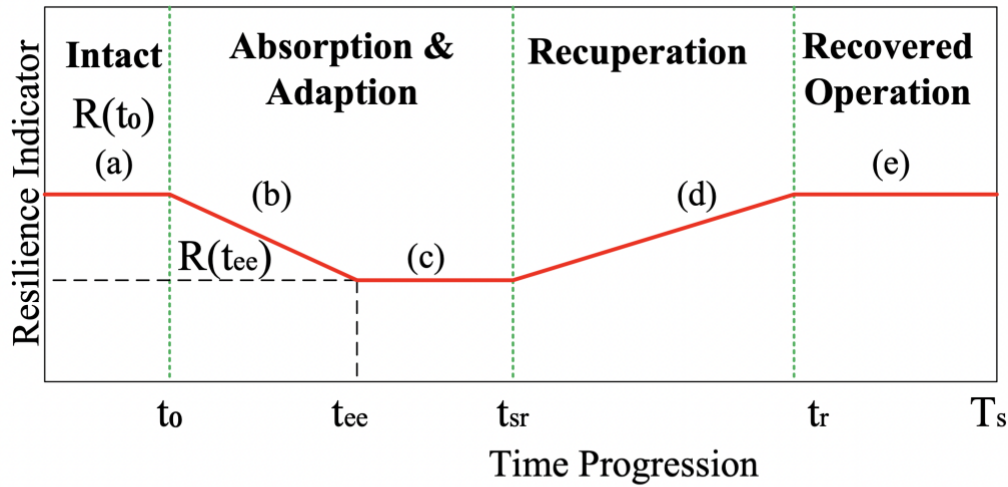
(a): Pre-disturbance state, (b): Event progression, (c): Post degraded state (d): I&O Recovery state, (e): Post recovery state

Figure 2.1 Conventional Trapezoid Model

The first phase, known as the intact phase, is a pre-contingency/pre-disturbance state, where the system operation is undamaged or unaffected. The performance indicator at this stage is ideally 100% and the system remains in an undamaged state until $t = t_0$. Considering the event begins at time $t = t_0$, the system moves into the second phase.

In the absorption and adaption phase, the system resiliency indictor decreases during event progression until t_{ee} and the system operates in a new state immediately after the event. The operational and infrastructure indicator remains at the post-disturbance state until $t = t_{sr}^{(o)}$ and $t = t_{sr}^{(i)}$ respectively. The total time duration of this phase measuring the

17

infrastructure and operational status of the power system can be represented as $\mathcal{T}_a^{(i)}$ and $\mathcal{T}_a^{(o)}$ respectively.

The third phase of the framework is called as recuperation phase. In this phase, restoration begins at t_{sr}, and the system tries to reach its pre-contingency state. Both the infrastructure and operational indicators slowly recover until t_r. This phase can also be called as restoration state. The infrastructure and operational resilience indicator of the system slowly restore until $t_r^{(i)}$ and $t_r^{(o)}$ respectively.

The final phase or the recovered operation indicates the measure of infrastructure and operational indicators during the post-recovery state. Unlike infrastructure resiliency, operational resiliency recovery is influenced by demand, generation availability, asset operational capability, and implementation of effective corrective actions. System resiliency during the post-recovery period can indicate an improved/deteriorated performance or the same pre-contingency performance of the system.

The resiliency measure depends on asset outages and human intervention during the recovery phase. A multiphase modified trapezoid model [15] is defined in this section for defining the system resiliency indicator as shown in Figure 3.2. Similar to the conventional trapezoid model (IORA), this multiphase modified trapezoid model has four phases, namely, intact, absorption, recuperation, and recovered operation. However, unlike the recuperation phase in the IORA model, the recuperation phase in system-level performance has three states, namely, operational recovery, quasi-recovered state, and infrastructure and operational (I&O) recovery. The infrastructure recuperation phase is a highly laborious and

time-consuming phase defining the recovery rate of the system after the disruption period. However, during this asset repairing period, the system operators can regain a part of the lost load and disconnected generators by implementing corrective operational actions, e.g., generator re-dispatch, power import from (export to) another area; this stage is defined as operational recovery in this work. Starting from t_{sr}, this state prolongs until t_{qr}.
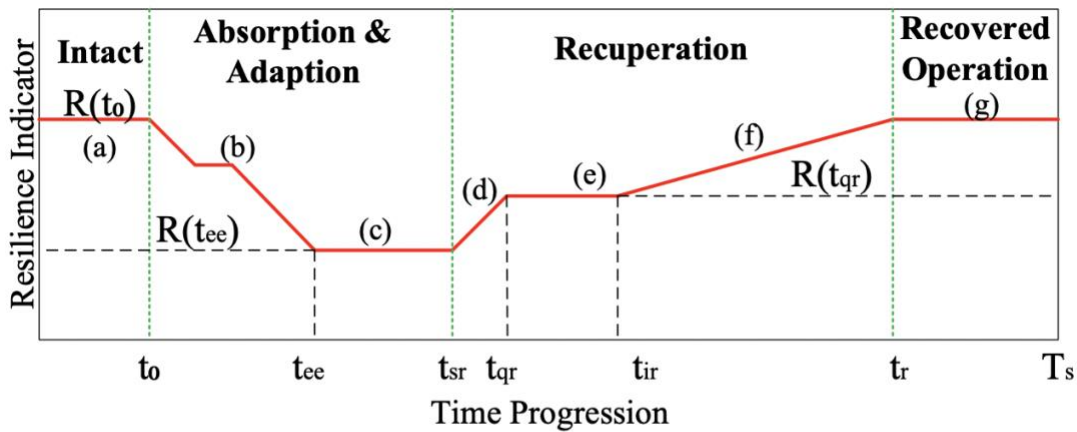
(a): Pre-disturbance state, (b): Event progression, (c): Post degraded state (d): Operational Recovery state, (e): Quasi-recovered state, (f): I&O Recovery state, (g): Post recovery state

Figure 2.2 Multiphase Modified Trapezoid Model

During the next state, known as the quasi-recovered state, a part of disconnected customers/generators and islanded buses/areas are regained back, and the system reaches a new operational state with a lower performance indicator compared to the targeted value. This state lasts until t_{ir}. I&O recovery state, being the third state, interprets the system performance improvement by recovering the infrastructural and operational characteristics of the network until t_r. Note that there can be multiple stages of operational recovery as more assets are repaired and new operational actions are implemented.

19

2.2.2. Aggregated Multiphase Trapezoid Model: System Resilience

Based on the multiphase trapezoid model, an aggregated multiphase trapezoid model considering transient decays and recoveries is defined in this chapter for system-level aggregated resilience evaluation as depicted in Figure 3.3.
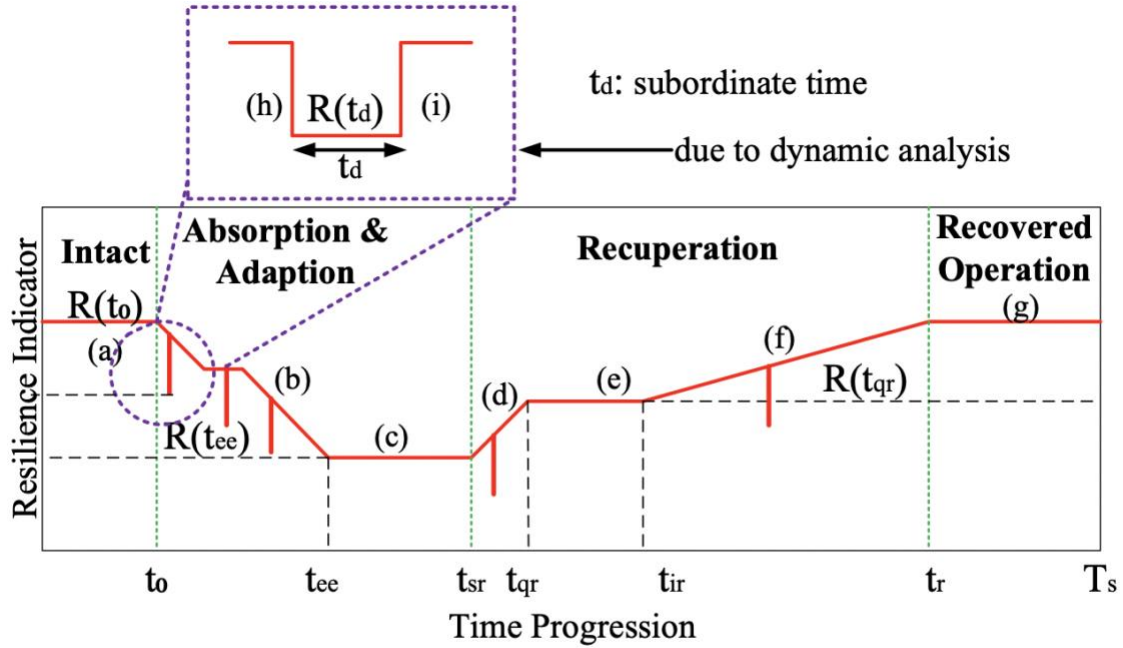
(a): Pre-disturbance state, (b): Event progression, (c): Post degraded state (d): Operational Recovery state, (e): Quasi-recovered state, (f): I&O Recovery state, (g): Post recovery state, (h): transient decay state, (i): transient recovery state

Figure 2.3 Aggregated Multiphase Trapezoid Model

Similar to the multiphase trapezoid model, the phases and states of the aggregated model remain exactly the same. However, there are two additional states namely, transient decay (h) and recovery (i) states corresponding to the dynamic analysis. The dips which are observed from the Figure 3.3 has the above mentioned states (g) and (i). At this state, the system operates at a lower resilience state for a time duration of t_d. t_d corresponds to the subordinate time. It is defined as the time duration during which the system remains at

20

a lower performance state. Note that t_d can extend between two states i.e., it can have longer time periods ranging between minutes and hours and they are highly dependent on the recovery standards and procedures followed by an operator during the event.

2.3   Definition of Resilience Metrics

The numerical metrics used to study the system response during extreme conditions are defined and discussed below.

(a)   Intact period ($\mathcal{T}_i$): The time duration in which I&O performance indicator remains unchanged/unaffected, and it can be formulated as,

$$\mathcal{T}_i = t_0 - t_0^-$$

(2.1)

where t_0^- represents the simulation start time.

(b)   Disruption rate ($\mathcal{D}_r$): Disruption or damage rate defines the rate of change of I&O resilience indicator during the event progression. The disruption rate for infrastructure resilience ($\mathcal{D}_r^{(i)}$) and operational resilience ($\mathcal{D}_r^{(o)}$) models are shown in Equations (3.2) and (3.3) respectively.

$$\mathcal{D}_r^{(i)}\Big|_{t_0 \to t_{ee}} = \frac{\mathcal{R}_i(t_0) - \mathcal{R}_i(t_{ee})}{t_{ee} - t_0}$$

(2.2)

$$\mathcal{D}_r^{(o)}\Big|_{t_0 \to t_{ee}} = \frac{\mathcal{R}_i(t_0) - \mathcal{R}_o(t_{ee})}{t_{ee} - t_0}$$

(2.3)

where $\mathcal{R}_i(t_0)$ and $\mathcal{R}_o(t_0)$ are I&O resilience indicator at time t_0, $\mathcal{R}_i(t_{ee})$ and $\mathcal{R}_o(t_{ee})$ are I&O resilience indicator at time t_{ee}. If the disruption variation is non-linear, the damage rate for different time samples can be estimated and can be weighted averaged for estimating the overall rate.

(c) Preparation time $(\mathcal{T}_p)$: Time duration in which I&O performance indicators remain at post-disturbance state. The infrastructure and operational preparation time can be written as given by Equations (3.4) and (3.5) respectively.

$$\mathcal{T}_p^{(i)} = t_{sr}^{(i)} - t_{ee} \tag{2.4}$$

$$\mathcal{T}_p^{(o)} = t_{sr}^{(o)} - t_{ee} \tag{2.5}$$

Here $t_{sr}^{(i)}$ and $t_{sr}^{(o)}$ correspond to infrastructure and operational recovery initiation time respectively.

(d) Recovery rate $(\mathfrak{R}_r)$: Restoration rate determines the gradient of I&O resilience indicator in the recuperation phase.

The infrastructure $(\mathfrak{R}_r^{(i)})$ and operational $(\mathfrak{R}_r^{(o)})$ recovery rates can be written as,

$$\mathfrak{R}_r^{(i)}\Big|_{t_{sr}^{(i)} \to t_r^{(i)}} = \frac{\mathcal{R}_i(T_s) - \mathcal{R}_i(t_{ee})}{t_r^{(i)} - t_{sr}^{(i)}} \tag{2.6}$$

$$\mathfrak{R}_r^{(o)}\Big|_{t_{sr}^{(o)} \to t_r^{(o)}} = \frac{\mathcal{R}_o(T_s) - \mathcal{R}_o(t_{ee})}{t_r^{(o)} - t_{sr}^{(o)}} \tag{2.7}$$

where $\mathcal{R}_i(T_s)$ and $\mathcal{R}_o(T_s)$ are I&O resilience indicator at time $t_{sr}^{(i)}$ and $t_{sr}^{(o)}$ respectively. $t_r^{(i)}$ and $t_r^{(o)}$ correspond to infrastructure and operational recovery end time respectively. If the recovery variation is non-linear, the indicators for different time samples are measured and a weighted averaged estimating the overall rate can be found.

(e) Recovery time $(\mathcal{T}_r)$: Time consumed by the system to regain I&O characteristics back to its original state or maximum recoverable state and it is given by Equations (3.8) and (3.9) respectively.

22

$$\mathcal{T}_r^{(i)} = t_r^{(i)} - t_{sr}^{(i)} \tag{2.8}$$

$$\mathcal{T}_r^{(o)} = t_r^{(o)} - t_{sr}^{(o)} \tag{2.9}$$

(f) Area under the curve (Λ_t): The area traced by I&O resilience trapezoid curves can be expressed as given by Equations (3.10) and (3.11) respectively.

$$\Lambda_t^{(i)} = \int_{t_0^-}^{t_0} \mathcal{R}_i \, dt + \int_{t_0}^{t_{ee}} \mathfrak{D}_r^{(i)} \, dt + \int_{t_{ee}}^{t_{sr}^{(i)}} \mathcal{R}_i \, dt + \int_{t_{sr}^{(i)}}^{t_r^{(i)}} \mathfrak{R}_r^{(i)} \, dt + \int_{t_r^{(i)}}^{T_s} \mathcal{R}_i \, dt \tag{2.10}$$

$$\Lambda_t^{(o)} = \int_{t_0^-}^{t_0} \mathcal{R}_o \, dt + \int_{t_0}^{t_{ee}} \mathfrak{D}_r^{(o)} \, dt + \int_{t_{ee}}^{t_{sr}^{(o)}} \mathcal{R}_o \, dt + \int_{t_{sr}^{(o)}}^{t_r^{(o)}} \mathfrak{R}_r^{(o)} \, dt + \int_{t_r^{(o)}}^{T_s} \mathcal{R}_o \, dt \tag{2.11}$$

(g) Absorption time ($\mathcal{T}_a$): Total Time period during which the system remains at absorption and adaption phase.

The infrastructure absorption time ($\mathcal{T}_a^{(i)}$), can be written as,

$$\mathcal{T}_a^{(i)} = t_{sr}^{(i)} - t_0 \tag{2.12}$$

The operational absorption time ($\mathcal{T}_a^{(0)}$), can be written as,

$$\mathcal{T}_a^{(o)} = t_{sr}^{(o)} - t_0 \tag{2.13}$$

2.4   Summary

Different linearized resilience models such as conventional and multiphase trapezoid models for steady-state resilience evaluation have been discussed. An aggregated multiphase trapezoid model has been proposed in this chapter with view of incorporating dynamic analysis into the resilience study. Finally, the resilience metrics and its numerical expressions are provided in this chapter.

CHAPTER 3

STOCHASTIC ASSESSMENT OF POWER SYSTEM RESILIENCE

Unlike deterministic approaches developed for traditional resilience analysis, power system response to high impact scenarios such as extreme weather conditions can cause cascading failures and outages in the grid. These extreme situations can cause power system assets failure and retirement in the grid. Power system resilience can be enhanced by incorporating stochasticity in system modelling and analysis. With a probabilistic risk assessment of each component, proper measures can be addressed to increase system robustness, adequacy, and healing capability. Thus, a probabilistic assessment approach has been developed in this chapter to capture the stochastic nature of the power system with the aim of modelling outage scenarios for electric power plants, transmission systems, and renewable plants. Moreover, the risk modelling on the power system can be represented as component status (operational and infrastructure status) based on which the system effects are captured to develop the resilience metrics.

3.1   Failure Probability Model and Scenarios for System Components

3.1.1   Wind Turbine Outage Model

With high penetration of renewable energy sources such as wind and PV, the power system response during these extreme weathers can cause major interruptions in the grid. For instance, the Texas 2021 winter storm has caused critical outages in the state for several weeks due to generation unavailability and wind turbine locking [1]. Thus, the wind turbine outage model needs to be incorporated to study the effect of net load variation in the system

resilience evaluation. Based on the power-wind characteristics of the wind turbine, the active power output can be determined based on the wind speed as shown in Equation (3.1).

$$P_t(v) = \begin{cases} 0 & 0 \le v < w_r \\ \frac{v^3 - w_i^3}{w_r^3 - w_i^3} & w_i \le v \le w_r \\ P_r & w_r \le v < w_0 \\ 0 & v > w_0 \end{cases} \tag{3.1}$$

where v is current wind speed (m/s), $P_t(v)$ is active power output for current wind speed measured in MW, P_r is rated active power output measured in MW, w_i, w_0 and w_r are cut-in, rated and cut-out speeds for wind turbine measured in m/s respectively. The wind turbines are locked and arrested from producing energy during high (above cut-out speed) and low (below cut-in speed) wind speed conditions. The power curve representing the operating characteristics of the GE 1.5 MW wind turbine extracted from [43] is depicted in Figure 3.1.
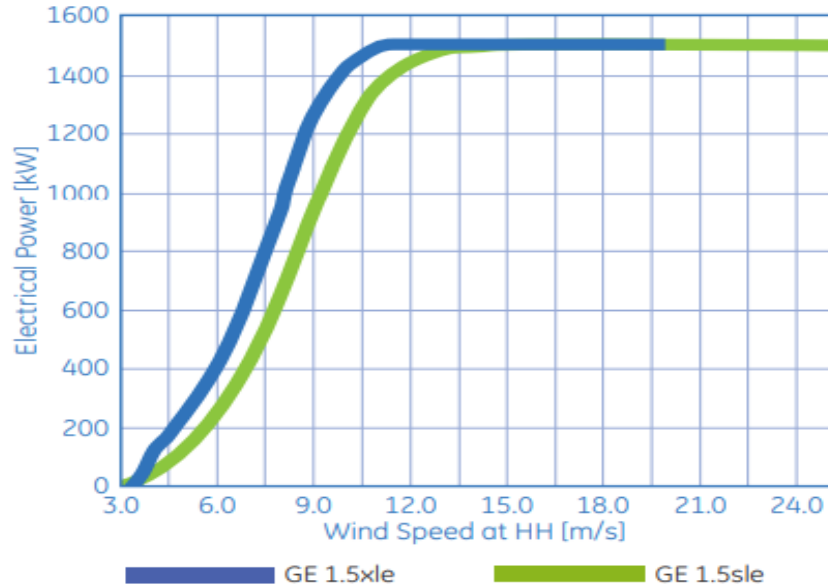
Figure 3.1 Power Curve of GE 1.5 MW Wind Turbine [43]

From Figure 3.1, the cut-in, rated and cut-out wind speeds for the GE 1.5sle structure are 3 m/s, 14 m/s and 25 m/s respectively. Though the 1.5sle is a classical

workhorse, it has been considered for the study since it has proven to be an efficient and reliable model [43].

3.1.2 Transmission Corridor

Fragility analysis is a probabilistic approach to determining the reliability of transmission networks (including transmission lines and towers) during extreme weather conditions and can be mathematically represented using Equation (3.2).

$$\vartheta(v_i) = \begin{cases} 0, & if \ v < v_{cr} \\ \vartheta(v), & if \ v_{cr} \leq v \leq v_{br} \\ 1, & if \ v > v_{br} \end{cases} \qquad (3.2)$$

where $\vartheta(v_i)$ is the failure probability of the transmission network for any wind speed, v_i (m/s) and $\vartheta(v)$ represents the failure probability of the transmission network for wind speed, v (m/s) when the wind speed is bounded within critical (v_{cr}) and breakdown wind speeds (v_{br}).
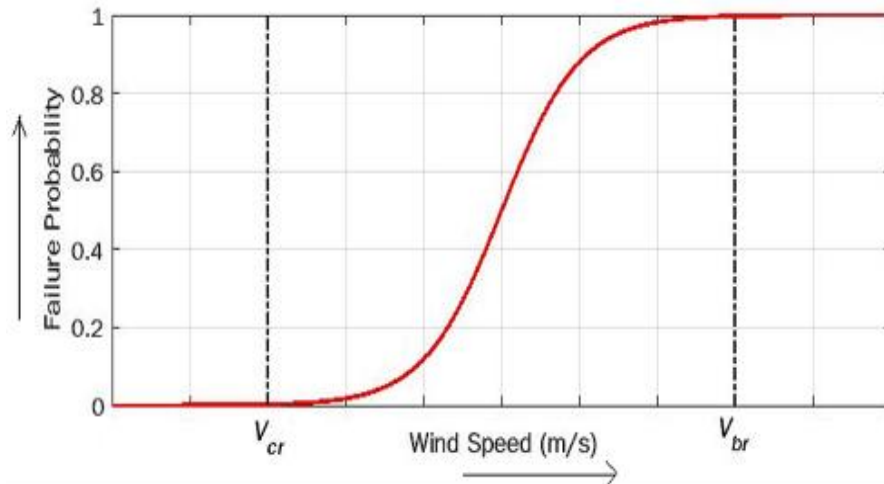
Figure 3.2 Generic Fragility Curve for Transmission Corridor [11]

For a wind speed below v_{cr}, the infrastructure and operation of the transmission network remain unaffected (i.e., zero failure probability) whereas, for a wind speed above

26

v_{cr} the reliability of the transmission network is altered based on the failure probability function. Wind speed above v_{br} collapses the structural and operational template of the network (i.e., 100% failure probability). A generic fragility curve representing the above framework extracted from [11] has been depicted in Figure 3.2.

The failure probability vs wind speed curve for less robust and more robust transmission corridors are extracted from [11] and shown in Figure 3.3.
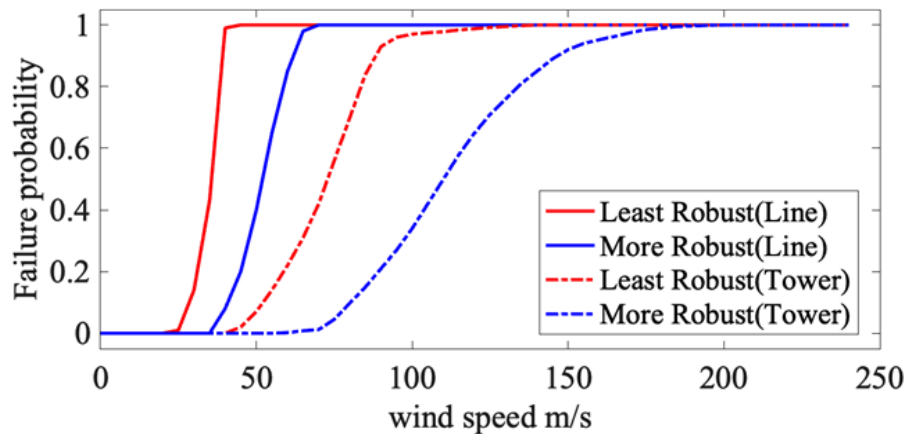
Figure 3.3 Fragility Curve for Transmission Corridor Extracted from [11]

3.2   Stochastic Resilience Assessment

The probabilistic resilience assessment incorporates system and hurricane stochasticity for a detailed analysis of resilience and risk assessment. As the power system is a highly uncertain network, implementing stochastic approach can be more realistic. The following sections briefly discuss the hurricane model, stochastic load model and probabilistic approach for resilience metrics estimation.

3.2.1   Hurricane Model

Based on the intensity of the hurricane, they are classified into five categories. The National Hurricane Center (NHC) grouped the hurricane categories based on Saffir-

Simpson Hurricane Wind Scale [44]. According to NHC, "The Saffir-Simpson Hurricane Wind Scale is a 1 to 5 rating based only on a hurricane's maximum sustained wind speed. This scale does not take into account other potentially deadly hazards such as storm surge, rainfall flooding, and tornadoes".

The Saffir-Simpson Hurricane Wind Scale calculates the amount of damage that could be caused by a hurricane. Hurricanes classified Category 3 and higher are known as major hurricanes, even though all hurricanes produce life-threatening winds [44]. The hurricane categories are tabulated based on their maximum sustained wind speed and their frequency of occurrence as shown in Table 3.1.

Table 3.1 Classification of Hurricanes Based on Saffir-Simpson Scale [44]

Categories	Maximum Wind speed (m/s)	Average Hurricanes Per Year
1	30-39	7.1
2	40-49	4.7
3 (major)	50-58	4.7
4 (major)	59-70	1.1
5 (major)	>70	0.2

The stochastic nature of the wind can be incorporated by following Monte Carlo Simulations (MCS) for resilience evaluation. Besides, it embeds the spatiotemporal nature of the hurricane through the transmission corridor. The wind profile and its frequency density distribution, based on the data obtained from [44], are depicted in Figure 3.4.
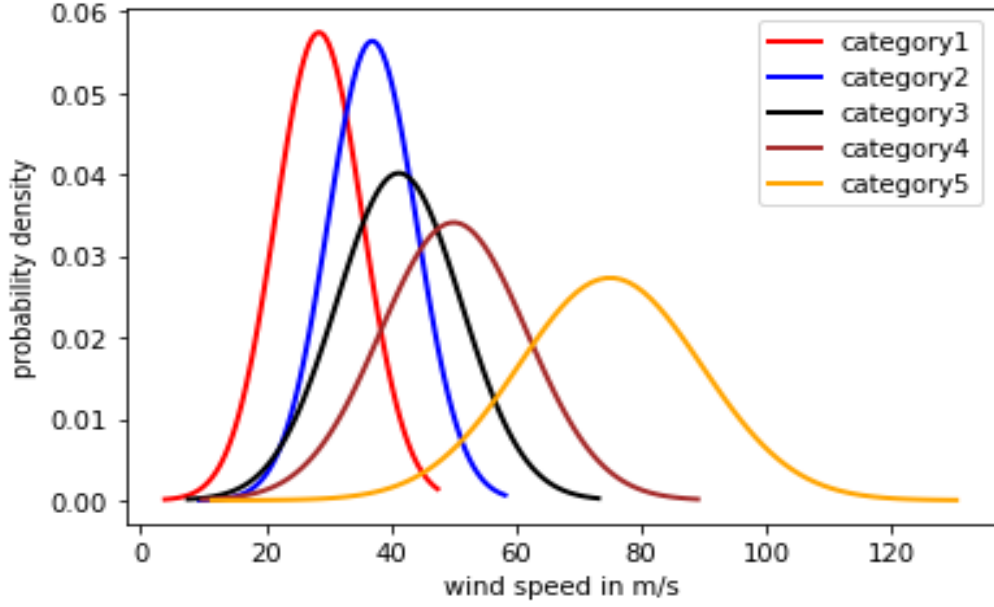
Figure 3.4 Probability Density Distribution Curve for Different Hurricane Categories

3.2.2 Stochastic Load Model

Unlike the deterministic approach, the stochastic approach includes load uncertainty in the resilience evaluation and has been implemented in this work. In the deterministic approach, the scheduled hourly bus loads are carried out for the resilience evaluation. On the contrary, the stochastic approach includes the load uncertainty due to the hurricane effects (wind uncertainty). The net hourly bus load, $P_{L,t}$, can be written as,

$$P_{L,t} = P_{L,t}^{sched} + P_t^{var} \tag{3.3}$$

where $P_{L,t}^{sched}$ represents the scheduled bus load in terms of percentage of full load, and P_t^{var} represents the uncertain load due to hurricane stochasticity.

3.2.3 Probabilistic Resilience Metrics

In this section, the probabilistic approach to estimate the resilience metrics is discussed. Metrics such as overall resilience and system toughness are derived and discussed below. The system resilience estimates the infrastructural and operational

resilience. The system toughness is used to quantify the grid robustness and sensitivity in response to the hurricane impact on the network.

(a)   System Resilience:

Let ε_i be any scenario for a given hurricane category and its probability of occurrence based on the event unfolding can be denoted as $\mathbb{P}(\varepsilon_i|v)$. If there are '$n$' scenarios, then the sum of the probabilities of each event can be written as,

$$\mathbb{P}(\varepsilon|v) = \sum_{i=1}^{n} \mathbb{P}(\varepsilon_i|v) = 1 \tag{3.4}$$

The overall infrastructure $\left(\Lambda_p^{(I)}\right)$ and operational resilience $\left(\Lambda_p^{(O)}\right)$ can be estimated as,

$$\Lambda_p^{(I)} = \sum_{i=1}^{n} \mathbb{P}(\varepsilon_i|v) \times \Lambda_i^{(I)} \tag{3.5}$$

$$\Lambda_p^{(O)} = \sum_{i=1}^{n} \mathbb{P}(\varepsilon_i|v) \times \Lambda_i^{(O)} \tag{3.6}$$

where $\Lambda_i^{(I)}$ and $\Lambda_i^{(O)}$ per unit values of infrastructure and operational resilience.

3.3   Steady-State Analysis

This section aims to focus on modelling wind turbine generators (WTGs) for power flow studies, unit commitment model for generation scheduling and optimal power flow technique for corrective action and generation dispatch for varying hourly bus loads.

3.3.1   Renewable Integration in the Grid

The representation of the wind plant for the steady-state analysis is highly important and depends on the type of machine being used for the analysis. For instance, the fixed speed wind turbine generators (WTGs) are modelled as negative load with constant reactive power equal to the amount being absorbed at the real power level considered for the study. These machines are integrated into the system as a PQ bus by modelling shunt capacitors for reactive power consumption at that bus [45]. Since type 3 and 4 wind

machines can provide reactive power support, they can be modelled as the conventional generator and can be integrated as PV buses into the system with appropriate reactive power limits.
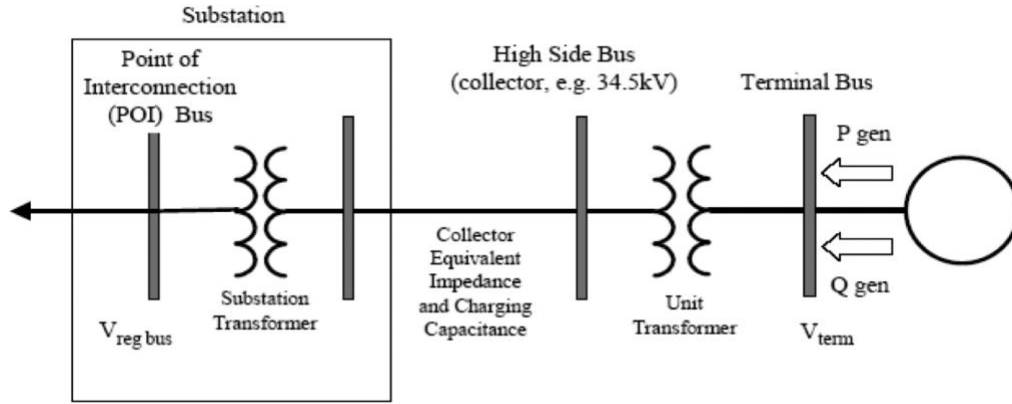
Figure 3.5 WTG Model for Power Flow Analysis [45]

Though the wind generators are decentralized at the plant level, the aggregated power is injected into the system through a collector-substation model. The equivalent aggregated model representing a single generating unit is valid for studying the system-level impact of wind resources penetration. A single-line diagram representing WTG modelling with a collector-substation system is depicted in Figure 3.5.

3.3.2   Unit Commitment

The unit commitment (UC) is performed to achieve system operation at minimum cost by committing the required available resources. The mathematical formulation for the UC [60] is used to determine the generator status and its generation level during each time and can be expressed as:

$$\min \sum_{t\in\mathcal{T}} \sum_{g\in\mathcal{G}} C_g P_g^t + C_g^{NL} u_g^t + C_g^{SU} v_g^t + \min C_L \sum_{t\in\mathcal{T}} \sum_{n\in\mathcal{N}} (D_n^t - d_n^t) \quad \forall g, \forall t \quad (3.12)$$

subject to

$$u_g^t P_g^{min} \leq P_g^t \leq u_g^t P_g^{max} \qquad \forall g, \forall t \qquad (3.13)$$

$$-\ell_k^t P_k^A \leq B_k\left(\theta_j - \theta_i\right) \leq \ell_k^t P_k^A \qquad \forall k, \forall t \qquad (3.14)$$

$$\sum_{g \in \mathcal{G}} P_g^t = \sum_{n \in \mathcal{N}} d_n^t \qquad \forall n, \forall t \qquad (3.15)$$

$$\sum_{t-\mathcal{T}_g^{up}+1}^{t} v_g^t \leq u_g^t \qquad \forall g, \forall t \qquad (3.16)$$

$$\sum_{t-\mathcal{T}_g^{down}+1}^{t} w_g^t \leq 1 - u_g^t \qquad \forall g, \forall t \qquad (3.17)$$

$$P_g^t - P_g^{t-1} \leq R_g^H u_g^{t-1} + R_g^{start} v_g^t \qquad \forall g, \forall t \qquad (3.18)$$

$$P_g^{t-1} - P_g^t \leq R_g^H u_g^t + R_g^{shut} w_g^t \qquad \forall g, \forall t \qquad (3.19)$$

$$u_g^t, v_g^t, w_g^t \in \{0,1\} \qquad \forall g, \forall t \qquad (3.20)$$

Equation (3.12) is the objective function aims in minimizing the total operating cost of the system and load shed cost incurred in the system. The system operating cost includes generation cost, no-load cost, and start-up cost at all time intervals (t) and for all generators (g). The linear cost inputs C_g, C_g^{NL}, and C_g^{SU} are linear cost (generation cost expressed in \$/MW), no-load cost and start-up cost (expressed in \$) of the generators that are remained and turned ON for all time periods. C_L represents the value of lost load in \$/MW. Equations (3.13) – (3.20) imposes actual system constraints on the optimization problem for scheduling real time generation status. The synchronous machine generation constraints caping the maximum and minimum active power limit is represented in equation (313). For offline generation units, the value of u_g^t is set to zero forcing no active power is generated by the corresponding machine. Equation (3.14) represent the active power limit constraints for any transmission branch (k) at all time intervals, t. The transmission line status (ℓ_k^t), denotes the line operational status at time, t. The line is considered online if

32

$\mathscr{b}_k^t$ is one, else the value of $\mathscr{b}_k^t$ is zero for the line remaining offline or tripped. The active power limits of the transmission corridor are determined based on the thermal rating of that branch. Equation (3.15) ensures generation-load balance constraint considering load shedding during the event progression and restoration phase of the simulation time. Equation (3.16), (3.17), (3.18) and (3.19) represents minimum uptime, downtime, ramp up and ramp down constraints for all generating units during the study. The variables v_g^t and denotes the turning ON and OFF status from the offline and online operation of the generating units for all time periods, t. Equation (3.20) ensures the variables u_g^t, v_g^t and w_g^t are binary (0 and 1). The status of the generators is obtained and utilized for solving optimal power flow.

3.3.3 AC Optimal Power Flow Technique

The optimal power flow technique is used to dispatch the generators for every period of bus load change in the system. Redispatch is carried out such that branch flow, node balance, generation-load balance and generation limit constraints are satisfied based on the generator status obtained from the unit commitment. The objective function for the optimal power flow is aimed to minimize load shedding during the event progression and recovery state. The pre-contingency and post-recovery states are aimed to conduct ACOPF optimizing the generation fuel cost. ACOPF has been solved using Siemens PSS®E (Power System Simulator for Engineering) version 35.2. The ACOPF model [46] for minimizing fuel cost and load shedding can be mathematically represented as follows,

$$\min \sum\nolimits_{\forall n_L} P_L^0 \left(1 - \psi_n^{(t)}\right) C_L \quad \forall t \in (t_e, t_r) \tag{3.21}$$

$$\min \sum_{\forall n_g} P_g^{(t)} C_g \quad \forall t \in T - \{(t_e, t_r)\} \tag{3.22}$$

subject to

$$U_g^{(t)} P_g^{min} \leq P_g^{(t)} \leq U_g^{(t)} P_g^{max} \quad \forall t \forall g \tag{3.23}$$

$$U_g^{(t)} Q_g^{min} \leq Q_g^{(t)} \leq U_g^{(t)} Q_g^{max} \quad \forall t \forall g \tag{3.24}$$

$$V_n^{min} \leq V_n^{(t)} \leq V_n^{max} \quad \forall t \forall n \tag{3.25}$$

$$\theta_n^{min} \leq \theta_n^{(t)} \leq \theta_n^{max} \quad \forall t \forall n \tag{3.26}$$

$$P_{ij}^{(t)} = V_i^2 (G_{i0} + G_{ij}) - V_i V_j (B_{ij} \sin \theta_{ij} + G_{ij} \cos \theta_{ij}) \, \forall t \forall k \tag{3.27}$$

$$Q_{ij}^{(t)} = -V_i^2 (B_{i0} + B_{ij}) + V_i V_j (B_{ij} \cos \theta_{ij} - G_{ij} \sin \theta_{ij}) \, \forall t \forall k \tag{3.28}$$

$$\sqrt{P_{ij}^{(t)^2} + Q_{ij}^{(t)^2}} \leq S_{ij}^A \quad \forall t \in T - \{(t_e)\} \forall k \tag{3.29}$$

$$\sqrt{P_{ij}^{(t)^2} + Q_{ij}^{(t)^2}} \leq S_{ij}^B \quad \forall t \in \{t_e\} \forall k \tag{3.30}$$

$$\psi^{min} \leq \psi_n^{(t)} \leq \psi^{max} \quad \forall t \in (t_e, t_r) \, \forall n \tag{3.31}$$

$$S_L^{(t)} = \psi_n^{(t)} S_L^0 \quad \forall t \in (t_e, t_r) \, \forall n \tag{3.32}$$

$$\sum_{n \in n_s} S_{ij}^{(t)} - \sum_{n \in n_r} S_{ij}^{(t)} = \sum_{\substack{n \in n_g \\ \forall g}} S_g^{(t)} - S_L^{(t)} \quad \forall t \, \forall n \tag{3.33}$$

where P_L^0 is the initial real power bus load in MW, $\psi_n^{(t)}$ is bus load multiplier at time t, ψ^{min} and ψ^{max} are the minimum and maximum allowable range for the load multiplier. C_L and C_g represent load shedding and generation fuel cost measured in \$/MW. $U_g^{(t)}$ is a parameter (non-variable entity in ACOPF model) representing the commitment status of the generator obtained from solving the UC problem. $P_g^{(t)}$, P_g^{min} and P_g^{max} are real power generated at time t, maximum and minimum capacity of real power generation

measured in MW. $Q_g^{(t)}$, Q_g^{min} and Q_g^{max} are reactive power generated at time t, maximum

and minimum capacity of reactive power generation measured in MVAR. $V_n^{(t)}$, V_n^{min} and

V_n^{max} are bus voltage at time t, maximum and minimum limit of bus voltage. $\theta_n^{min}, \theta_n^{max}$

are maximum and minimum bus voltage angles, respectively, measured in degrees. $\theta_n^{(t)}$

represents instantaneous bus voltage angle measured in degrees. $P_{ij}^{(t)}$ and $Q_{ij}^{(t)}$ are real and

reactive power flow on the branch between buses i and j. G_{i0} and B_{i0} are real and imaginary

parts of the shunt admittance at bus i respectively. G_{ij} and B_{ij} are real and imaginary parts

of the line admittance between buses i and j respectively. θ_{ij} is the bus voltage angle

difference between buses i and j. S_{ij}^A and S_{ij}^B are continuous and long-term emergency

(LTE) thermal ratings of the line measured in MVA respectively. $S_L^{(t)}$ and S_L^0 represent

effective and initial bus load measured in MVA. T represents the total simulation hour,

$\{t_e\}$ is set representing event progression period, $\{(t_e, t_r)\}$ is a set representing the time

period between event initiation and recovery end time. $U_g^{(t)}$ represents the commitment

status of the generator at time t. n_s and n_r represent the set of sending and receiving end

buses based on the direction of net branch flow.

     Equation (3.21) represents the objective function for minimizing load shedding

during event progression, post degraded state and recuperation state. (3.22) represents the

objective function for minimizing fuel costs, utilized during pre-contingency and post-

recovery states. In addition to linear cost curves, PSS®E has the capability of incorporating

quadratic, exponential and polynomial fuel cost curves as well. PSS®E OPF has been built

based on the conventional AC power flow technique and it requires a swing bus for solving

the same. The real and reactive power generation is limited within its capacity by the constraints mentioned in Equations (3.23) and (3.24) respectively. The bus voltage and bus voltage angle constraints are modelled using Equations (3.25) and (3.26) respectively. Equations (3.27) and (3.28) represent the mathematical equation to estimate real and reactive power flow on branches between buses i and j respectively. Equations (3.29) and (3.30) represent the continuous and LTE thermal rating constraints for transmission branches respectively. LTE is a 24-hour emergency thermal capacity of the line during extreme scenarios. Thus, the line capacity can be increased to operate at LTE during the event progression state. Continuous thermal rating of transmission lines can be implemented during the rest of the simulation period. Equation (3.31) represents the load multiplier constraint. Equation (3.32) estimates online apparent bus loads during the simulation hour. Constraints (3.31) and (3.32) are specially used for minimizing bus load adjustments based OPF technique. They are neglected in the fuel cost optimization model. Node-balance constraint is governed by Equation (3.33). It is also assumed the steady-state is assumed to be stable after re-dispatching the generation committed units using the optimal power flow technique.

3.4   Summary

The importance of implanting stochasticity in the resilience evaluation is highlighted followed by modelling hurricane and bus loads for different scenarios using Monte Carlo Simulation approach. Besides, the mathematical formulation of the system analysis techniques used in steady-state evaluation of resilience studies for a network with wind penetration is discussed.

CHAPTER 4

TEST CASE AND DYNAMIC MODELS

Though the steady-state operation of the power system is analyzed for different scenarios and disturbances and at various timestamps, it is also equally important to perform short-term time domain simulations (STTDS) on the system following the event/contingency to assess its dynamic response. Thus, this chapter focuses on modelling dynamic models for generator, exciter, governor, bus loads and protection devices. Moreover, this chapter also briefs the dynamic modelling of wind and solar resources in the interest of monitoring system behaviour during renewable penetrations in the electric grid. The dynamic models are constructed in PSS®E (Power System Simulator for Engineering) version 35.2, high performance transmission planning and analysis tool developed by Siemens.

4.1   Test System Description

The IEEE reliability test system (1996) or RTS, obtained from [47], is used for resilience study and the single line diagram of the same is depicted in Figure 4.1. RTS is a three-area test case where all the areas are electrically identical i.e., in terms of generation capacity, branch rating and peak bus loads. It consists of 99 conventional generators (33 in each area), 104 transmission lines, 57 bus loads (19 in each area) and other technical details favouring the system infrastructure are shown in Table 4.1. The given model is a conventional RTS network, obtained from [47], and does not have renewable resource penetrations.
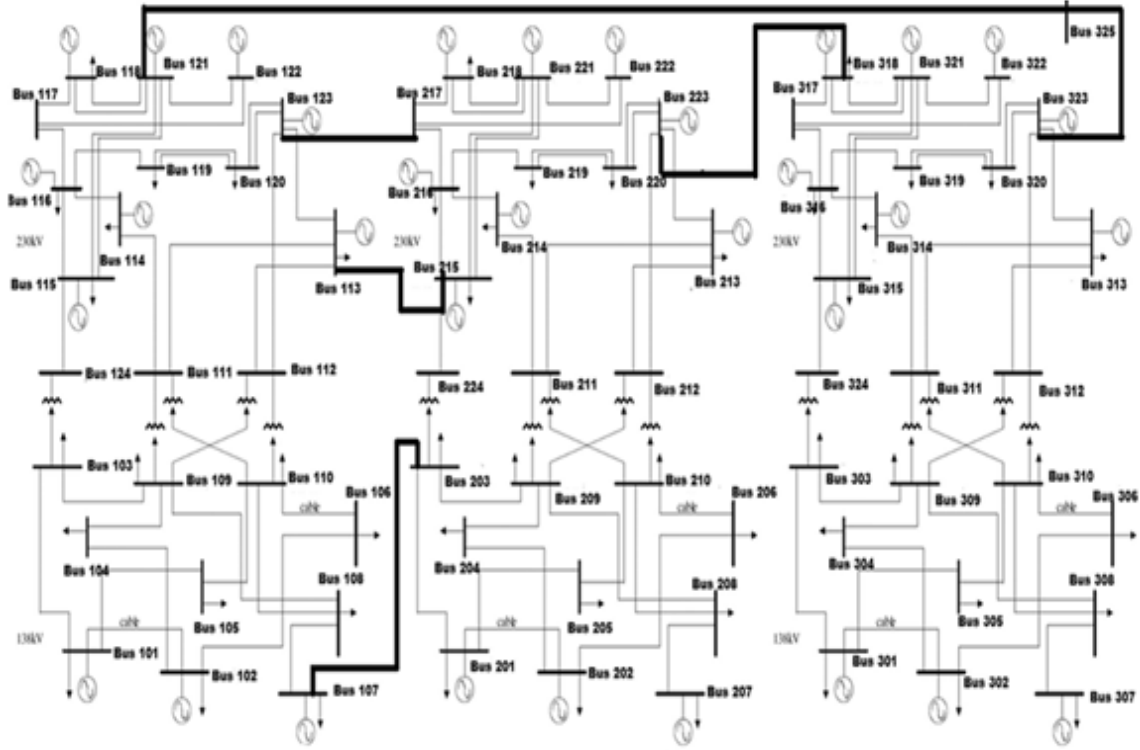
Figure 4.1 One-line Diagram of IEEE Reliability Test System (1996)

From Figure 4.1, it can be observed that there are five tie lines connecting these three regions supporting the power sharing capability among the areas. Note that taking these tie lines offline can make the system going unstable as they are vital for stability analysis.

Table 4.1 IEEE RTS'96 test details [47]

Parameters	Features
Buses	73
Areas	3
Total generation capacity	14.5 GW (15202 MVA)
Total peak bus loads	8550 MW (8725 MVA)
Base Voltages	138 kV and 230 kV

Figure 4.2 One-line Diagram of Modified IEEE RTS System

40

A modified RTS network with 20% wind penetration provided in Figure 4.2 is considered for this work. The corresponding wind plants are added at buses 123, 223 and 323 corresponding to areas 1, 2 and 3 respectively. Each wind plant can generate 750 MW at 0.9 power factor for the rated wind speed condition.
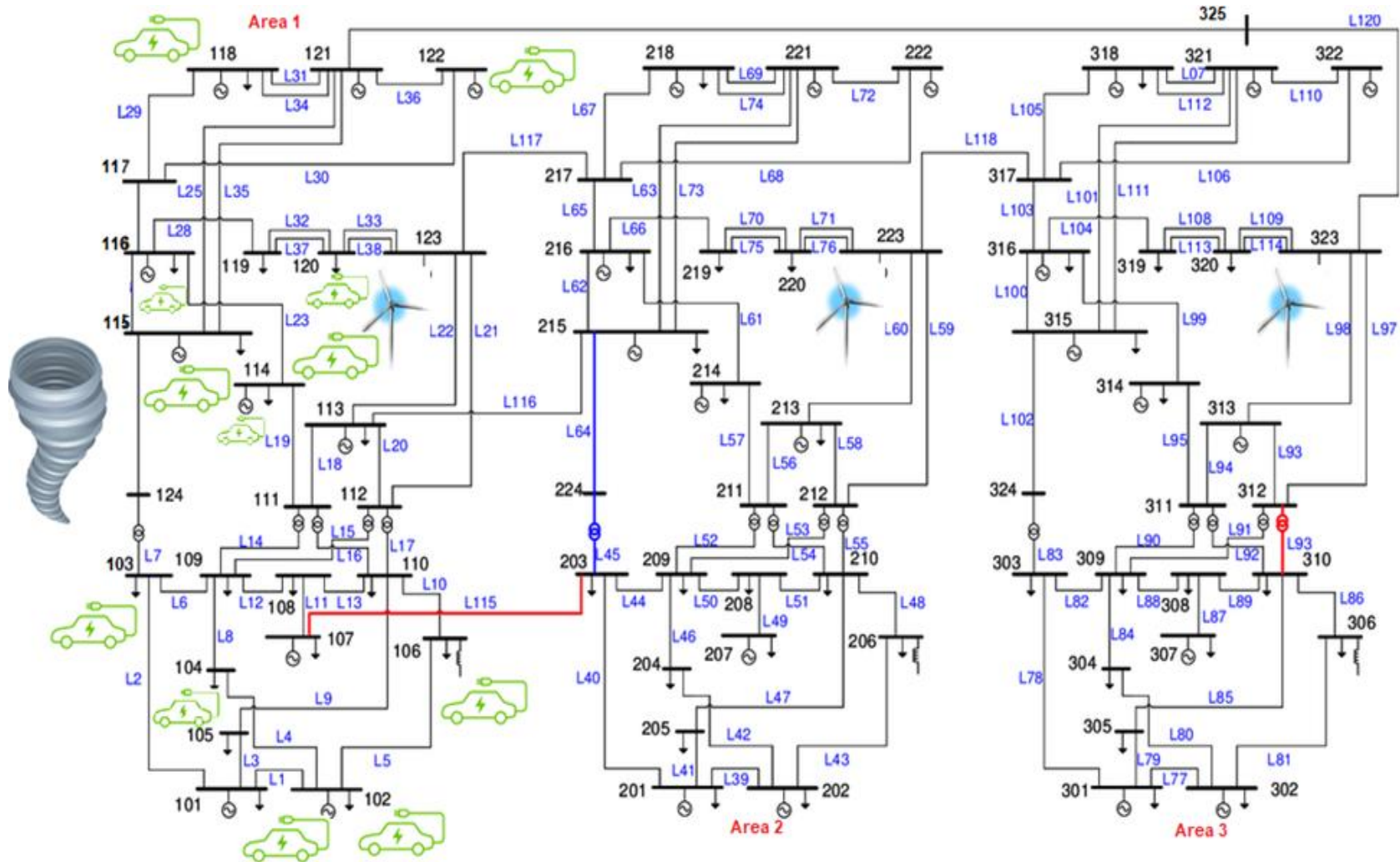
To append wind penetration in the conventional grid, certain procedures are followed. One such rule is known as 2/3 decommitment-1/3 redispatch rule, which are followed by NERC for system analysis with renewable penetration in the grid [48]. The rule applies to conventional steam power plants dominated electric grid. If a 3 MW wind plant to be added to the network, 2 MVA of steam plant capacity must be decommitted and 1 MW of dispatching steam plant output power is required. With nuclear plants in the network, this work modifies the above procedure by considering the 1 MW rule applied to the nuclear plants instead of the steam plants. For the current study, the hydro and gas plants remain same as they play a major role in frequency support in reliable grid operation.

With the above modified rule, for 750 MW wind penetration at area 1, 500 MVA capacity of steam plant requires decommitment and 250 MW capacity redispatching applied for nuclear plants. With these modifications accomplished, the plant is added at bus 123 through collector-substation model mentioned in Chapter 3. In similar fashion, identical wind plants each of 750 MW generation capacities are added to the areas 2 and 3 at buses 223 and 323 respectively.

4.2   Conventional Plant Model

Conventional power plants such as steam, gas turbine, coal and nuclear plants consist of synchronous machines, exciters, governors, and boilers (reactor). In STTDS,

these components such as generators, exciters and governors are represented by differential-algebraic equations. These equations (representing plant models) are connected to power system networks using algebraic equations. Thus, dynamic values representing the dynamic behaviour of the system are considered for the modelling. All the dynamic models representing the plant components considered for this work are widely being used and accepted by Western Electric Coordinating Council (WECC) [49].

4.2.1. Synchronous Machine Model

The detailed model of the synchronous generator is actively represented using E'' model, which is the most widely used simplified model for electromechanical stability studies in practice. This model can also be called voltage behind sub transient reactance. Equations (4.1) to (4.6) represent the electrical and mechanical characteristics of the detailed synchronous machine model. Assumptions considered and derivations of the equations are briefed in chapter 4 of [50].

$$\dot{\lambda}_D = \frac{1}{\tau''_{do}} \sqrt{3} E'_q - \frac{1}{\tau''_{do}} \lambda_D + \frac{1}{\tau''_{do}} (x'_d - x_l) i_d \tag{4.1}$$

$$\sqrt{3}\dot{E}'_q = \frac{1}{\tau'_{d0}} \sqrt{3} E_{FD} + \frac{(x_d - x'_d)(x''_d - x_l)}{\tau'_{d0}(x'_d - x_l)} i_d - \frac{\sqrt{3}}{\tau'_{d0}} \left[1 + \frac{(x_d - x'_d)(x'_d - x''_d)}{(x'_d - x_l)^2} \right] E'_q$$

$$+ \frac{(x_d - x'_d)(x'_d - x''_d)}{\tau'_{d0}(x'_d - x_l)^2} \lambda_D \tag{4.2}$$

$$\dot{\lambda}_Q = \frac{1}{\tau''_{qo}} \sqrt{3} E'_d - \frac{1}{\tau''_{qo}} \lambda_Q + \frac{1}{\tau''_{qo}} (x'_q - x_l) i_q \tag{4.3}$$

$$\sqrt{3}\dot{E}'_d = \frac{-(x_q - x'_q)(x''_q - x_l)}{\tau'_{q0}(x'_q - x_l)} i_q - \frac{\sqrt{3}}{\tau'_{q0}} \left[1 + \frac{(x_q - x'_q)(x'_q - x''_q)}{(x'_q - x_l)^2} \right] E'_d$$

$$- \frac{(x_q - x'_q)(x'_q - x''_q)}{\tau'_{q0}(x'_q - x_l)^2} \lambda_Q \tag{4.4}$$

42

$$2H\dot{\omega} = T_m - e_q''i_q/3 - e_d''i_d/3 - D\omega. \tag{4.5}$$

$$\dot{\delta} = \omega - 1 \tag{4.6}$$

The above differential equations are combined with the following algebraic equations.

$$e_q'' = \frac{x_d''-x_l}{x_d'-x_l}\sqrt{3}E_q' + \frac{x_d'-x_d''}{x_d'-x_l}\lambda_D \tag{4.7}$$

$$e_d'' = \frac{x_q''-x_l}{x_q'-x_l}\sqrt{3}E_d' - \frac{x_q'-x_q''}{x_q'-x_l}\lambda_Q \tag{4.8}$$

These equations are used in power system tools such as PSLF and PSS®E to solve transient stability analysis with the machine model coined as GENROU, which is used in this work. Parameters for GENROU are provided in Appendix A.1.1.

4.2.2. Excitation System

The effect of the excitation system on transient stability studies is vital since it plays a major role in improving the first swing by arresting the sudden acceleration (deceleration) of the machine when subjected to major disturbances. This mechanism is carried out by fast adjustment of machine internal flux and ruling out the threat of instability. Modern excitation systems can be effective in two ways. Firstly, in reducing the severity of machine swings when subjected to large impacts by reducing the magnitude of the first swing and by ensuring that the subsequent swings are smaller than the first [50]. Secondly, there are situations where various oscillation modes reinforce each other during later swings, which along with inherent weak system damping can cause transient instability. Properly compensated very fast, high response excitation system can overcome these problems and increase power transfer limit by improving its transient response. Thus, a static exciter

representing a modern fast excitation system can be used for the dynamic analysis of the network. Besides, to study the actual response of the synchronous generation, exciter should be dynamically modelled as well.

IEEE ST1 static excitation model (1980), the most commonly used exciter, is chosen for the study and its block diagram is shown in Figure 4.3. Parameters for the exciter are obtained from [51] and provided in Appendix A.1.2. The static exciter model is constructed using the EXST1 model available in the PSS®E model library.
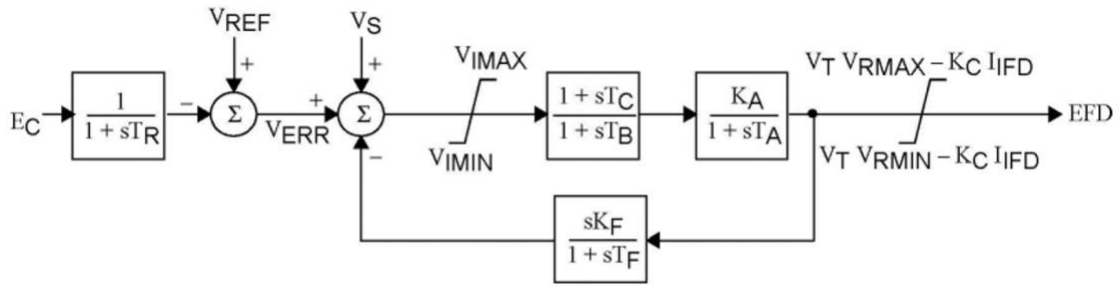
$V_S = \text{VOTHSG} + \text{VUEL} + \text{VOEL}$

Figure 4.3 Block diagram of IEEE ST1 Excitation Model (1980) [53]

ST1 is a potential-source controlled-rectifier exciter model in which excitation power is supplied through a transformer located at generator terminals or unit auxiliary bus and it is regulated by a controlled rectifier. This excitation model is capable of transient gain reduction by suitably appending time constants in the feedforward path or feedback path by proper selection of feedback loop parameters. Detailed explanation, working, design and application can be found in [50] and [51].

4.2.3. Governor Model

The governor models are designed to represent the power system response for stability studies since they actively participate in changing the mechanical power input

provided any major disturbance/demand change occurred in the system. Governors are used to arrest the frequency drop/increase and bring it back to its nominal value of 60 Hz for the power grid in the United States of America (USA) using primary and secondary frequency control. As US power grids operate with stringent frequency variation from their nominal value, the governor model is of paramount importance. Different governors such as steam (nuclear), hydro and gas turbine governors are realized using PSS®E models TGOV1, HYGOV and GGOV1 respectively. The block diagrams of TGOV1, HYGOV and GGOV1, obtained from [52], are given in Figures 4.4, 4.5 and 4.6 respectively. TGOV1 is a basic steam turbine governor model, and it represents the reheater time constant effect for a steam turbine. R is the maximum allowable speed droop and it's typically 5% for US power plants.
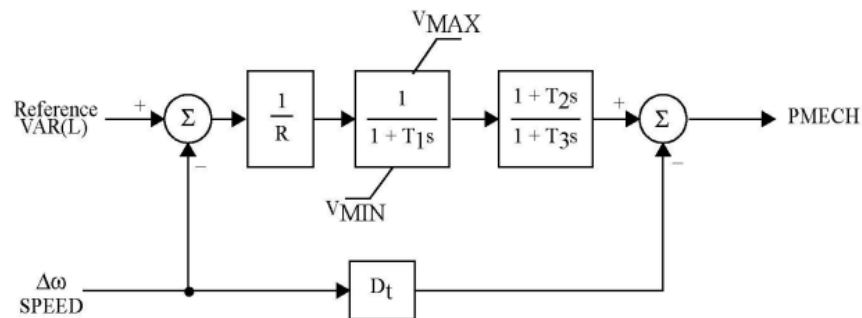
Figure 4.4 Simplified Block Diagram of TGOV1 [52]

HYGOV represents a basic hydropower plant governor model with a simple hydraulic representation of penstock with unrestricted head race and tailrace, and no surge tank. The turbine model is valid for a full range of plant operations i.e., from no load to maximum sluice gate opening. This governor model can be used to realize dashpot-type mechanical governors (e.g., Woodward, English Electric) as well as dashpot-equivalent electrohydraulic governors (e.g., ASEA). As acceleration governing (derivative action) is

45

only employed in particular scenarios in most interconnected systems, this action has not

been included in the model [52].

Figure 4.5 Block Diagram of HYGOV [52]

Figure 4.6 Block Diagram of GGOV1 [52]

GGOV1 is used to model different prime movers controlled by PID (Proportional-Integral-Derivative) controllers. For the study, this model is used to represent gas turbine governors. Various parameters of the model create the versatility of tuning its application for heavy-duty engines, single shaft combined cycle turbines, diesel engines and simple hydro turbines in dams having short water column lengths and minimal effects of water inertia. Design parameters of TGOV1, GGOV1 and HYGOV are given in Appendix A.3, A.4 and A.5 respectively.

4.3   Wind Turbine Generator Model

Type 3 also called DFIG (doubly fed induction generator) wind turbine generators are the most popular model for power generating applications and its schematic extracted from [52] is shown in Figure 4.7. In this arrangement, the stator is directly connected to the grid whereas the rotor is connected through a power electronic back-to-back converter to the grid. Through slip rings, the rotor is connected to a machine-side converter. The rotor side converter is electrically coupled to the grid side converter (GSC) through a DC link capacitor connected to the grid through a three-phase transformer. The generator speed can be controlled mechanically by operating the rotor network at variable frequencies. At super-synchronous speed, the power injected into the grid is the sum of the power available at stator terminals and the power processed by the grid side converter. At sub-synchronous speed, the net power injected by the machine into the grid is the difference between the stator power and power absorbed by GSC. No power is exchanged between the rotor and the grid at synchronous speed.

The dynamic models for type 3 WTGs are available in the Siemens PSS®E model library. The type 3 WTGs model connectivity to the grid can be depicted in Figure 4.8. A WTG consists of four components namely, generator/converter, converter control, wind turbine and pitch control models. The frequency-power response curve for WTG extracted from [52] is represented in Figure 4.9 and used in this work.
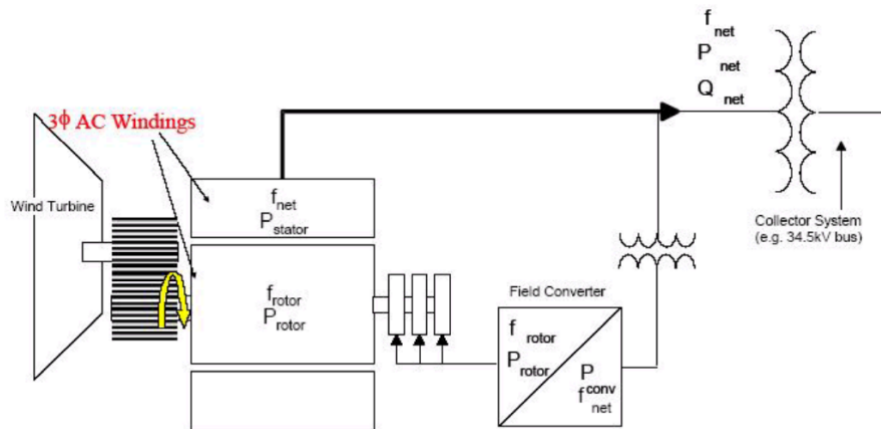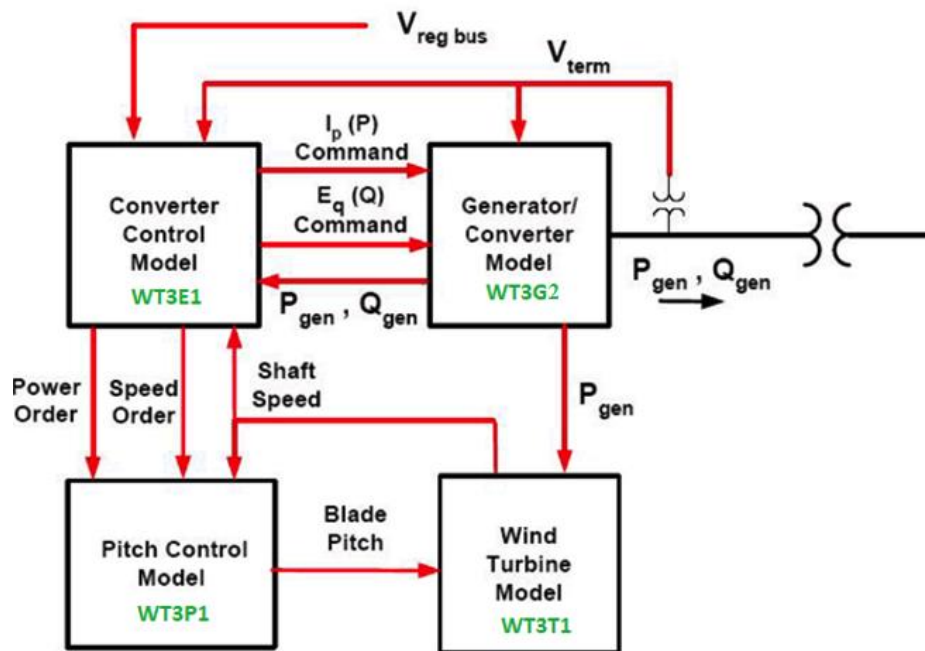

Figure 4.7 Schematic of Type 3 WTG [52]

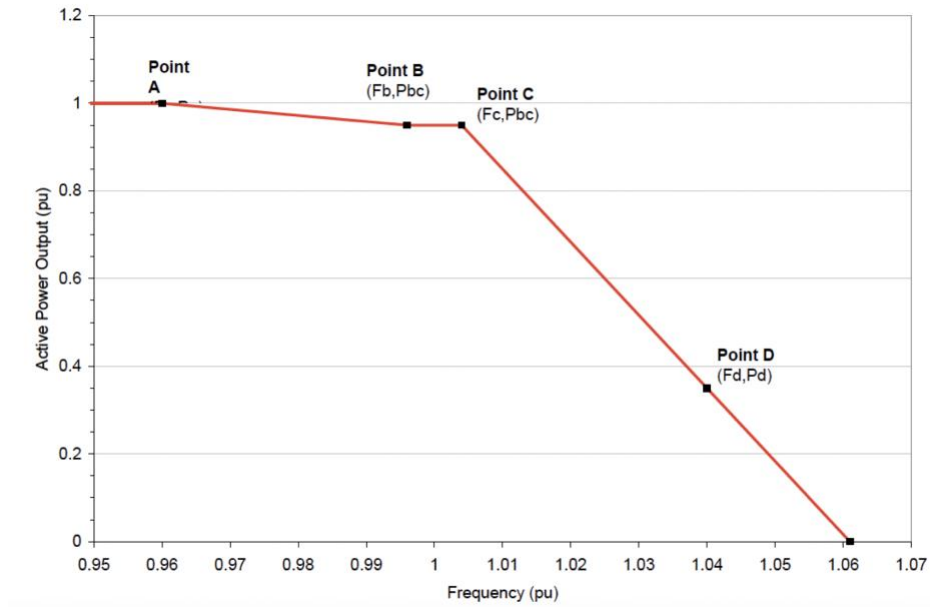Figure 4.8 GE Type 3 WTG Dynamic Model Connectivity

Figure 4.9 Frequency-Power Droop Characteristics [52]

(a)   Generator/Converter Model:

The generator/converter model obtained from [53] is shown in Figure 4.10. The power is injected by modelling the generator as a controlled current source. The model has both high voltage reactive current logic and low voltage active current logic to control active and reactive power injection based on the operator's decision of control. The model has two input signals namely WEQCMD and WIPCMD. These commands are respectively triggered based on controlling the reactive and active power injection to the grid respectively. In this work, the reactive power control (or constant power factor control) has been implemented. WT3G2 model available in the PSS®E model library has been used for the converter/generator model.

(b)   Converter Control Model:

The converter control model exhibits two types of control namely, (i) reactive power control and (ii) active power control as shown in Figure 4.11. Based on the operator's

decision, the control will be implemented. The logic for reactive power control is depicted in Figure 4.11(a).
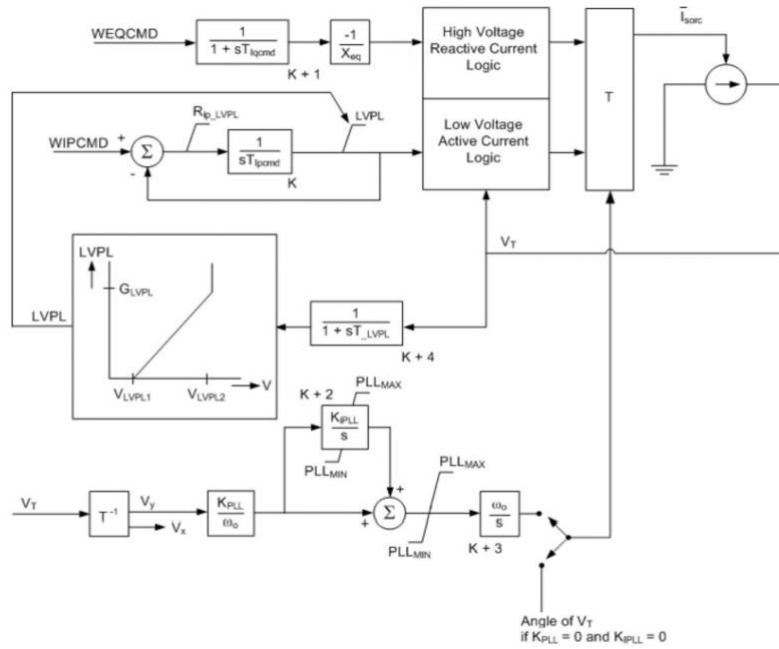

Figure 4.10 Generator/Converter Model for Type 3 WTG [53]
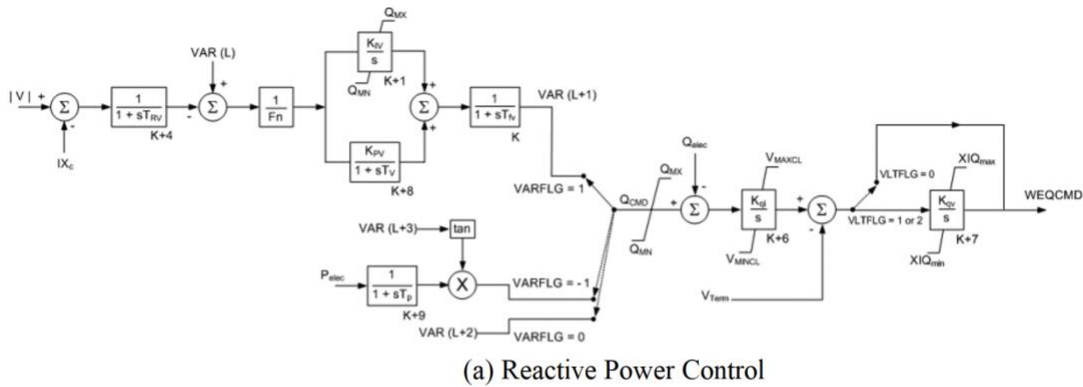
(a) Reactive Power Control
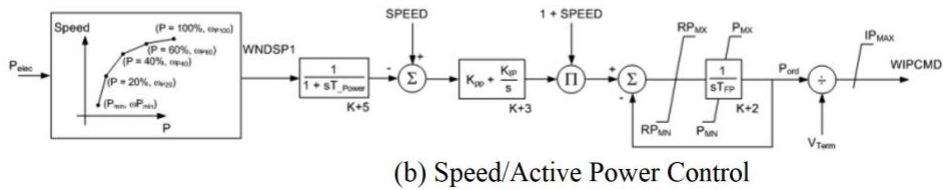
(b) Speed/Active Power Control

Figure 4.11 Converter Control Model for Type 3 WTGs [53]

Three modes of reactive power control include constant Q, constant power factor and constant voltage, which can be decided based on proper parameter settings. Similarly, the active power (torque) control, shown in Figure 4.11(b), implements maximum power point tracking from the WTG and injects the same to the grid. Selecting this mode of control makes the turbine operate at a rated speed corresponding to rated wind power for different wind velocities. In this work, reactive power control is selected. The Siemens PSS®E model used for the converter control is WT3E1.
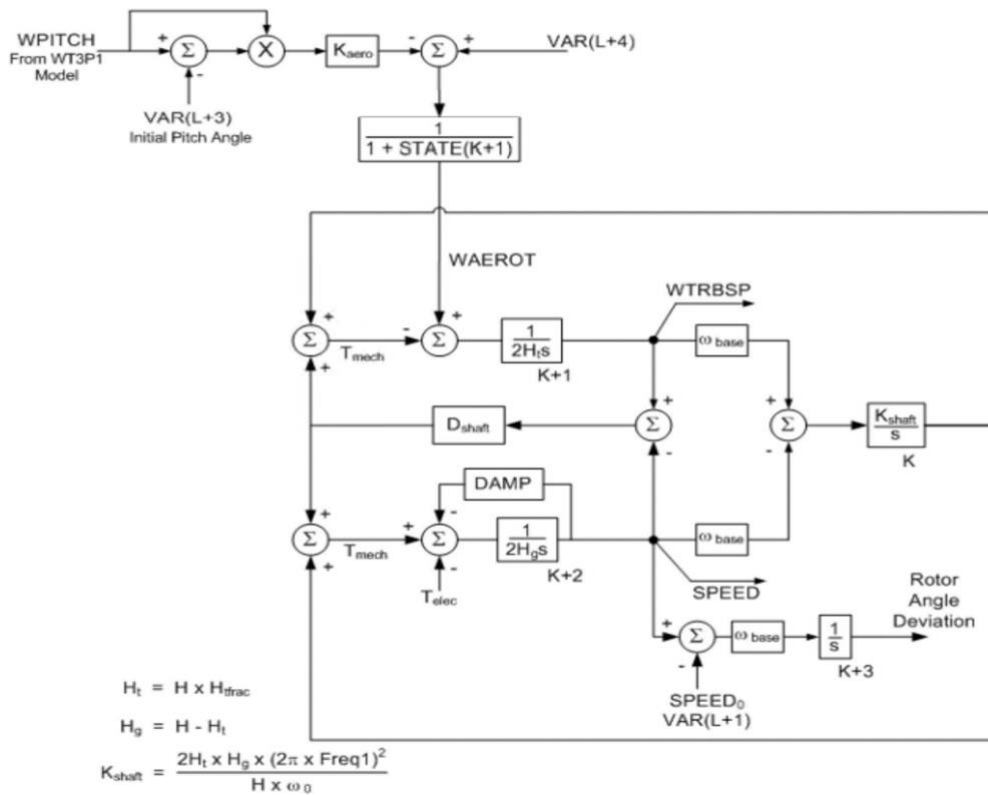
Figure 4.12 Mechanical System Model for Type 3 Wind Generator [53]

51

(c)   Wind Turbine and Pitch Control Model:

The drivetrain or wind turbine model for the type 3 WTG is depicted in Figure 4.12. The model has two options such as one-mass and two-mass models. In this work, the one-mass model has been used. WT3T1, available in the PSS®E library, has been used for dynamic modelling of the type 3 WTG. The pitch control model for type 3 WTG (WT3P1) available in the PSS®E library is shown in Figure 4.13. The parameters for the type 3 WTG model have been provided in Appendix A.1.4.

Figure 4.13 Pitch Control Model for Type 3 Wind Generator [53]

4.4   Protection Components Model

Relays are used for diverse purposes such as regulation, monitoring, synchronization, and protection. Modelling protection relays is critical for power system analysis, operation and planning.
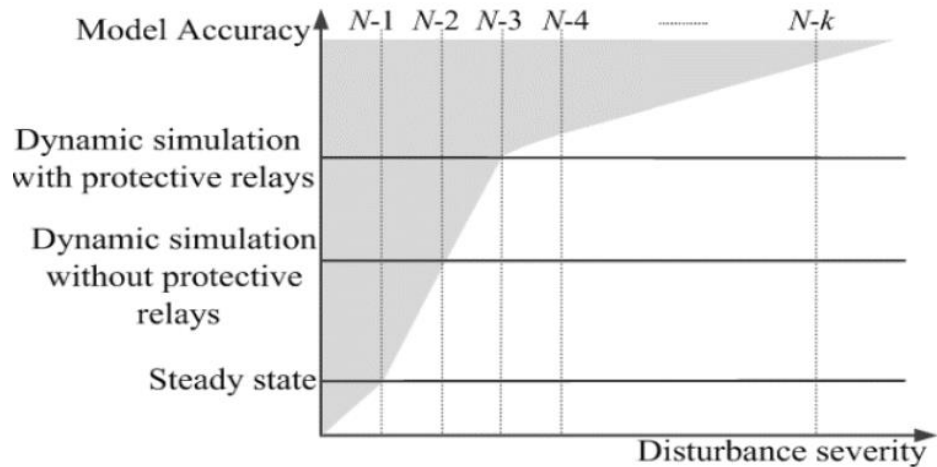
Figure 4.14 Conceptual Description of the Analysis Required for Studying Varying Catastrophic events

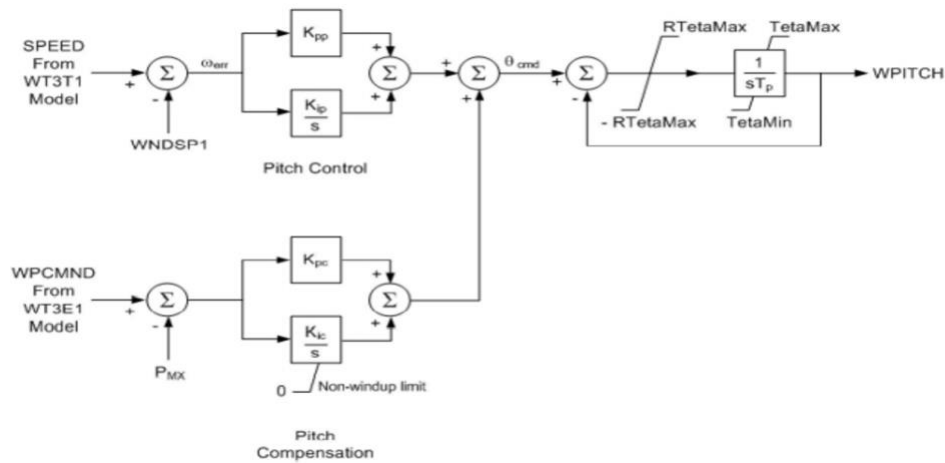The primary objective of the power system is to provide reliable customer service and to minimize the extent and time of outages when serious/intolerable events occurred. Protective relays operate under such conditions to arrest the instability spread. Thus, relays are required to model for dynamic security assessments. Moreover, with an increase in contingencies/outages severity, the system model accuracy can be improved by implementing a protection model in the networks as shown in Figure 4.14. This sub-section briefs the modelling of distance, load and generator relays for power system infrastructure and operational protection.

4.4.1. Distance Relay Model

Distance relay is used for the protection of transmission lines against carrying excessive electric current greater than its rating which can be caused because of faults and short circuit conditions. The electrical distance between the relay and the fault location is measured by a distance relay. These relays respond to voltage, current, and voltage-current angles. These values can be calculated using relay impedance, which is proportional to the

53

fault distance. Typically, these relays are programmed to trip whenever a fault occurs within a fractional distance 'h' of the relay point as shown in Figure 4.15. This fraction is known as the "reach setting," which indicates that if a fault develops in this section of the line, the relay will trip immediately. If the fault is beyond this reach point, the relays will trip with a programmed time delay. If a fault occurs at the reach point, the impedance measured at relay A is

$$Z_R = \frac{V_1}{I_L} = hZ_L \qquad (4.9)$$
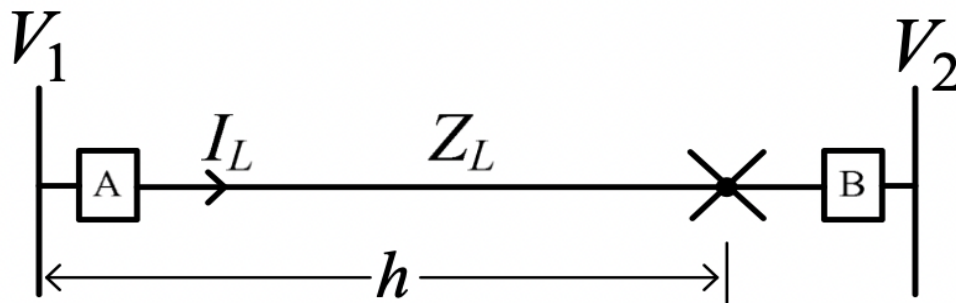
Figure 4.15 Reach Setting of Distance Relay [54]

Commercial relays have three zones of protection namely zone 1, zone 2 and zone 3 as shown in Figure 4.15. There are three different types of relays namely, impedance relay, mho relay and admittance relay. Mho relay being more popular and inherently directional is used in this work and its relay characteristics are depicted in Figure 4.16. Different zones of protection of distance relay operation are pictorially depicted in Figure 4.17 [50]. The reach point and time delay for relay operation for three zones are tabulated in Table 4.2 [50]. The distance relay available in the PSS®E model library used for the study is DISTR1.
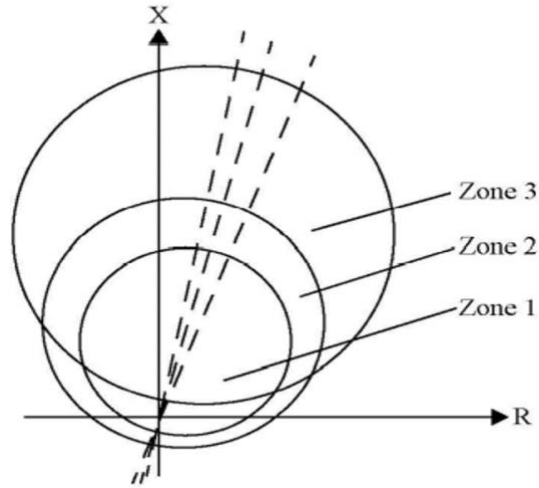
Figure 4.16 Mho Distance Relay Characteristics [53]
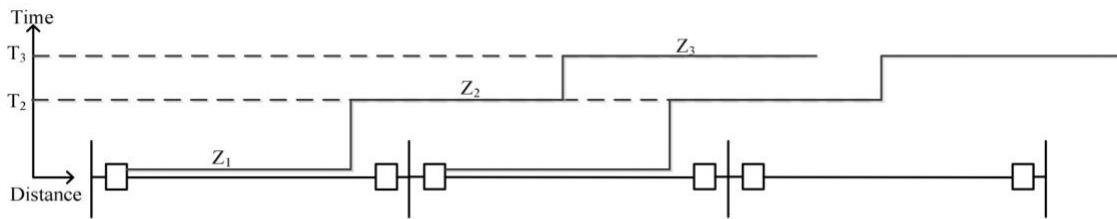
Figure 4.17 Zones of Protection for Distance Relay [50]

Table 4.2 Distance Relay Parameters [50]

Zones	Reach point	Time delay
1	80%-90%	0 s
2	At least 120%	0.25 s
3 (backup zone)	At least 220 %	1-2 s

4.4.2. Under-Voltage/Frequency Load Relay

Modelling load shedding relays in the power system help in maintaining the generation-load balance by avoiding frequency instability and voltage collapse at certain

regions of the network. Under-frequency load shedding (UFLS) helps in maintaining system frequency to operate at (near to) nominal frequency (60 Hz). Since the turbine-governor cannot perform corrective actions at low frequency (< 58.5 Hz), it is of ultimate importance to maintain the frequency (and generation-load balance) by shedding excess bus loads. This protection scheme helps in arresting frequency drop by shedding a certain percentage of bus loads at different stages of frequency. Note the relay trips of the entire bus load if the frequency hits the lowest threshold according to NERC reliability standards. The parameter setting for the UFLS scheme is shown in Table 4.3.

Table 4.3 UFLS Scheme Attributes [55]

UFLS Stage	Frequency Threshold (Hz)	Minimum Relay Time Delay (s)	Breaker Delay (s)	Load Shed (pu)	Cumulative Load shed (pu)
1	59.5	0.05	0.02	0.1	0.1
2	59.2	0.05	0.02	0.2	0.3
3	58.8	0.05	0.02	0.2	0.5

Table 4.3 represents the UFLS setting attributes for Eastern Interconnection distribution providers and transmission owners with 100 MW or more peak net load according to NERC reliability standard [55]. Voltage collapse in power systems is becoming a frequently occurring phenomenon in diverse parts of the world due to large deficits in spinning reserves and reactive power generation, reactive demand spikes and single-phase air-conditioners stalling and so on. This voltage decrement in that particular region can potentially create cascading blackouts in a few minutes to hours following the disturbance occurrence. Under-voltage load shedding (UVLS) can act as a protection

model, which performs load shedding at buses where voltage dip is severe, and its recovery is time-consuming. It ensures the required percent of load shedding is performed such that the voltage is recovered back to its minimum (or greater than the minimum) operating limit. WSCC group has developed the standard by performing Q-V and P-V analyses and validated the same by confirming the results with each other. Moreover, the group has also carried out fast dynamic simulations, long time dynamic simulations, security constrained OPF and various tools for insights regarding voltage stability and collapse phenomena [56]. UVLS parameter settings are obtained from the standard and shown in Table 4.4.

Table 4.4 UVLS Scheme Attributes [55]

UVLS Stage	Voltage Threshold (Hz)	Relay Time Delay (s)	Breaker Delay (s)	Load Shed (pu)	Cumulative Load shed (pu)
1	0.95	0.75	0.05	0.3	0.3
2	0.85	1.00	0.05	0.5	0.8

Under-voltage/frequency load shedding (UVFLS) relay model is realized using PSS®E user-defined model UVUFBLU1.

4.4.3. Under/Over-Voltage Generator Relay

Various reasons such as loss of load, defective voltage regulator, manual human errors and speed acceleration can cause generator voltage to increase beyond the continuous maximum operation limit. This increased voltage at generator terminals can cause insulation breakdown and can cause damage to the machine itself. Generators can continuously operate at a maximum threshold of 1.05 pu. If the machine terminal voltage

is prevailing at (or greater than) 1.15 pu. for more than 0.5 seconds, then the machine must be tripped offline according to the NERC reliability rules and regulations [57].

Similarly, the under-voltage operation of the machine can be caused due to local/remote incremental load, loss of generation and deceleration which can lead to voltage collapse affecting the system stability. Thus, the generators are designed to operate at a lower threshold of 0.95 pu. of base voltage. Machines are tripped offline if the operating voltages are at 0.90 pu. of rated voltage for a period of 4 seconds and more (Figure 4.18). These relays are realized using the model NRCGP3U available in the PSS®E model library. The relay parameter settings are shown in Table 4.5.
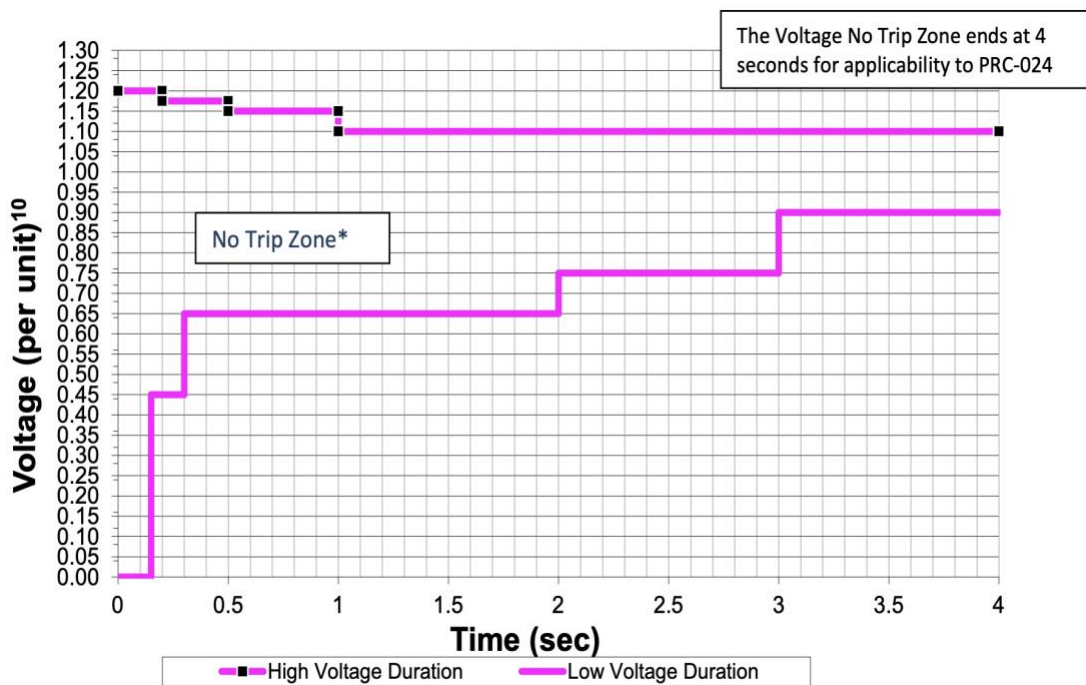

Figure 4.18 Voltage Protection Settings for Western Interconnection [57]

Table 4.5 UOVGT Parameters [57]

High Voltage Standard		Low Voltage Standard	
Voltage (pu)	Minimum Time(s)	Voltage (pu)	Minimum Time(s)
≥ 1.200	0.00	< 0.45	0.15
≥ 1.175	0.20	< 0.65	0.30
≥ 1.150	0.50	< 0.75	2.00
≥ 1.100	1.00	< 0.90	3.00
< 1.100	4.00	≥ 0.90	4.00

4.4.4. Under/Over-Frequency Generator Relay (UOFGT)

Under-frequency generator trip (UFGT) actions are triggered due to the generator operating around 0.90 to 0.96 pu. of nominal frequency, which can be due to load spikes. Due to sudden load increment, the kinetic energy stored in the rotating mass is used for generating excess current by decelerating itself. Due to the deceleration, the frequency drops, which should be taken care of by turbine-governor actions to arrest the frequency drop. However, UFGT comes into play if the drop is intolerable and cannot be handled by the governor's actions (Table 4.6).

Over-frequency generation can occur if there is an excess generation in the system and to maintain generation-load balance, synchronous machines are tripped. In general, to avoid any damage to synchronous machines, they are tripped offline beyond (at) minimum and maximum frequency threshold. NERC reliability standard for under/over-frequency

generator tripping schemes for the Eastern Interconnection system, obtained from [57], is depicted in Figure 4.19.

Table 4.6 UOFGT Parameters [57]

High Frequency Standard		Low Frequency Standard	
Frequency (Hz)	Minimum Time (s)	Frequency (Hz)	Minimum Time (s)
≥ 61.7	Instantaneous trip	≤ 57.0	Instantaneous trip
≥ 61.6	30	≤ 57.3	0.75
≥ 60.6	180	≤ 57.8	7.5
< 60.6	Continuous operation	≤ 58.4	30
		≤ 59.4	180
		>59.4	Continuous operation
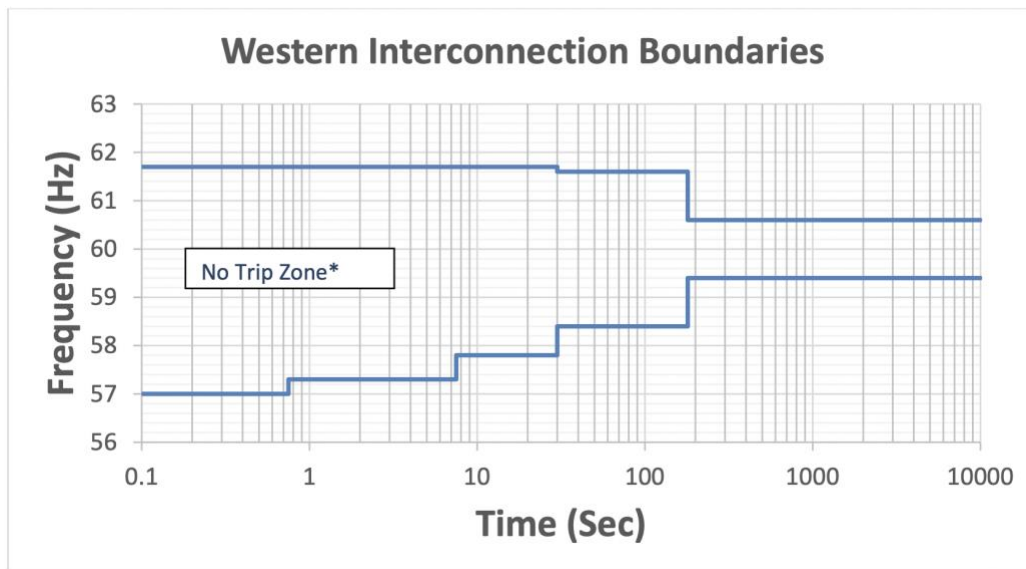
Figure 4.19 Design Performance and Modelling Curves for Under/Over Frequency Generation Tripping [57].

Figure 4.19 represents the minimum and maximum frequency threshold generator trip values for different time periods. The minimum and maximum values can be set at 57.3 Hz and 61.6 Hz respectively. Generator operations at (and below) these values are automatically tripped offline without any delay. NRCGP3U model is used for realizing the UOFGT relay model in PSS®E.

4.5   Summary

In this chapter, the test system description and modification of conventional RTS network by incorporating 20% wind penetration based on 2/3decommitment-1/3redispatch rule have been discussed. Furthermore, the WECC approved dynamic models of synchronous generators, exciters, governors, DFIG based wind power plants and protection models are discussed.

CHAPTER 5

RESULT ANALYSIS AND DISCUSSIONS

Resilience evaluation results based on Monte-Carlo simulations (MCS) have been focused to discuss in this chapter. The generation of diverse outage scenarios for different hurricane categories is discussed and the corresponding MCS based resilience evaluation approach is tested on the power system model described in Chapter 4. The steady-state and aggregated results are obtained for different scenarios using the power system tool Siemens PSS®E and probabilistic metrics are evaluated. Python 2.7 has been employed to automate and perform resilience evaluation.

5.1   Scenario Assumption

Following are the assumptions considered throughout the period of the simulation study.

(i)   The resilience study is carried out for a power system against a hurricane affecting only area 1. The event initiates at $t = 51$ and prolongs for a period of 25 hours.

(ii)   The simulation is carried out for 400 hours assuming the availability of the labour force after the hurricane event. The simulation hours can extend up to a period of 600 to 750 hours based on the storm intensity level.

(iii)   The study is carried out only for transmission level and the bus loads are modelled as lumped constant power load model. The corresponding base hourly bus loads are scheduled based on the active and reactive power demand during the winter season on weekdays/weekends.

(iv)   The fragility model of the transmission networks is designed assuming that the 138 kV and 230 kV systems as normal (less robust) and more robust corridors, respectively.

(v)   Any outages that happened in the system during the event progression are not recovered back during the next simulation hour within the event period for steady-state analysis. However, the assets lost during transient stability analysis are regained back within the next 20 minutes despite this recovery might take an even longer period in real-time scenarios. During event progression, the long-term thermal rating (24-hour rating) and short-term thermal rating (15-min rating) for the branches are considered for steady-state and dynamic analyses, respectively.

5.2   Deterministic Approach

A deterministic model assumes certainty in all aspects. In this approach, the study is carried out for a determined load schedule and winter wind profile. This approach solves for one hurricane scenario and does not include power system uncertainty in the model. The deterministic approach that has been followed in this study to define and evaluate the resilience metrics is depicted in Figure 5.1. The process involves conducting steady-state and dynamic analysis of the system at each hour of event propagation to calculate the resilience metrics. Transient stability analysis with modelling protection schemes—including distance relays, under frequency load/generator shedding, and under voltage load/generator shedding schemes—as well corrective actions are carried out at each hour of the event period. The transient stability studies evaluate system dynamic stability and identify the lines that may be tripped (due to overload conditions or unstable power swings)

and the loads/generators that are shed during that period. The results of transient stability (including line tripping and generator/load shedding) are utilized to make the related updates in the steady-state system topology at every time step. A steady-state analysis of the updated system involving AC optimal power flow (ACOPF) is performed with minimization of the bus load adjustment (amount of shed load) as the objective function.
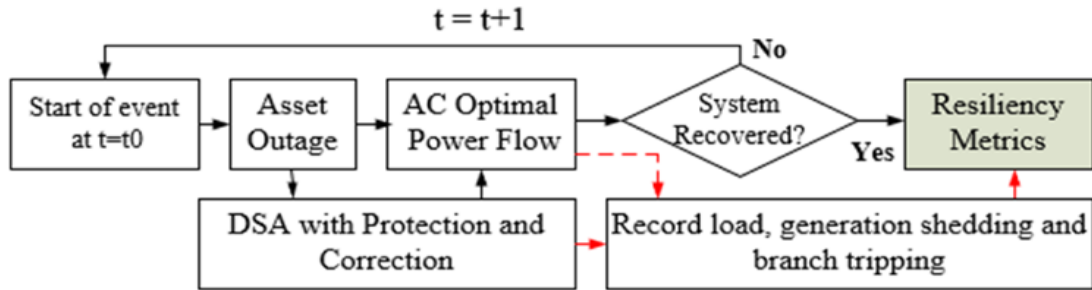

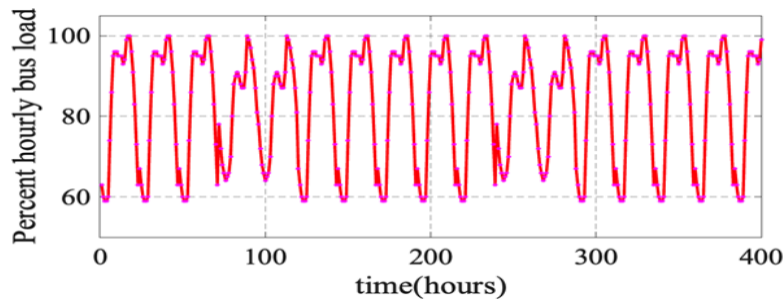Figure 5.1 Deterministic Approach to Evaluate Resilience Metrics
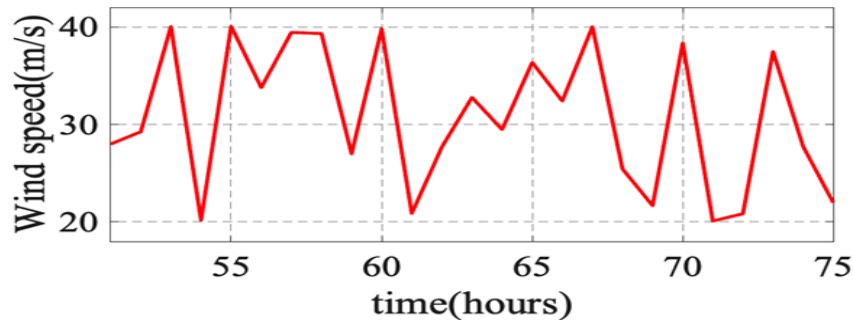

Figure 5.2 Winter load profile

Figure 5.3 Wind speed profile

The hourly load profile and wind speed variation during the event progression are depicted in Figures 5.2 and 5.3, respectively. The fragility model representing transmission

line/tower failure probability with respect to different wind speeds for less robust and more robust systems is extracted from [11] and is shown in Figure 3.3.

5.2.1. Steady-State Results

AC optimal power flow module of PSS®E is used for steady-state analysis to minimize the load shedding at each bus. The steady-state infrastructure and operational resilience indicators based on the availability of generators, served bus loads, and connected transmission lines are plotted in Figures 5.4, 5.5, and 5.6 respectively.
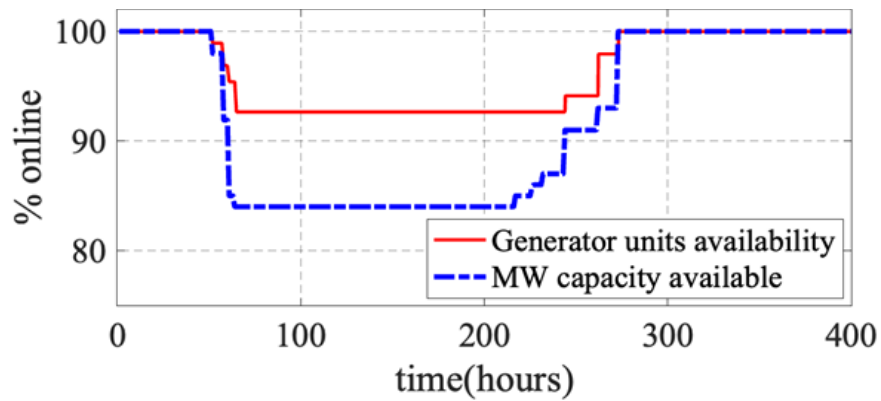

Figure 5.4 Hourly generator units and active power capacity availability
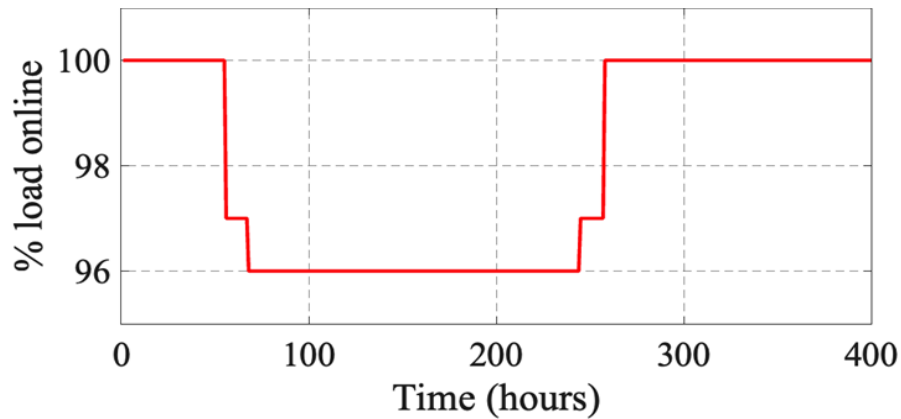

Figure 5.5 Percentage of load connected

There are 99 generation units in the test case, and during the event progression, a total of 15 units become offline because of bus islanding due to line outages, decreasing the available generation capacity from 14,550 MW to 13,530 MW at the end of the event.

65

As a result of the isolation of load buses due to the hurricane effect, approximately 4% of the load is shed.
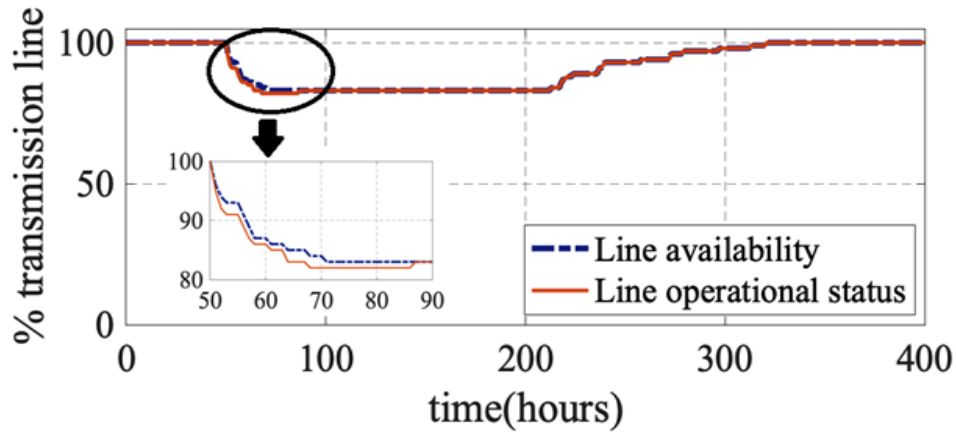
Figure 5.6 Percentage of transmission line connection/availability status

Table 5.1 Steady-State Resilience Metrics

Metrics	Generator		Branch		Load
	IR	OR	IR	OR	OR
D_r (%/hr)	-0.667	-0.306	-0.75	-0.71	-0.167
$\mathfrak{R}_r$ (%/hr)	0.301	0.023	0.077	0.148	0.307
τ_r (hr)	47	47	234	108	13
Λ_t (pu)	0.952	0.994	0.918	0.92	0.981

In Figure 5.6, there are two curves representing the operational statuses of the transmission lines (solid line) and the infrastructure availability of the transmission lines (dashed line). The dashed line represents the number of transmission lines that were not damaged by the hurricane whereas the solid line represents the operational status of all transmission lines. A transmission branch becomes operationally unavailable due to bus islanding or complete damage because of the event. However, the line is infrastructurally

66

available if not damaged by the event. The recovery time for the towers and lines that are damaged depends on their mean time to repair rates obtained from the IEEE RTS data [47].

The curves in Figure 5.6 match the modified trapezoid model discussed in Chapter 2. The resilience metrics provided in Chapter 2 for the generation units, loads, and transmission corridors are calculated and are provided in Table 5.1. In Table 5.1, IR and OR refer to infrastructure resilience and operational resilience, respectively.

5.2.2. Aggregated Results

Aggregated results include the steady-state and dynamic analysis results. Transient stability analysis based on rotor angle stability is carried out for a time period of 15 seconds. The branch rating is set to STE (15-min emergency rating). The branch status is updated (disturbance is introduced) 1 second after the study initiation time. The step size for the simulation is 0.0083 s (which is half of the 60 Hz cycle period). The dynamic performance of the system in terms of transient load shedding and generator shedding around the corresponding simulation hour is plotted in Figures 5.7 and 5.8 respectively.
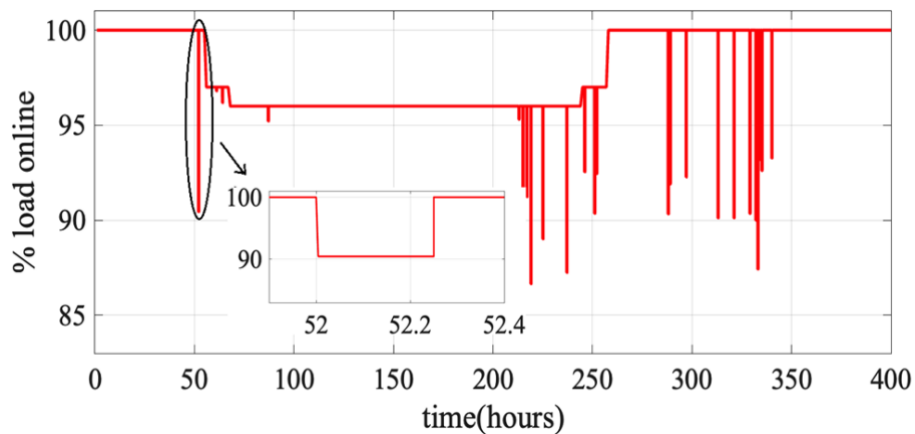
Figure 5.7 Percentage load online-aggregated model

Both the generator and load curves have dips at certain hours during the simulation. These dips in the curves are due to the transient generator and load shedding which can be recovered after a period of 20 minutes based on the above assumption. Figures 5.7 and 5.8 represent the aggregated results and reveal the actual number of generators and loads that become offline during the event.
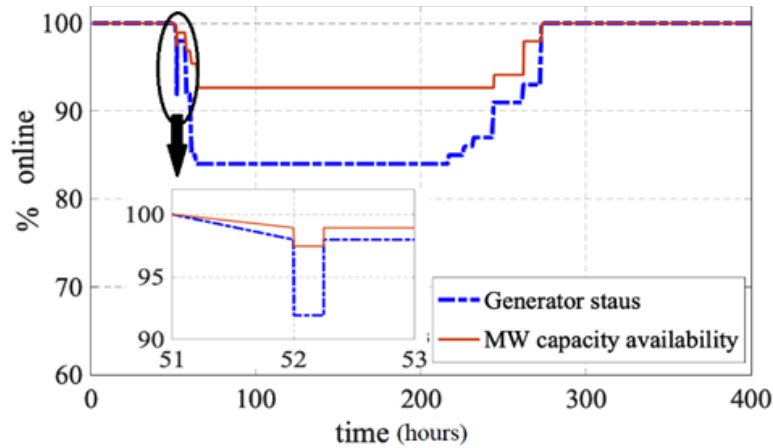
Figure 5.8 Percentage generators and active power capacity availability-aggregated model
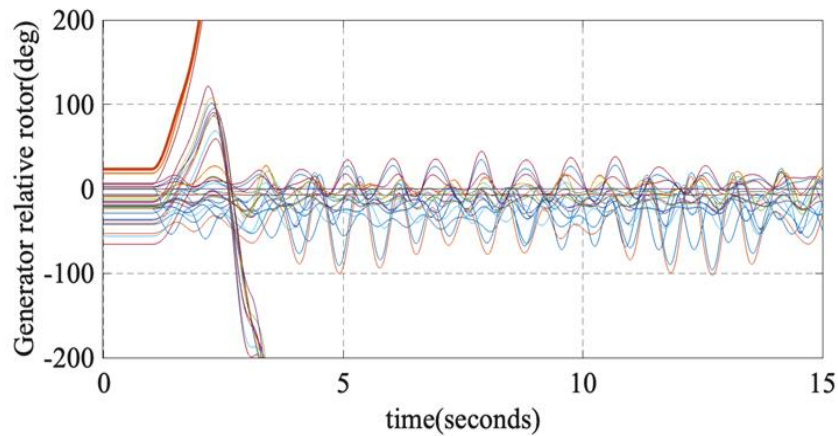
Figure 5.9 Relative rotor angle of machines at hour 52 without corrective action

It is observed that a load drop of 83.6% occurs at simulation hour of 237 because of reconnecting generator bus 122. These dips in the generator and load curves (generator/load shedding) are not observed in the steady-state analysis. Thus, the steady-state analysis alone

is not sufficient for having a realistic assessment of the system resilience since the system

stability and the dynamic response of the system are important to monitor. The following

paragraphs brief the importance of dynamic analysis after a major disturbance by providing

an instance where an intense outage happened causing system instability during the study.

Figure 5.10 Relative rotor angle of machines at hour 52 with corrective action

Figure 5.11 Percentage of the generators online in the two cases of with and without implementing protective actions

During transient stability studies, the stability of the system is evaluated by monitoring the relative rotor angles, voltages and bus frequency of the connected machines. One such instance during the simulated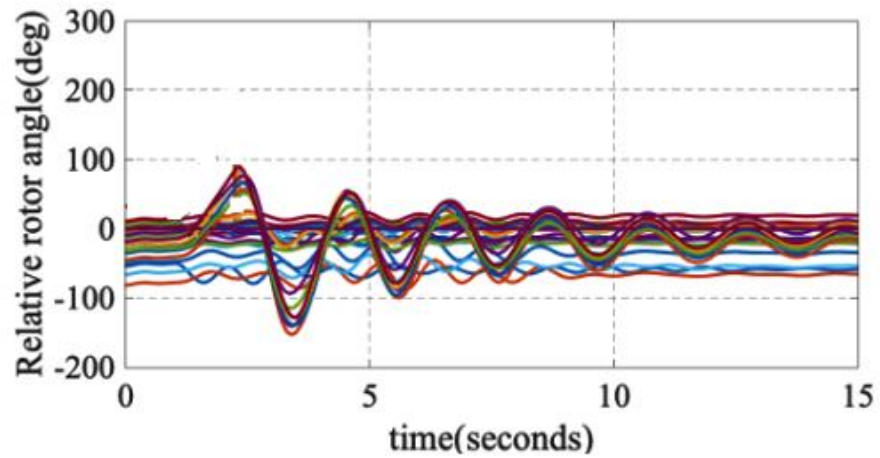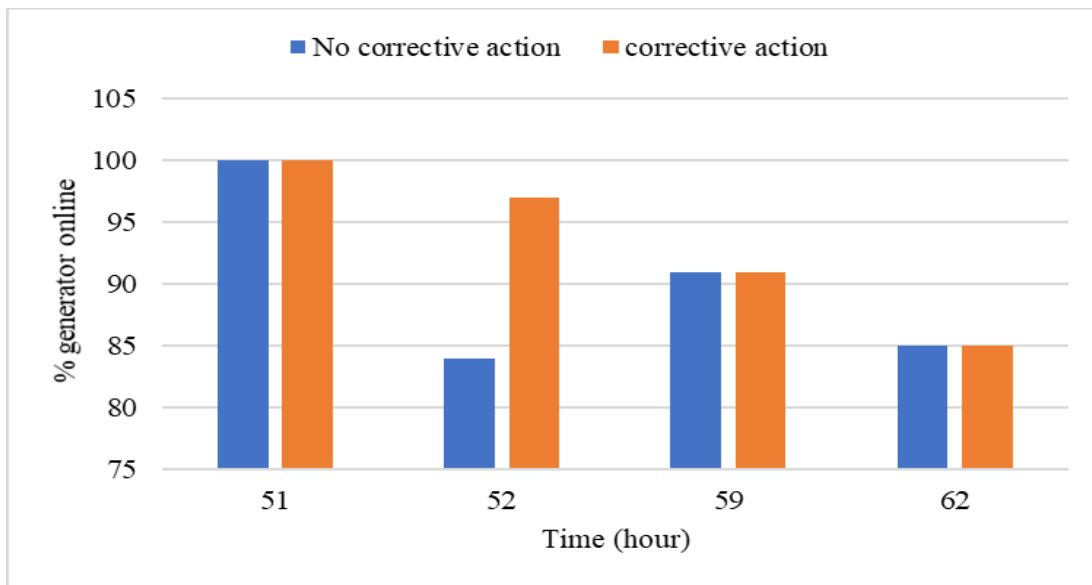 event that can jeopardize system stability occurred at hour 52. If proper corrective actions have not been taken within the effective time, the tripping of the line between Arnold 230 kV and Aston 230 kV buses at hour 52 can jeopardize system stability. Due to the hurricane effect at hour 52, the transmission line between buses 114 and 117 is damaged. Due to this tripping action, the machines at bus 122 started losing synchronism and this action of losing synchronism is observed at generators connected to buses 114, 115, 116, and 123 in area 1. Because of unstable power swings at generator buses 325 and 223, the two tie branches 325-121 and 318-223 are tripped by distance relay operation causing line overloading. It is also further observed that almost all machines located in area 2 and area 3 lost their synchronism at this hour.

The relative rotor angles of the generators at hour 52 are shown in Figure 5.9. Actions such as generators tripping at bus 122 by out-of-step relay can prevent system instability in this case. This action makes the system stable and prevented distance relay misoperation and the consequent tripping of the tie lines. The relative rotor angles of the generators after applying the corrective actions are shown in Figure 5.10. As can be seen in this figure, no generator loses its synchronism with respect to the rest of the system.

The generator shedding with and without corrective actions at hour 52 is compared in Figure 5.11. As can be seen, with corrective actions being implemented at hour 52, the percentage of the generators remaining online increased substantially. Similarly, the load shedding can be compared for the mentioned cases. At hour 52, the load shedding has

reduced from 94.5% to 8.1% by implementing the corrective actions, which shows that the remedial actions prevent the system from collapsing and losing all its load. The system resilience metrics based on the aggregated results of the system are computed and tabulated in Table 5.2. In Table 5.2, IR and OR refer to infrastructure resilience and operational resilience respectively.

Table 5.2 Aggregated Resilience Metrics

Metrics	Generator		Branch		Load
	IR	OR	IR	OR	OR
D_r (%/hr)	-0.667	-0.306	-0.75	-0.71	-0.16
$\mathfrak{R}_r$ (%/hr)	0.301	0.023	0.077	0.148	0.021
τ_r (hr)	47	47	234	108	187
Λ_t (pu)	0.918	0.96	0.918	0.92	0.976

Comparing the disruption, recovery rate, and area under the curve metrics of the aggregate results, it is observed that their values are less than that in the steady-state studies since steady-state studies do not consider system instability, transient load/generator shedding, and line tripping. The existing steady-state (trapezoid) resilience model is not sufficient for analysing system resilience as it neglects dynamic stability, transient load shedding and transmission line tripping. These issues are addressed in dynamic studies and specific corrective actions are implemented to make the system operate in stable condition. Besides, the multiple stages of recovery can be visualized in the aggregated trapezoid model, which cannot be observed in the conventional trapezoid model.

5.3   Stochastic Approach

The deterministic approach does not include uncertainty and stochasticity in the resilience studies. [11] carries out resilience evaluation based on a steady-state deterministic approach. However, the modern power system is a stochastic network and highly uncertain to predict its response. In order to encounter the gap between the deterministic approach and real-time analysis, stochasticity is incorporated in this work by following a probabilistic approach as briefly discussed below.

The stochastic analysis incorporates the stochastic nature of hurricane speeds, system assets and power system loads. The hurricane model contains three categories as mentioned in Chapter 3. The outage scenarios have been generated based on the Monte Carlo simulations considering wind uncertainty and component states. The stochastic nature of the line outage depends on the failure probability curve as a function of wind speed mentioned in Chapter 3.

For the case of stochastic load representation, the mathematical equation (3.2) provided in Chapter 3 has been utilized. The load variability due to high EV penetration causing a steep increase/decrease in the load curve has been used in this work. The following situations are considered for generating outage scenarios:

(i)   Fuel interruption: Due to extreme cold, wells and pipes stopped delivering fuel to natural gas power plants. Coal plants and nuclear plants are knocked offline as well [1].

(ii)   Wind turbine blades are frozen during winter storms as in the Texas outage [1].

(iii)   Wind turbines are prone to permanent damage at high wind speeds [58].

(iv)   Line overload/fault/complete damage (trip) due to storms (insulation failure).

(v)   Incorrect action of tie-line (or sensitive branch) trip by the operator due to incorrect state estimation.

(vi)   Insulation flashover/failure due to impurities (caused by sandstorm, windstorm), damage and heating (caused by the hurricane, winter storm, or wildfire) – must consider the age of the insulator as well as how fast the breakdown occurs.

It is assumed that the available conventional generators can support part of net load variation based on the wind uncertainty during pre and post-hurricane conditions based on the generator ramping capability.

Figure 5.12 represents the probabilistic approach for evaluating power system resilience against different categories of hurricanes. Each outage scenario is generated based on the MCS approach and if there are disturbances or outages sensed, a transient stability study is performed for a period of 15 seconds. The system stability is ensured at the end of each DSA (dynamic security assessment) time step, and system convergence tolerance is met by performing ACOPF. If the convergence has not met its requirements, the system is checked for any island. By isolating the islands, ACOPF has been evaluated again to avoid any steady-state violations. Different trials are performed for each hurricane category. At the end of each scenario, resilience metrics are estimated. For every hurricane category, probabilistic metrics are evaluated.
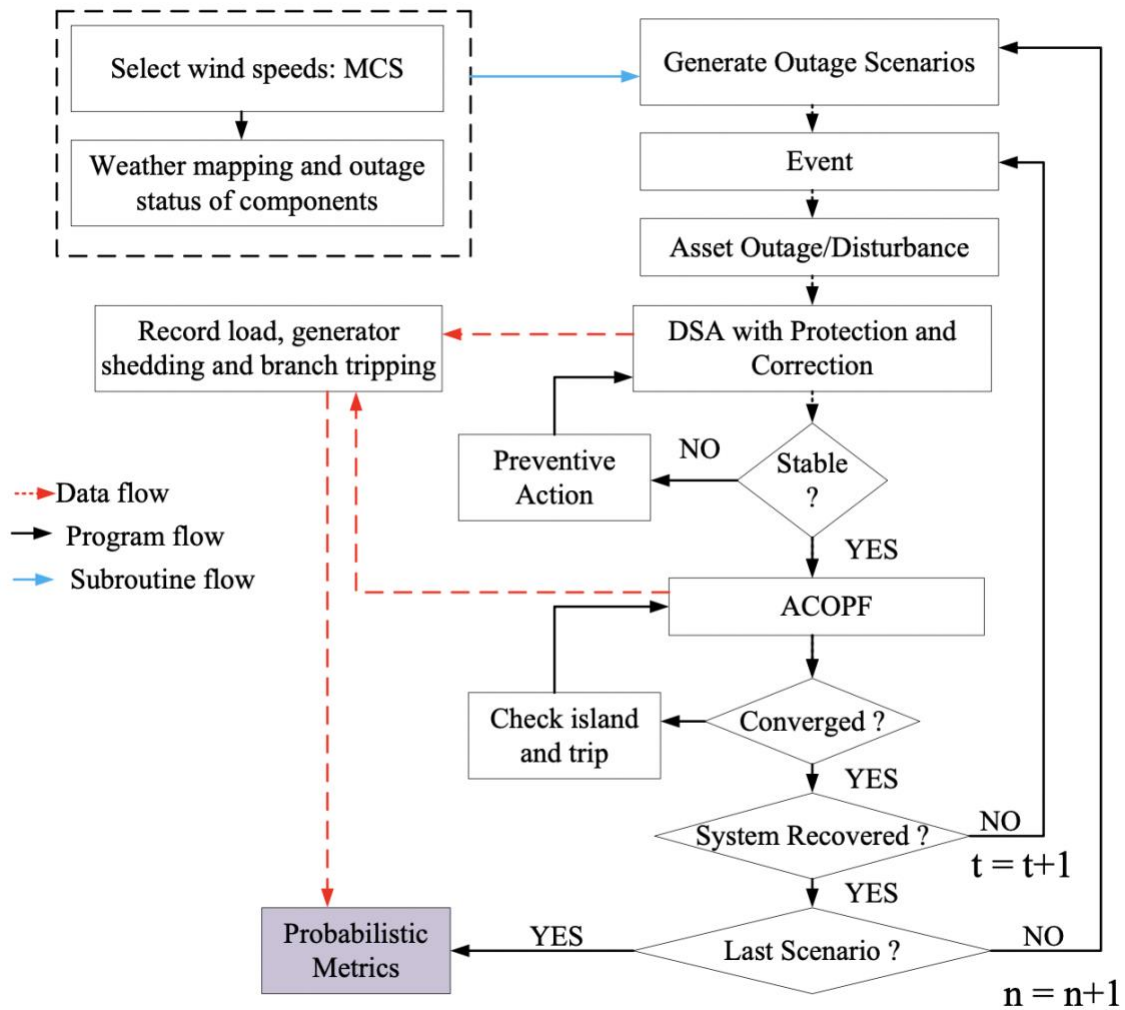
Figure 5.12 Probabilistic Approach for Resilience Evaluation

5.3.1 Steady-State Results

Using the MCS-based stochastic approach, the optimal power flow has been solved to estimate steady-state resilience metrics. The steady-state resilience evaluation with sudden peaks and dips in hourly net load and component loss for different categories of hurricanes has been evaluated and quantified in terms of the resilience indices. Table 5.3 represents the resilience indices estimated based on the probabilistic approach discussed in Chapter 3.

Table 5.3 Steady-State Resilience Indices

Metric	Category 1	Category 2	Category 3
$\Lambda_p^{(O)}$	0.9912	0.9803	0.9542
$\Lambda_p^{(I)}$	0.9968	0.9528	0.9239

Three classes such as 1, 2 and 3 indicate the resilience evaluation against the hurricane categories 1, 2 and 3 and their corresponding resilience metrics have been plotted as shown in Figures 5.13-5.20. Figure 5.13 represents the number of offline transmission lines for the three classes. Each class consist of 50 scenarios.
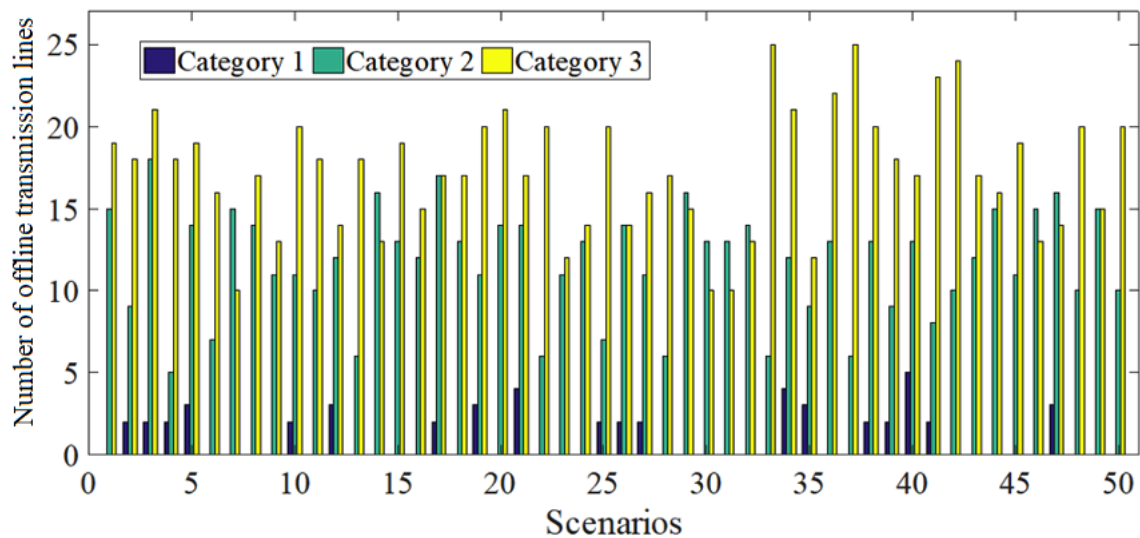
Figure 5.13 Offline Transmission Corridors Record for Different Hurricane Categories

The disruption and recovery rates of the power system components (transmission line and generator) for the three different classes are depicted in Figures 5.14 and 5.15 respectively. The recovery time required for each component regain back to its original operational state is determined for different scenarios and for hurricane categories as depicted in Figure 5.16.
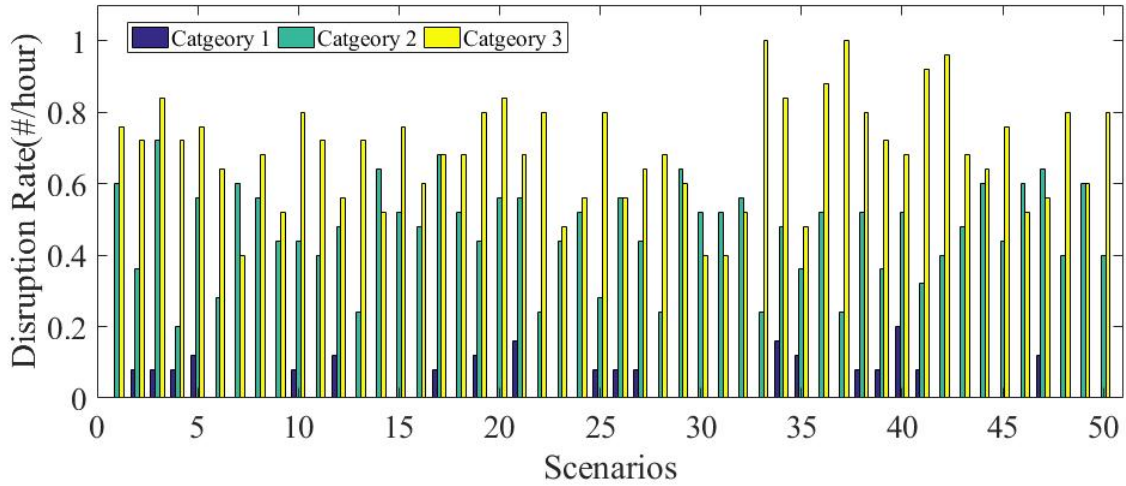
Figure 5.14 Component Disruption Rate for Different Hurricane Scenarios

Figure 5.15 Recovery Rate of Components for Different Hurricane Scenarios

From Figure 5.13, the minimum and the maximum number of transmission lines gone offline for three hurricane categories are tabulated in Table 5.4. The peak and least values of the component's disruption rate and recovery time for different hurricane categories are tabulated in Table 5.5.

Figure 5.16 Component Recovery Time for Different Hurricane Scenarios
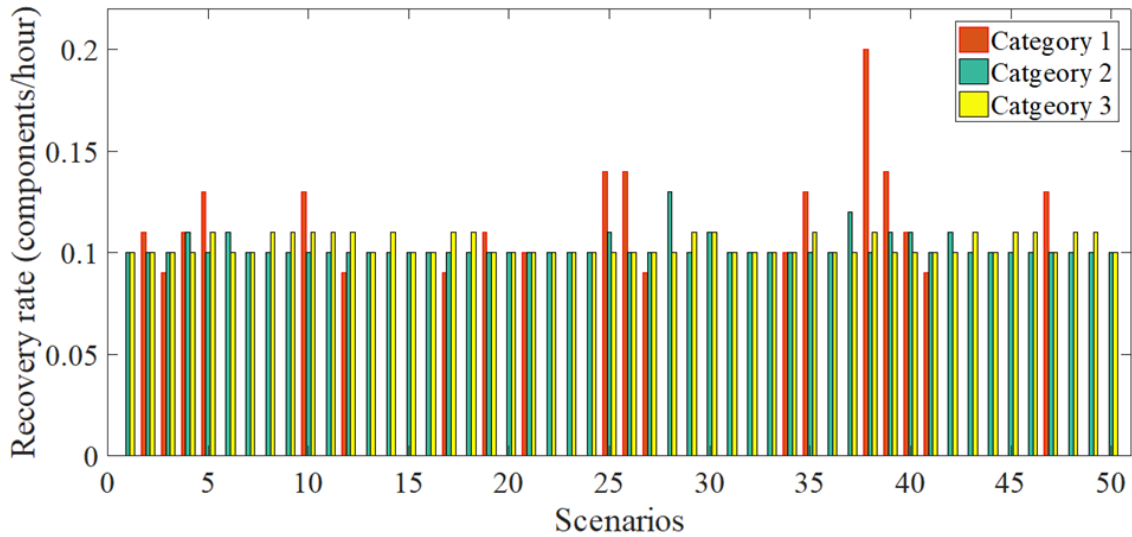
Table 5.4 Peak and Least Values of Offline Transmission Lines for Different Hurricane Categories

	Category 1	Category 2	Category 3
Maximum lines	5	5	25
Minimum lines	0	17	13

Table 5.5 Peak and Least value of Component's Disruption Rate and Recovery Time for Different Hurricane Categories

	Disruption Rate (lines/hour)		Recovery Time (hours)	
	Min. value	Max. value	Min. value	Max. value
Category 1	0	0.2	0	38
Category 2	0.2	0.72	35	169
Category 3	0.4	1.12	80	234

From Figure 5.15, the highest recovery rate of 0.2 lines/hour is observed for category 1 hurricanes for scenario 8. For category 1 hurricanes, there are missing red bars indicating zero transmission line damage. For category 2 and 3 hurricanes, the recovery rate swings between 0.1 lines/hour and 0.11 lines/hour. A peak value of 0.136 lines/hour is observed for scenario 28 for a category 2 hurricane.

The maximum and total load shed records for different hurricane categories are depicted in Figures 5.17 and 5.18 respectively. The load disruption rate, recovery rate and system recovery time are shown in Figures 5.19, 5.20 and 5.21 respectively.
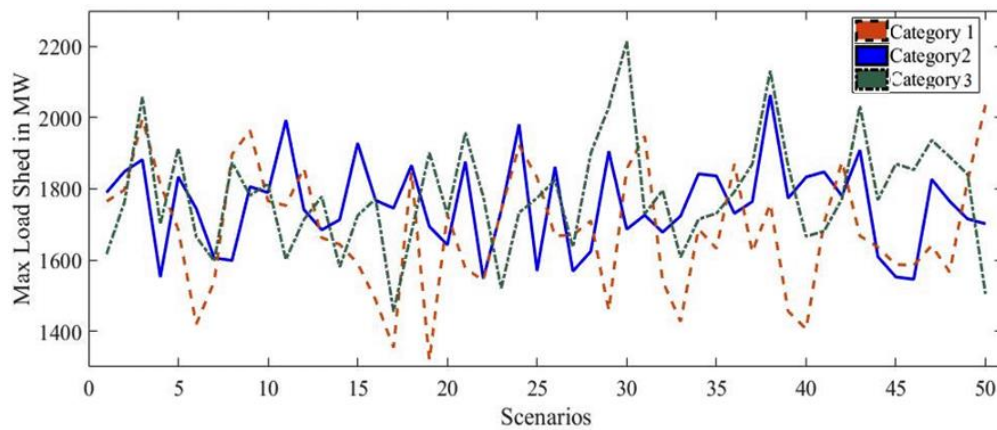
Figure 5.17 Maximum Load Shed Record–Operational Resilience
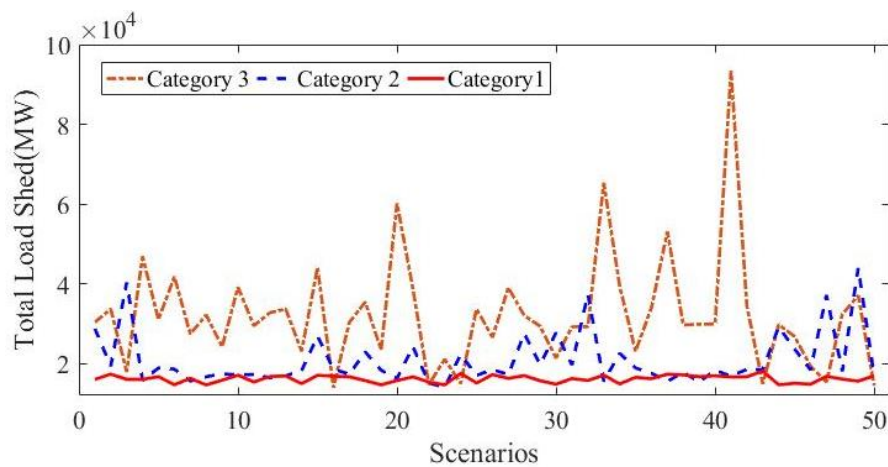
Figure 5.18 Total Load Shed Record–Operational Resilience

78
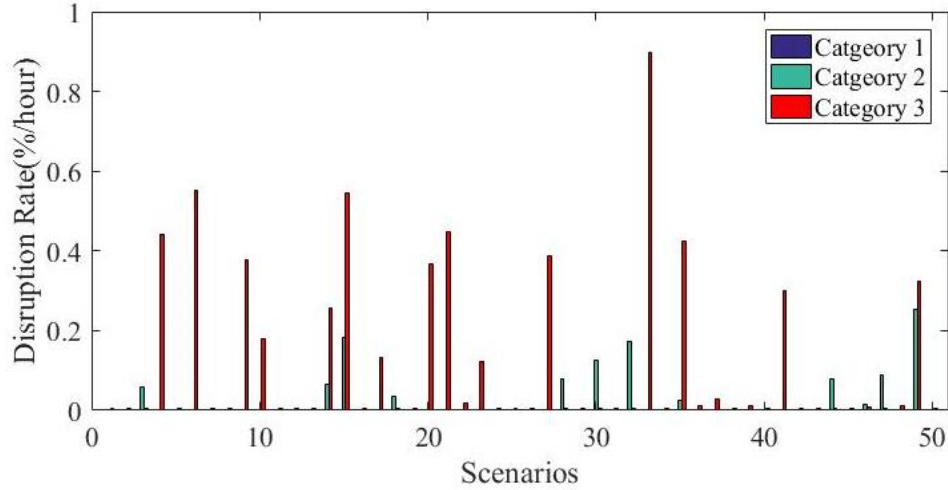
Figure 5.19 Load Disruption Rate–Operational Resilience
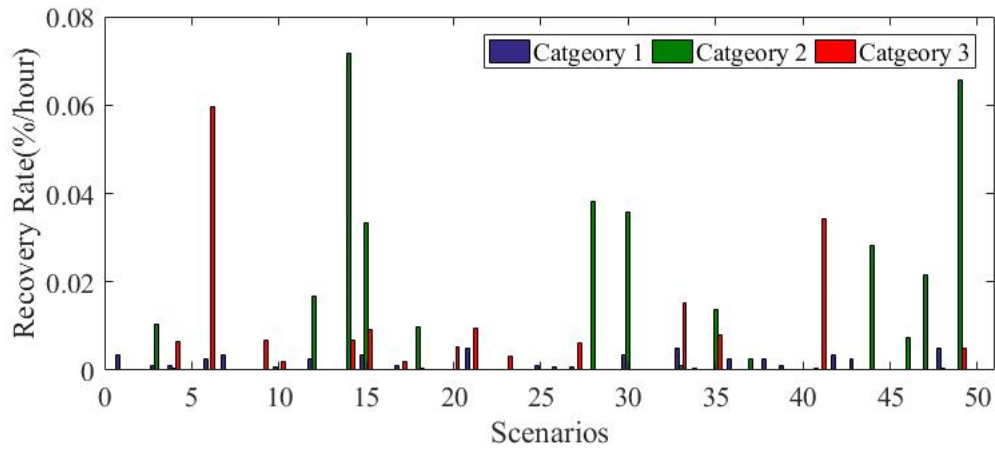
Figure 5.20 Load Recovery Rate–Operational Resilience

From Figures 5.17 and 5.18, the peak values of maximum and total load shedding records for three hurricane categories are tabulated in Table 5.6. The peak and least values of the load disruption rate and recovery time fo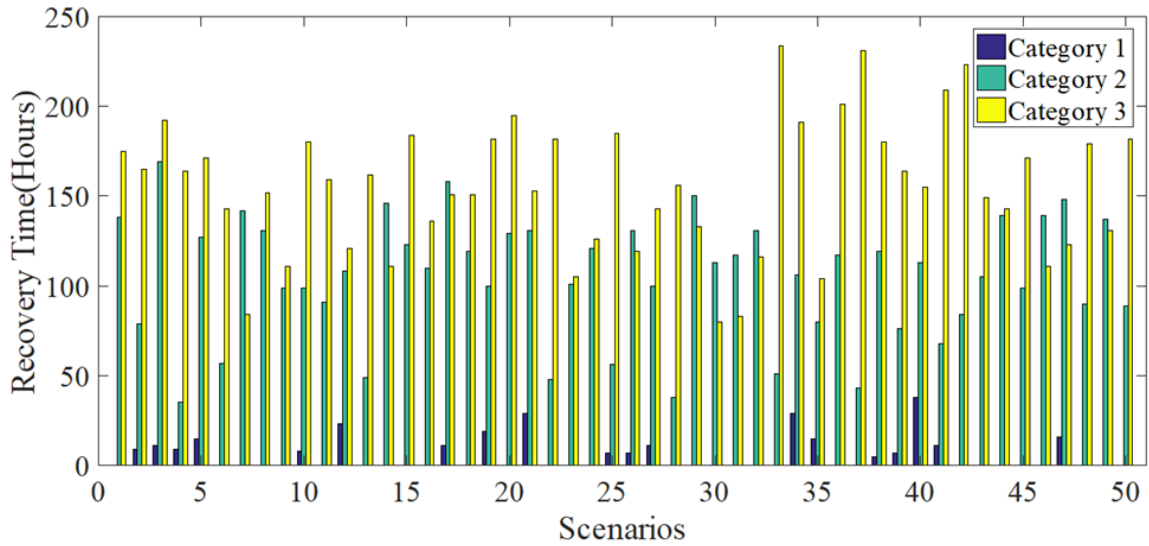r different hurricane categories are tabulated in Table 5.7. From Figure 5.18, it is observed that the worst scenario is 41 for a category 3 hurricane. From Figure 5.20, the recovery rate is smaller for category 3 hurricanes compared to category 1 and category 2 hurricanes.
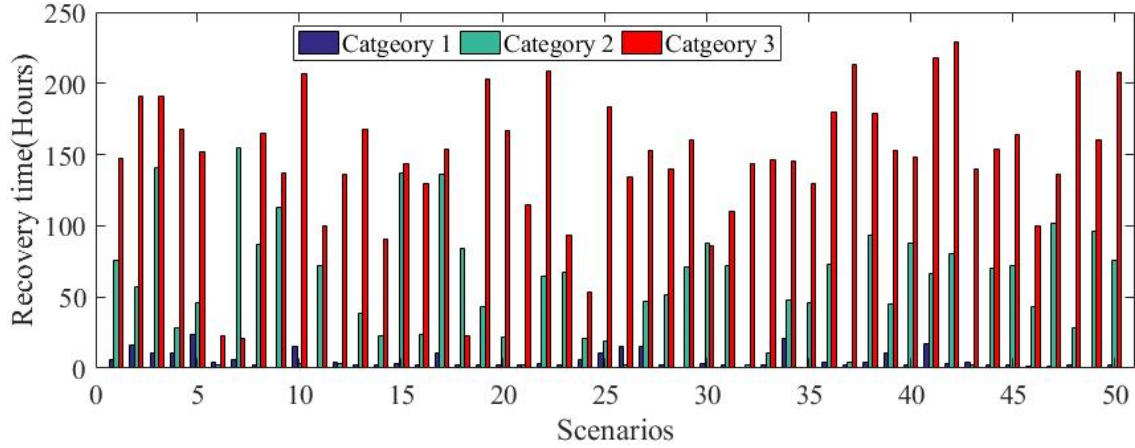
Figure 5.21 System Recovery Time–Operational Resilience

Table 5.6 Peak Values of Maximum and Total Load Shed for Diverse Hurricane Categories

	Category 1	Category 2	Category 3
Maximum Shed (MW)	2031	2158	2200
Total Shed (MW)	97040.9	46583.3	12067.4

Table 5.7 Peak and Least value of Operational Disruption Rate and Recovery Time for Different Hurricane Categories

	Disruption Rate (%/hour)		Recovery Time (hours)	
	Min. value	Max. value	Min. value	Max. value
Category 1	0	0.931	0	32
Category 2	0.085	0.285	35	157
Category 3	0.063	0.593	32	231

From Table 5.7, it is observed that category 1 hurricane has the highest disruption rate based on the disruption metric proposed in [11]. However, the load shedding results (Figures 5.17 and 5.18) clearly provide the worst-case scenarios. This is due to the

estimation of average disruption rate i.e., considering variation is linear and end values for calculation. For instance, the load at hour 51 can be 91% rated load while the load can be 63% at hour 75. Thus, the total and maximum load shed records have been proposed to have a clear view of worst-case scenarios.

Figure 5.22 Area Under the Curve-Infrastructure Resilience

Figure 5.23 Area Under the Curve-Operational Resilience

The system infrastructure and operational resilience indicators for different hurricane categories are plotted in Figures 5.22 and 5.23 respectively. The area under the component vs time curve for different scenarios and hurricane categories is calculated and
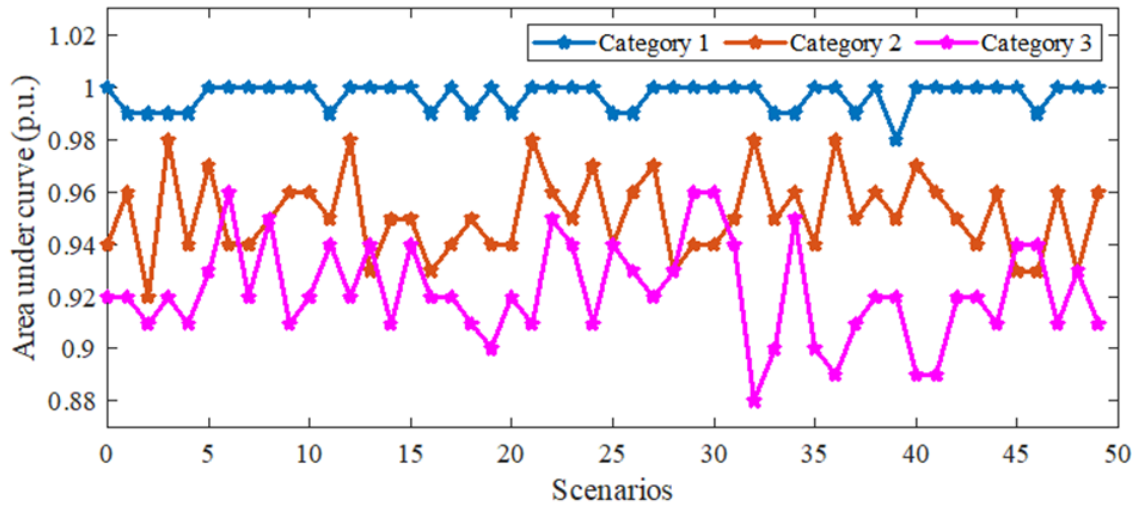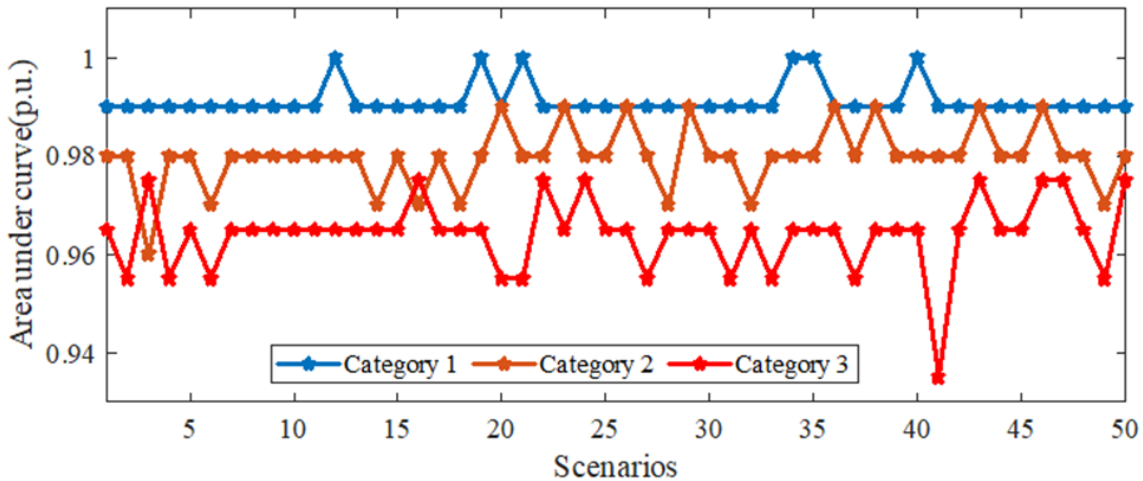
it is known as the system infrastructure resilience indicator. Similarly, the area under the % load online vs time curve for different scenarios and hurricane categories is known as the system operational resilience indicator.

From Figure 5.22, a minimum $\Lambda_t^{(i)}$ of 0.926 is observed for scenario 41 for a category 3 hurricane. The maximum disruption occurs in scenario 36. But the minimum value of $\Lambda_t^{(i)}$ is observed at 41 due to a smaller recovery time compared to scenario 36. From Figure 5.23, the curve dips are visible for scenarios 32 and 36 for a category 3 hurricane. The above assertion can be supported based on the following discussion.

In scenarios 32 and 36, there are cases such as non-supportive steam plants due to lack of fuel for power generation, and complete damage of 3 wind turbines in the wind plant at Area 1 due to failure of rotor brakes. In scenario 36, two conventional steam plants at buses 116 and 123 each having a capacity of 155 MW go offline due to fuel unavailability at t=63 and 64 respectively. Thus, a total capacity of 310 MW has been reduced from the system's overall generation capability. This unprecedently situation caused a complete load shedding at buses 114 and 109. Besides at t=64, 60% and 30% load shedding have been observed at buses 119 and 120 due to the offline plant at bus 123.

Low probable chances such as two steam plants at buses 116 and 123 going offline at the same instant can be a critical situation simulated at t=63. At t=63, the partial loads are knocked off at buses 106, 113, 119 and 120 and a complete load shedding is observed at buses 108, 109 and 114 causing an overall load shedding of 1275 MW at Area 1. Besides, 10 MW of load shedding is observed at buses 208 and 209 at area 2 due to the loss of generation plants. This is because of three tie-lines running between buses 123-217 (line

1), 113-215 (line 2) and 107-203 (line 3). The tie line 1 and 3 export power from area 1 to area 2.

In scenario 41, three wind turbines are completely damaged reducing the WT generators from 500 to 497 respectively. Thus, the plant capacity is reduced from 750 MW to 745.5 MW. This loss does not have an impact on the operational state of the system. Contemporarily, in the case of scenario 36, due to the sudden tripping of wind plants at t=51 for category 2 and 3 hurricanes, there are load sheds observed at area 1. This shedding can be decreased during the next hour by realigning the generator commitment status.

5.3.2   Aggregated Model

Aggregated results include the steady-state and dynamic analysis results. The step size for the dynamic simulation is 0.0083 s (which is half of the 60 Hz cycle period). The maximum and total load shed records are depicted in Figures 5.24 and 5.25 respectively. The system aggregated infrastructure and operational resilience indicators for different hurricane categories are illustrated in Figures 5.26 and 5.27 respectively.
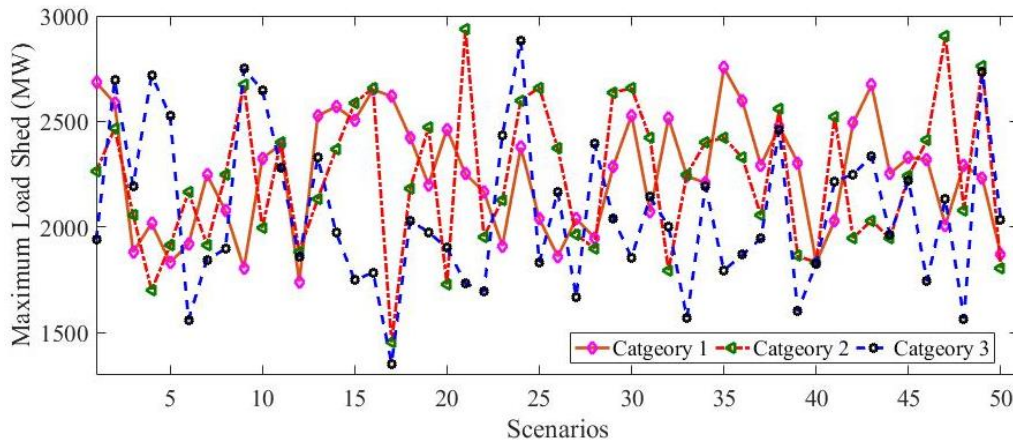
Figure 5.24 Maximum Load Shed Record–Aggregated Operational Resilience
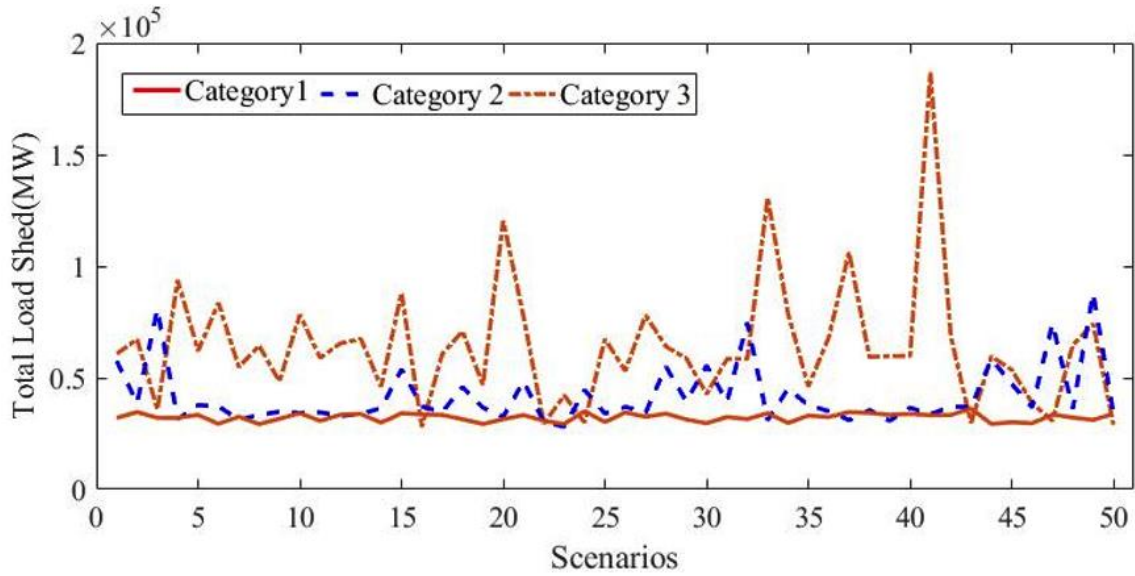
Figure 5.25 Total Load Shed Record–Aggregated Operational Resilience
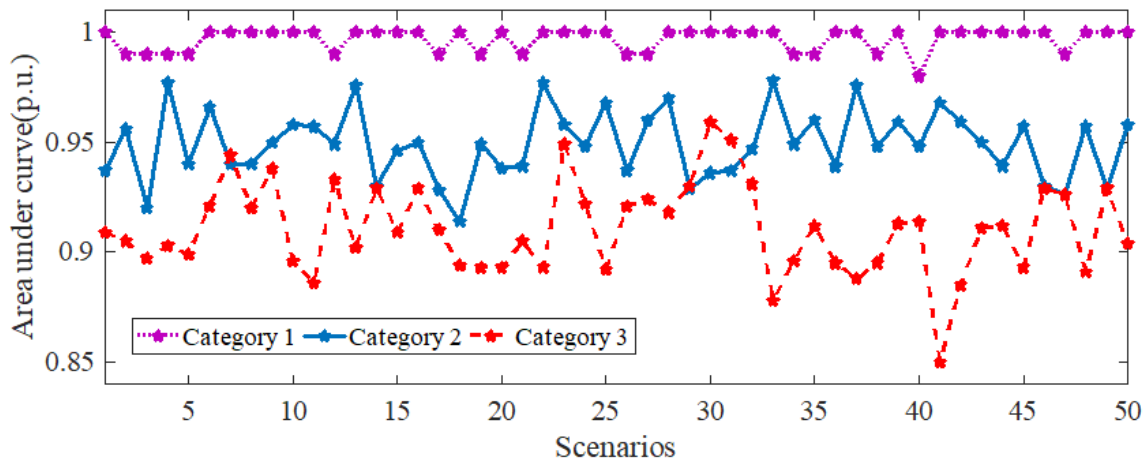
Figure 5.26 Aggregated System Infrastructure Resilience Indicator for Different Scenarios

From Figure 5.26, scenarios 11, 18 and 36 for a category 3 hurricane have a considerable difference in $\Lambda_t^{(i)}$ values for steady-state and aggregated case estimation. This is due to the dynamic effects in terms of relay operation caused due to faults and the generation loss in the system.
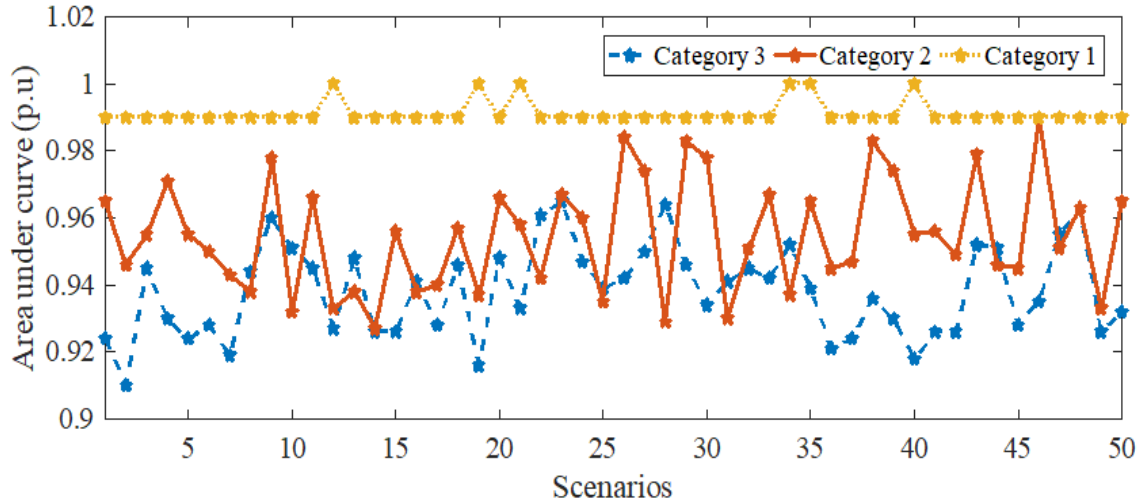
Figure 5.27 Aggregated System Operational Resilience Indicator for Different Scenarios

Comparing Figure 5.23 and Figure 5.27, the values of $\Lambda_t^{(o)}$ are more or less the same since there are certain cases of generator shedding due to protective actions. All the cases discussed in the dynamic studies are stable. Due to the sudden loss of a wind plant during the category 2 and 3 hurricanes, there are cases of load shedding observed in the system. One such case is scenario 36 from category 3 which is discussed in test study 1.

(a)　　　Test Study 1: Loss of Wind Plant in Area 1

As the wind plant at area 1 going offline, a UFLS relay operation has been observed. Due to this situation, the load buses at areas 1, 2 and 3 experienced under-frequency load shedding relay operation around a time period of 2.92, 2.94 and 3.3 seconds respectively. The frequencies of load buses where relay operation has been triggered for areas 1, 2 and 3 are depicted in Figures 5.28, 5.29 and 5.30 respectively.
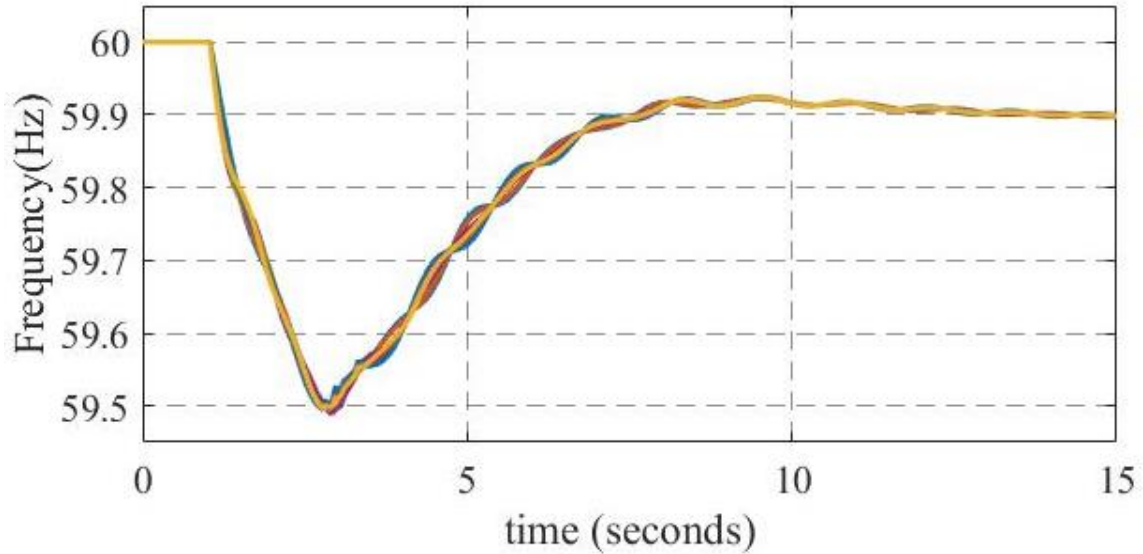
Figure 5.28 Frequency of Load Buses at Area 1 after the loss of Wind Plant
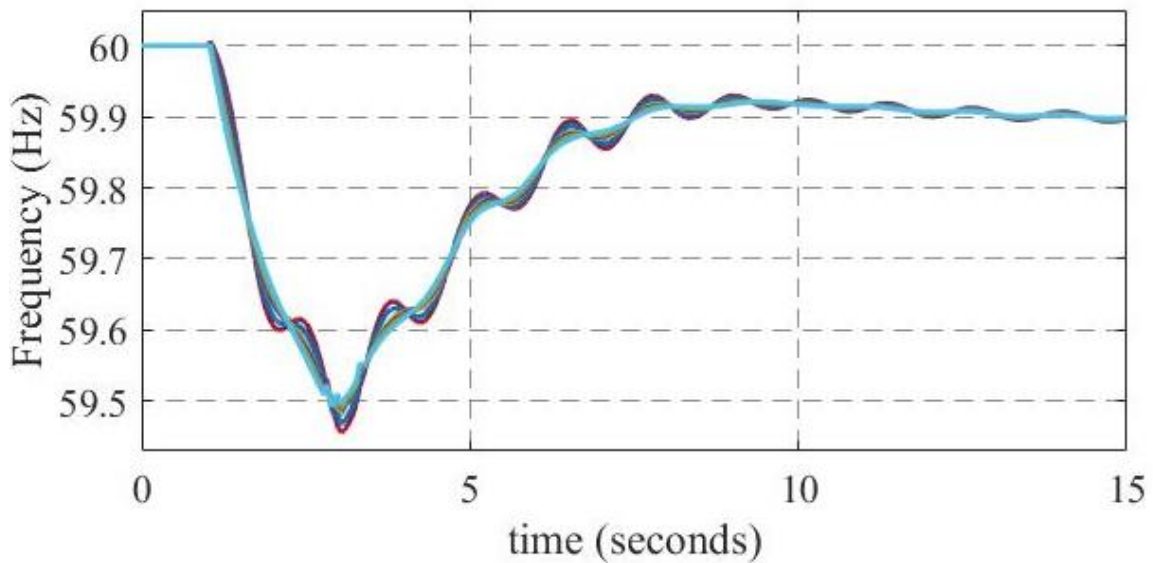
Figure 5.29 Frequency of Load Buses at Area 2 after the loss of Wind Plant

At t=2.92 seconds, buses 107-109, 113-116, 118-120 in area 1 experienced the first stage of UFLS relay operation (10% load shedding) as shown in Figure 5.28. The frequencies reached a value of 59.5 Hz at t=2.92 s. At t=2.94 seconds, buses 201-210, 213-216 and 218 in area 2 experienced the first stage of UFLS relay operation (10% load

shedding) as shown in Figure 5.29. The frequencies reached a value of 59.47 Hz at t=2.94 s. Compared to area 1, area 2 has higher load shedding. This is due to the sudden tripping of the 650 MW generating wind plant which contributed to exporting power from area 1 to area 2 through three tie lines.
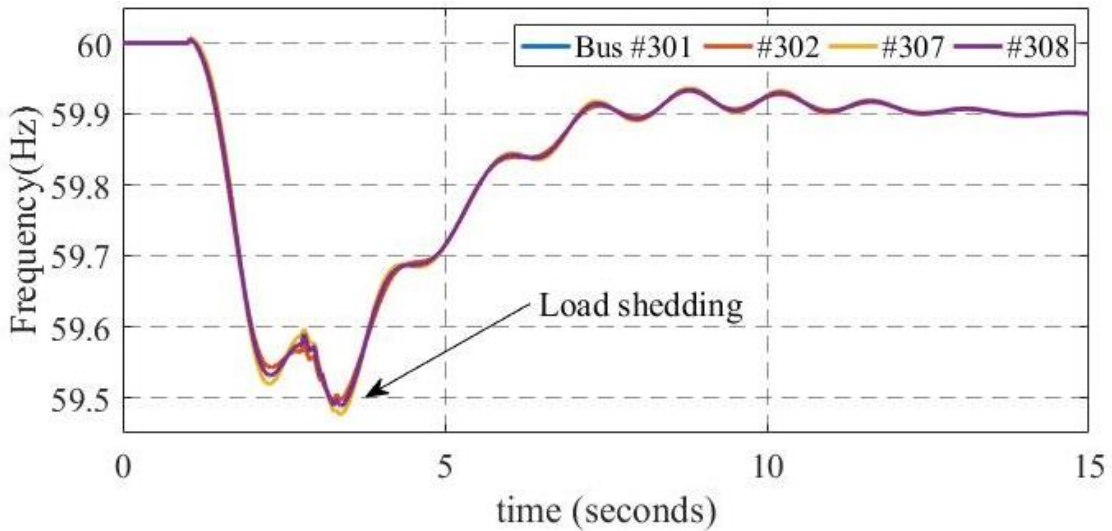
Figure 5.30 Frequency of Load Buses at Area 3 after the loss of Wind Plant
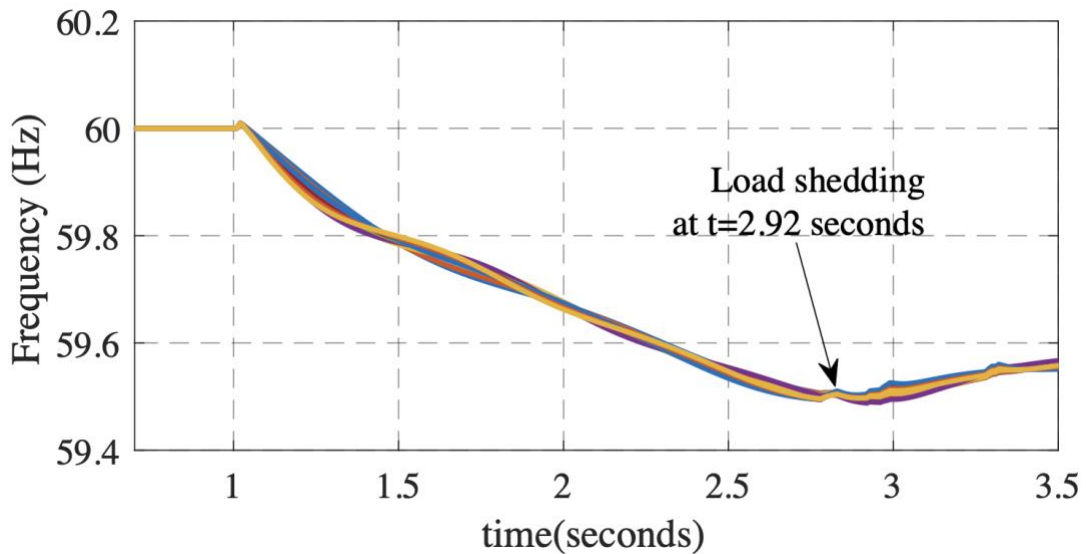
Figure 5.31 Initial Change in Frequency of Load Buses at Area 1 after losing Wind Plant

87
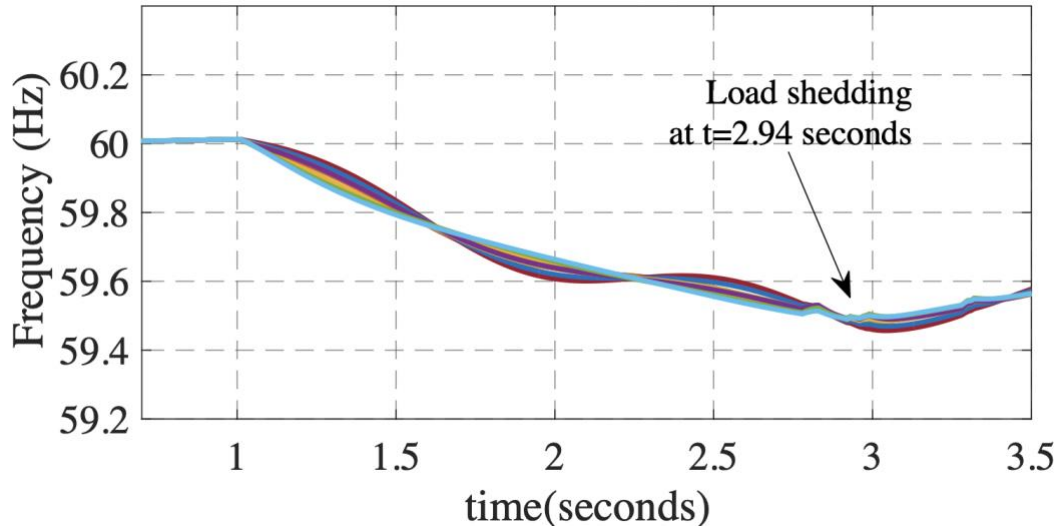
Figure 5.32 Initial Change in Frequency of Load Buses at Area 2 after losing Wind Plant
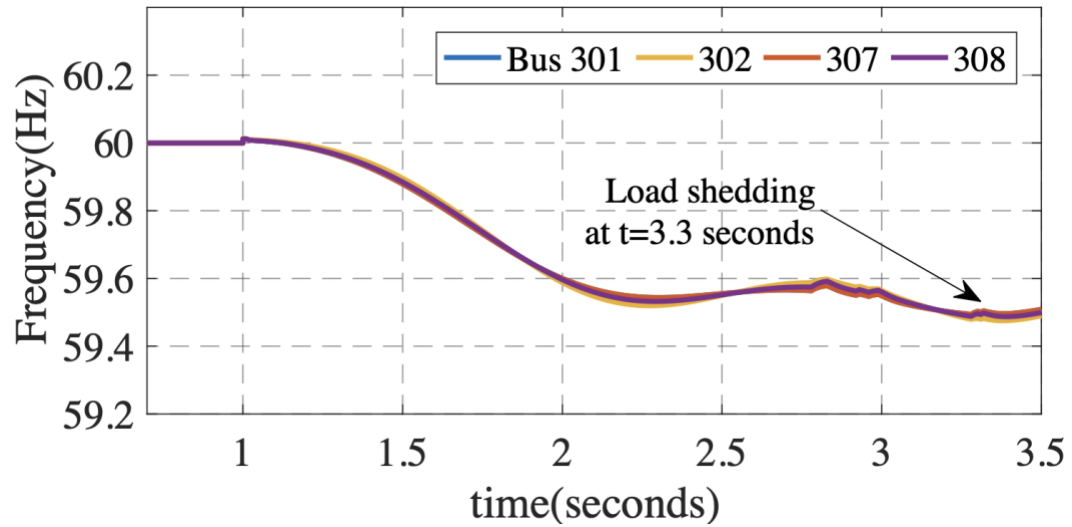
Figure 5.33 Initial Change in Frequency of Load Buses at Area 3 after losing Wind Plant

Table 5.8 Frequency Change and RoCoF for Load Buses at Areas 1, 2 and 3

Areas	Δf (Hz)	t_{nadir} (s)	ROCOF (Hz/s)	f_{nadir} (Hz)
1	-0.5	2.92	-0.2604	59.5
2	-0.53	2.94	-0.2732	59.47
3	-0.503	3.3	-0.2187	59.497

At t=3.3 seconds, buses 301, 302, 307 and 308 in area 3 experienced the first stage of UFLS relay operation (10% load shedding) as shown in Figure 5.30. The frequencies reached a value of 59.497 Hz at t=3.3 s. Partial load shedding is observed at area 3 due to a decrease in power transfer capability in the tie line between areas 1 and 3.

The initial change in frequency for load buses at areas 1, 2 and 3 are plotted in Figures 5.31, 5.32 and 5.33 respectively. These frequency change (Δf), time period taken to reach frequency nadir (t_{nadir}), rate of change of frequency (ROCOF) and frequency nadir (f_{nadir}) for these load buses are estimated and shown in Table 5.8.

(b)   Test Study 2: Debris and Insulation Failure

In scenario 19, due to the hurricane effect, events such as insulation failure of the components and debris are implemented as shown in Table 5.9. The events are initiated at time t = 2 seconds. At t=1 second, a transmission line (108-109) is ripped down due to the hurricane. At t=2.1 seconds, line 121-122 is ripped down due to the hurricane.

Table 5.9 Event Description

Event	Fault types	Location	Duration	Resemblance
1	Bus fault	Bus 116	3 cycles	(Plant) Insulation failure
2	Line fault	122-121	4 cycles	Debris
3	Line fault	121-325	4 cycles	Debris
4	Line fault	121-115	6 cycles	(Transmission) Insulation failure
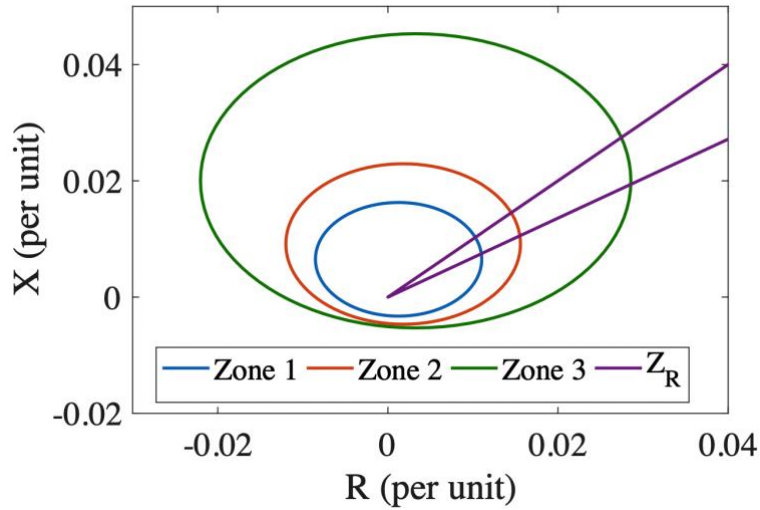
(a)
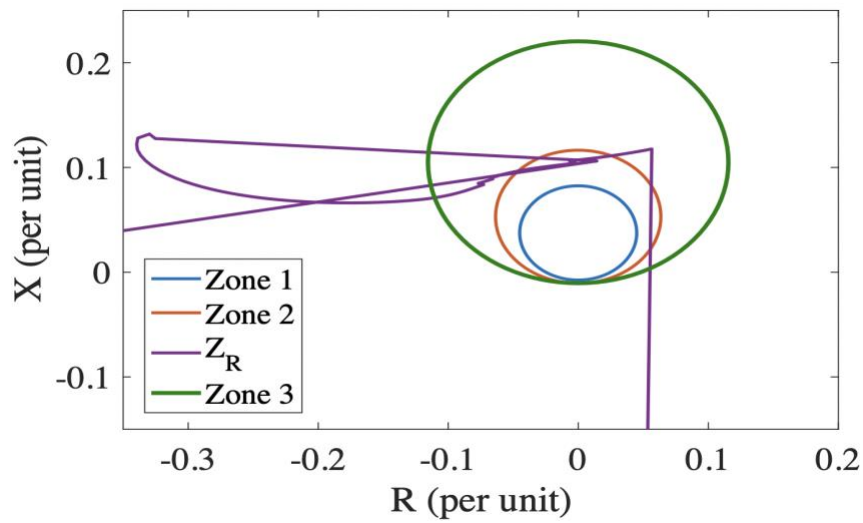
(b)

Figure 5.34 Relay Impedance (Z_R) Trajectories for Lines (a) 116-119 and (b) 117-122

Due to these events, distance relay, UVLS and out-of-step relays have been operated resulting in branch tripping, load shedding and generators shedding respectively. The impedance trajectory for lines 116-119 and 117-122 are shown in Figures 5.34 and 5.35 respectively. The bus voltage profiles, real power on transmission lines, relative rotor angle and real power generated by synchronous machines are depicted in Figures 5.35, 5.36, 5.37 and 5.38 respectively.
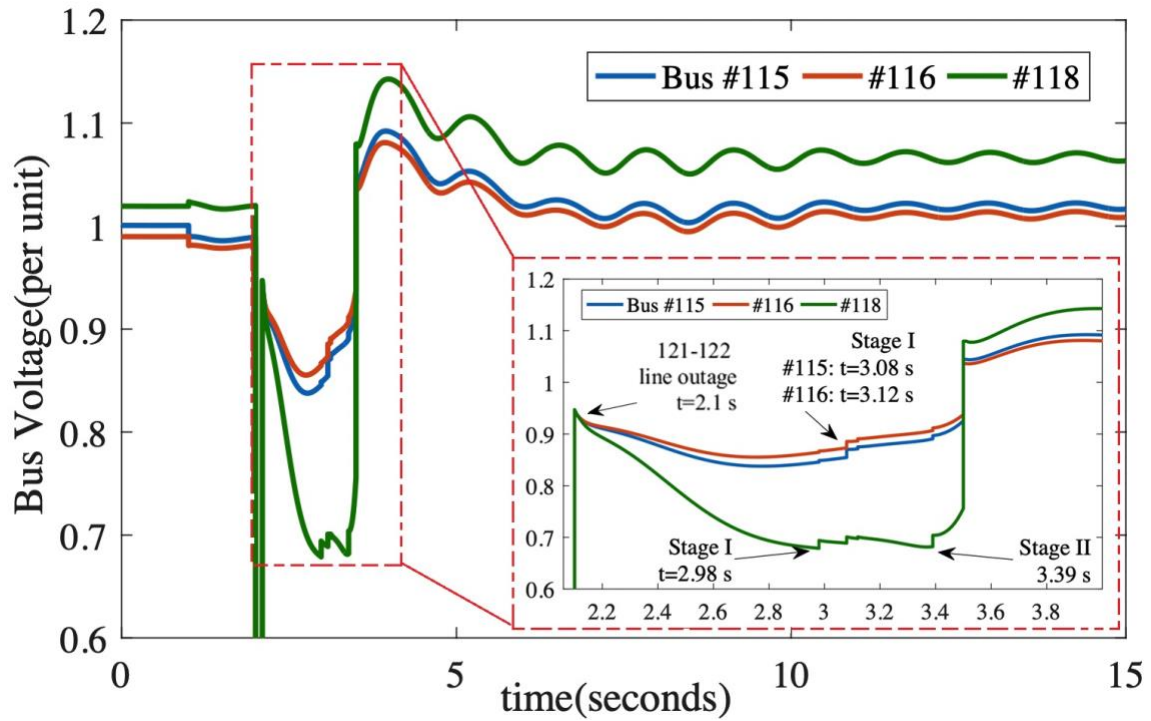
Figure 5.35 Voltage Profile for Buses 115, 116 and 118
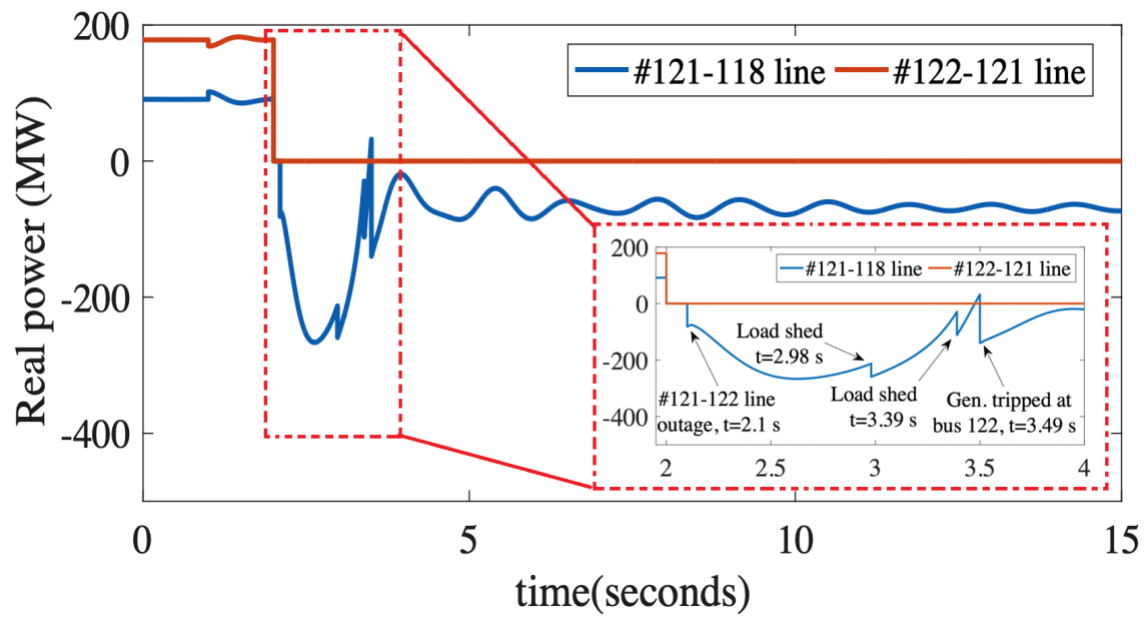
Figure 5.36 Real Power of Lines 121-118 and 122-121
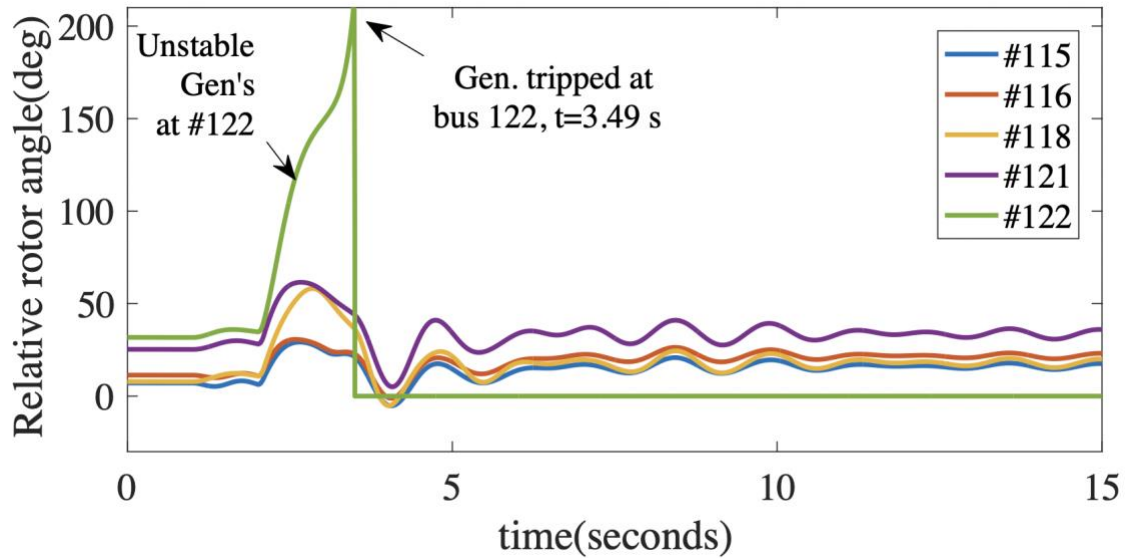
Figure 5.37 Relative Rotor Angle of Generators at Buses 115, 116, 118, 121 and 122
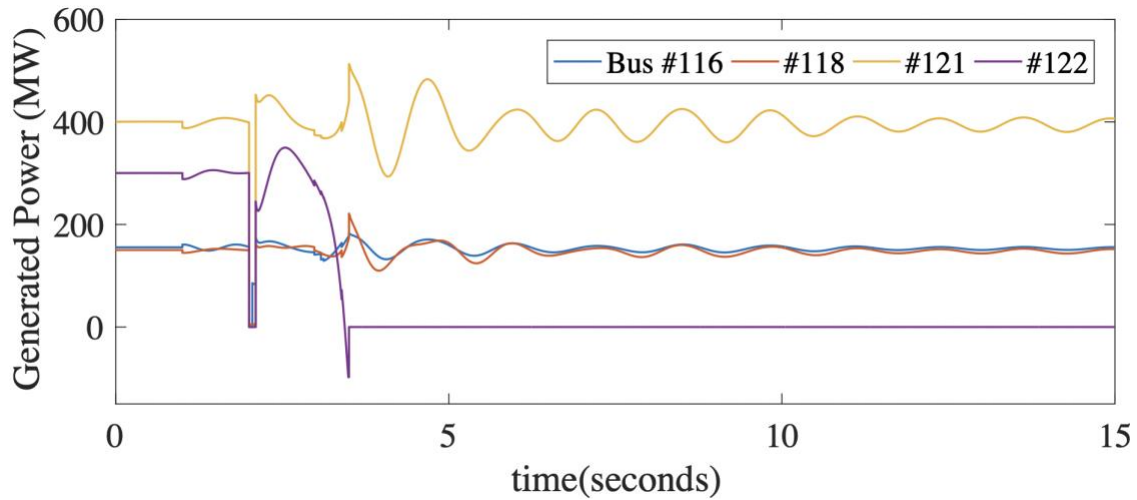
Figure 5.38 Real Power Generated at Buses 116, 118, 121 and 122

At t=2.03 seconds, the transmission line 116-119 trips due to distance relay operation as the relay trajectory enters zone 1 of mho distance relay as shown in Figure 5.34(a). Due to the fault at the near end of bus 122, Z_R enters zone 2 and stays until the fault gets cleared as observed in Figure 5.34(b). Once the fault has been cleared, Z_R leaves the relay zone and loops around in the third quadrant until t=3.4 seconds. At 3.4 seconds,

the impedance trajectory enters the third zone and remained until t=3.5 seconds. At t=3.5 seconds, Z_R leaves the relay operating zone due to generator shedding at bus 122.

At t=2.1 seconds, due to the outage of line 121-122, the voltage at buses 115,116 and 118 decreased and initiated UVLS operation as observed in Figure 5.35. At t=2.98 seconds, the initial stage of UVLS has been triggered to shed a 104.17 MW (21.27 MVAR) load at bus 118 followed by a 99.86 MW (20.16 MVAR) and 24.51 MW (4.9 MVAR) load sheds at buses 115 and 116 respectively. Despite the load shed at bus 118, the further decrement in bus voltage has caused stage II UVLS operation which knocked off a load of 173.81 MW (35.45 MVAR) at t=3.39 seconds. With all these actions, the bus voltages increased and plummeted to 1.1 pu at t=3.49 seconds. Among other buses, bus 118 was highly affected due to real power (export) dependency from bus 122 via the transmission line 121-122 which has gone offline due to the hurricane as shown in Figure 5.36. It can be observed that the real power on line 121-118, decreased from 128 MW due to line outage and finally settles at -55 MW.

Due to outage of the line 121-122, the machines at bus 122 started going unstable as their rotor angles begin increasing at t=2.1 seconds and reaches 180° at t=3.48 seconds. The out-of-step logic operation has been triggered as the rotor angles have exceeded the maximum threshold value which resulted tripping of 6 hydro units at bus 122 as depicted in Figure 5.37. Thus, a total load shedding of 402.35 MW (81.78 MVAR) has been observed. This scenario can create a huge impact on system stability if these buses have heavy-duty motor loads and power electronic drives such as variable frequency drives (VFDs).
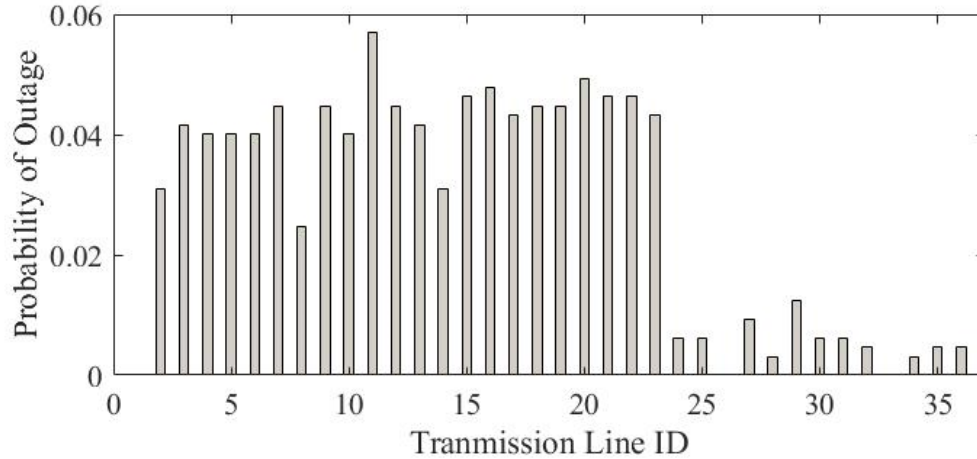
Figure 5.39 Outage Probability of Transmission Lines in Area 1

The frequency of transmission line outages in area 1 due to different hurricane categories is depicted in Figure 5.39. It can be observed that lines 26 and 33 have zero outage probability as they are substation incoming and outgoing lines. Transmission lines 24-36 correspond to more robust corridors, and they are affected during category 3 hurricanes. Line 27, 29 and 35 are the tie lines. Line 11 has the highest outage probability of 0.0585. Table 5.10 shows the aggregated probabilistic resilience metrics quantifying operational and infrastructural resilience. From the table, it can be observed that aggregated indices are smaller compared to steady-state indices considering the transient load/generation shedding and branch tripping.

Table 5.10 Aggregated Resilience Indices

Metric	Category 1	Category 2	Category 3
$\Lambda_p^{(O)}$	0.9912	0.9544	0.9079
$\Lambda_p^{(I)}$	0.9968	0.9409	0.8835

5.4   Summary

In this chapter, results obtained from steady-state and proposed approaches considering dynamic studies are compared in terms of the infrastructure and operational resilience metrics. Furthermore, the importance of the stochastic resilience evaluation over the deterministic approach is highlighted and their results are compared for a better understanding of the power system response to such a highly uncertain event.

CHAPTER 6

CONCLUSION AND FUTURE SCOPE

6.1   Discussions and Conclusion

This work analyzes the steady-state and dynamic effects of hurricanes on the power system's resilience. The studies are conducted on the IEEE modified reliability test system 1996. An aggregated trapezoid model has been developed based on the extension of the conventional multiphase trapezoid model. The system-level resiliency model is introduced and is quantified based on the resiliency metrics including disruption rate, recovery rate, recovery time, absorption time, and area under the curve. Disruption rate, recovery rate, and area under the curve metrics are modified and proposed based on the aggregated results obtained from the steady-state and transient stability analysis. Moreover, the importance of including transient stability analysis in power system resiliency studies and its effects on evaluating the system's operational status such as load shedding and generation shedding is evaluated in this work.

The system stability has been evaluated throughout the event period, and the impact of implementing proper corrective actions on preventing system instability and improving the resilience metrics are analysed. Finally, the resiliency metrics for steady-state and aggregate results are computed and compared. It can be observed that the area under the curve, disruption rate, and recovery rate metrics are highly impacted in the dynamic analysis due to the presence of dips in load and generator status curves. In addition to the existing steady-state analysis, the dynamic analysis tool paved the way for realizing the system operational status that can closely mimic the actual system performance.

96

A probabilistic approach based on MCS has been proposed and utilized in modelling hurricanes, outage scenarios, transmission fault types, load scheduling and wind generation. It can be observed that there are certain crucial scenarios such as failure of system recovery to pre-event state (wind turbine damages), generation going offline due to inadequate fuel availability and transmission faults. During such scenarios, the following cases have been reported.

(i) The neighbouring areas have reported considerable load shedding and high frequency drops with huge ROCOF values.

(ii) Distance relay operation followed by tripping of machines at area 1 and load shedding.

(iii) Line outage due to hurricane followed by a fault caused load shedding and triggers out-of-step generator protection logic.

In addition to the existing deterministic steady-state resilience approach, the stochastic aggregated analysis tool paved the way for realizing the system operational status that can closely mimic the actual system performance.

6.2   Future Scope

During this work, some of the following difficulties were experienced and the following improvements can be made in future works.

(i) Metrics Evaluation: With more uncertainty incorporated in the network, the load shedding curves follow irregular patterns, which can be difficult to estimate the area under the curve. Discrete evaluation techniques for irregular bodies categorised into multiple known areas can be followed.

(ii)   Load Modelling: In this work, the loads are considered as a constant impedance model. However, the grids are dominated by frequency and voltage-dependent models. Thus, a complex load model with VFD (variable frequency drive) supported single phase and three-phase induction motors can be considered for future study to analyse scenarios such as fault-induced delayed voltage recovery and voltage stalling for resilience evaluation.

(iii)   Renewable Dominant Networks: In this work, 20% wind penetration was considered. With the high penetration of renewable resources (solar and wind), the resilience evaluation can be more challenging and uncertain. Future work can incorporate renewable penetration up to 100% based on the recent success of CAISO on 100% renewable penetrated grid operation.

(iv)   Distribution Network Modeling: Since the above analysis is constricted to the transmission system, the obtained load shedding results cannot be 100% predictable. There can be the isolation of loads due to distribution outages as well which cannot be modelled for the above transmission network. Thus, a transmission-distribution network can be effectively used for resilience evaluation in future.

REFERENCES

[1]   J. T. Austin Energy Institute (2021, July). The Timeline and Events of February 2021 Texas Electric Grid Blackouts. [Online]. Available: https://www.puc.texas.gov/agency/resources/reports/UTAustin_(2021)_EventsFebruary2021TexasBlackout_(002)FINAL_07_12_21.pdf.

[2]   Joshua W. Busby *et al.*, "Cascading risks: Understanding the 2021 winter blackout in Texas", *Energy Research & Social Science*, vol. 77, pp. 1-10, July 2021.

[3]   K. Amadeo, "Hurricane Harvey Facts, Damage and Costs", [Online]. Available: https://www.lamar.edu/_files/documents/resilience-recovery/grant/recovery-and-resiliency/hurric2.pdf.

[4]   National Infrastructure Advisory Council, "Critical Infrastructure Resilience Final Report and Recommendations", September 2009.

[5]   Presidential Policy Directive/PPD-21, The White House. [Online]. Available: https://obamawhitehouse.archives.gov/the-press-office/2013/02/12/presidential-policy-directive-critical-infrastructure-security-and-resil.

[6]   Electric Power Research Institute (2016), *Electric Power System Resiliency: Challenges and Opportunities*. [Online]. Available: https://www.epri.com/research/products/000000003002007376.

[7]   National Academies of Sciences, Engineering and Medicine, "Enhancing the Resilience of the Nation's Electricity System", 2017. [Online]. Available: https://nap.nationalacademies.org/catalog/24836/enhancing-the-resilience-of-the-nations-electricity-system.

[8]   U.S. Energy Information Administration-EIA-Independent Statistics and Analysis, Available [Online]: https://www.eia.gov/todayinenergy/detail.php?id=50316.

[9]   K. Tierneyand, M. Bruneau, *Conceptualizing and Measuring Resilience: A Key to Disaster Loss Reduction*. The National Academies of Sciences, Engineering and Medicine, *Transportation and Research, News*, vol. 250, May-Jun. 2007.

[10]   M. Panteli and P. Mancarella, "Influence of extreme weather and climate change on the resilience of power systems: Impacts and possible mitigation strategies," *Elect. Power Syst. Res.*, vol. 127, pp. 259–270, 2015.

[11]   M. Panteli, P. Mancarella, D. N. Trakas, E. Kyriakides and N. D. Hatziargyriou, "Metrics and Quantification of Operational and Infrastructure Resilience in Power Systems," in IEEE Transactions on Power Systems, vol. 32, no. 6, pp. 4732-4742, Nov. 2017, doi: 10.1109/TPWRS.2017.2664141.

[12]   U.S. Energy Information Administration-EIA-Independent Statistics and Analysis, Available [Online]: https://www.eia.gov/todayinenergy/detail.php?id=49556.

[13]   B. Chiu, R. Roy and T. Tran, "Wildfire Resiliency: California Case for Change," in IEEE Power and Energy Magazine, vol. 20, no. 1, pp. 28-37, Jan.-Feb. 2022, doi: 10.1109/MPE.2021.3122730.

[14]   T. Pultarova, "Cyber security - Ukraine grid hack is wake-up call for network operators [News Briefing]," in Engineering & Technology, vol. 11, no. 1, pp. 12-13, February 2016, doi: 10.1049/et.2016.0116.

[15]   S. Chanda, A. K. Srivastava, M. U. Mohanpurkar and R. Hovsapian, "Quantifying Power Distribution System Resiliency Using Code-Based Metric," in IEEE Transactions on Industry Applications, vol. 54, no. 4, pp. 3676-3686, July-Aug. 2018, doi: 10.1109/TIA.2018.2808483.

[16]   E. Al-Ammar and J. Fisher, "Resiliency assessment of the power system network to cyber and physical attacks," 2006 IEEE Power Engineering Society General Meeting, 2006, pp. 7 pp.-, doi: 10.1109/PES.2006.1709089.

[17]   D. L. Donaldson, M. S. Alvarez-Alvarado and D. Jayaweera, "Power System Resiliency During Wildfires Under Increasing Penetration of Electric Vehicles," 2020 International Conference on Probabilistic Methods Applied to Power Systems (PMAPS), 2020, pp. 1-6, doi: 10.1109/PMAPS47429.2020.9183683.

[18]   Executive Office of President and U. S. Department of Energy. *Economic Benefits of Increasing Electric Grid Resilience to Weather Outages*. [Online]. Available: https://www.energy.gov/sites/prod/files/2013/08/f2/Grid%20Resiliency%20Report_FINAL.pdf.

[19]   H. Sabouhi, A. Doroudi, M. Fotuhi-Firuzabad and M. Bashiri, "Electrical Power System Resilience Assessment: A Comprehensive Approach," in IEEE Systems Journal, vol. 14, no. 2, pp. 2643-2652, June 2020, doi: 10.1109/JSYST.2019.2934421.

[20]   S. Zuloaga and V. Vittal, "Quantifying Power System Operational and Infrastructural Resilience Under Extreme Conditions Within a Water-Energy Nexus Framework," in IEEE Open Access Journal of Power and Energy, vol. 8, pp. 229-238, 2021, doi: 10.1109/OAJPE.2021.3084577.

[21]   Y. Yang, W. Tang, Y. Liu, Y. Xin and Q. Wu, "Quantitative Resilience Assessment for Power Transmission Systems Under Typhoon Weather," in IEEE Access, vol. 6, pp. 40747-40756, 2018, doi: 10.1109/ACCESS.2018.2858860.

[22]   M. Mahzarnia, M. P. Moghaddam, P. T. Baboli and P. Siano, "A Review of the Measures to Enhance Power Systems Resilience," in IEEE Systems Journal, vol. 14, no. 3, pp. 4059-4070, Sept. 2020, doi: 10.1109/JSYST.2020.2965993.

[23]   M. Panteli, D. N. Trakas, P. Mancarella and N. D. Hatziargyriou, "Boosting the Power Grid Resilience to Extreme Weather Events Using Defensive Islanding," in IEEE Transactions on Smart Grid, vol. 7, no. 6, pp. 2913-2922, Nov. 2016, doi: 10.1109/TSG.2016.2535228.

[24]   R. Moreno et al., "From Reliability to Resilience: Planning the Grid Against the Extremes," in IEEE Power and Energy Magazine, vol. 18, no. 4, pp. 41-53, July-Aug. 2020, doi: 10.1109/MPE.2020.2985439.

[25]   T. Lagos et al., "Identifying Optimal Portfolios of Resilient Network Investments Against Natural Hazards, With Applications to Earthquakes," in IEEE Transactions on Power Systems, vol. 35, no. 2, pp. 1411-1421, March 2020, doi: 10.1109/TPWRS.2019.2945316.

[26]   G. Fu et al., "Integrated Approach to Assess the Resilience of Future Electricity Infrastructure Networks to Climate Hazards," in IEEE Systems Journal, vol. 12, no. 4, pp. 3169-3180, Dec. 2018, doi: 10.1109/JSYST.2017.2700791.

[27]   R. Moreno et al., "Microgrids Against Wildfires: Distributed Energy Resources Enhance System Resilience," in IEEE Power and Energy Magazine, vol. 20, no. 1, pp. 78-89, Jan.-Feb. 2022, doi: 10.1109/MPE.2021.3122772.

[28] M. Panteli and P. Mancarella, "Modeling and Evaluating the Resilience of Critical Electrical Power Infrastructure to Extreme Weather Events," in IEEE Systems Journal, vol. 11, no. 3, pp. 1733-1742, Sept. 2017, doi: 10.1109/JSYST.2015.2389272.

[29] N. Alemazkoor et al., "Hurricane-Induced Power Outage Risk Under Climate Change is Primarily Driven by the Uncertainty in Projections of Future Hurricane Frequency", Sci Rep 10, 15270 (2020), doi: 10.1038/s41598-020-72207-z.

[30] Maia-Silva, D., Kumar, R. & Nateghi, R. The critical role of humidity in modeling summer electricity demand across the United States. Nat Commun 11, 1686 (2020).

[31] Perera, A. T. D., Nik, V. M., Chen, D., Scartezzini, J. L., & Hong, T. (2020). Quantifying the impacts of climate change and extreme climate events on energy systems. Nature Energy, 5(2), 150-159.

[32] Reyna, J., Chester, M. Energy efficiency to reduce residential electricity and natural gas use under climate change. Nat Commun 8, 14916 (2017).

[33] P. Gautam, P. Piya and R. Karki, "Resilience Assessment of Distribution Systems Integrated With Distributed Energy Resources," in IEEE Transactions on Sustainable Energy, vol. 12, no. 1, pp. 338-348, Jan. 2021, doi: 10.1109/TSTE.2020.2994174.

[34] V. Chalishazar et,.al., "Power System Resilience Metrics Augmentation for Critical Load Prioritization", Pacific Northwest National Laboratory, January 2021.

[35] H. T. Nguyen, J. Muhs and M. Parvania, "Preparatory Operation of Automated Distribution Systems for Resilience Enhancement of Critical Loads," in IEEE Transactions on Power Delivery, vol. 36, no. 4, pp. 2354-2362, Aug. 2021, doi: 10.1109/TPWRD.2020.3030927.

[36] H. Aki, "Demand-Side Resiliency and Electricity Continuity: Experiences and Lessons Learned in Japan," in Proceedings of the IEEE, vol. 105, no. 7, pp. 1443-1455, July 2017, doi: 10.1109/JPROC.2016.2633780.

[37] R. Eskandarpour, "Power System Resilience Enhancement Using Artificial Intelligence", Ph.D. Dissertation, University of Denver, August 2019.

[38]   Q. Zhou et.al., "Distributed control and communication strategies in networked microgrids," IEEE Communications Surveys & Tutorials, vol. 22, pp. 2586–2633, Sep. 2020.

[39]   H. Hui, Y. Ding and M. Zheng, "Equivalent Modeling of Inverter Air Conditioners for Providing Frequency Regulation Service," in IEEE Transactions on Industrial Electronics, vol. 66, no. 2, pp. 1413-1423, Feb. 2019, doi: 10.1109/TIE.2018.2831192.

[40]   H. Hui, Y. Ding, T. Chen, S. Rahman and Y. Song, "Dynamic and Stability Analysis of the Power System With the Control Loop of Inverter Air Conditioners," in IEEE Transactions on Industrial Electronics, vol. 68, no. 3, pp. 2725-2736, March 2021, doi: 10.1109/TIE.2020.2975465.

[41]   H. Hui, Q. Yang, N. Dai, H. Zhang, Y. Ding and Y. Song, "Anticipatory Control of Flexible Loads for System Resilience Enhancement Facing Accidental Outages," 2021 International Conference on Power System Technology (POWERCON), 2021, pp. 844-849, doi: 10.1109/POWERCON53785.2021.9697825.

[42]   U.S.-Canada Power System Outage Task Force, *Final Report on the August 14, 2003 Blackout in the United States and Canada: Causes and Recommendations,* April 2004.

[43]   GE Energy, 1.5 MW Wind Turbine Brochure [Online]. Available: https://geosci.uchicago.edu/~moyer/GEOS24705/Readings/GEA14954C15-MW-Broch.pdf.

[44]   National Weather Service, Saffir-Simpson Hurricane Scale [Online]. Available: https://www.weather.gov/mfl/saffirsimpson.

[45]   E. Muljadi, presentation notes, Spring 2007, University of Colorado.

[46]   Siemens PSS®E version 35.2 (2020). *Program Operation Manual*.

[47]   Grigg. C and et al., "The IEEE reliability test system-1996. A report prepared by the Reliability Test System Task Force of the Application of Probability Methods Subcommittee," *IEEE Trans. Power Syst.*, vol. 14, no. 3, pp. 1010–1020, Aug. 1999.

[48]   N. W. Miller, K. Clark and M. Shao, "Frequency responsive wind plant controls: Impacts on grid performance," 2011 IEEE Power and Energy Society General Meeting, 2011, pp. 1-8, doi: 10.1109/PES.2011.6039137.

[49]   Western Electric Coordinating Council (May 2022), *WECC Approved Dynamic Model Library* [Online]. Available: https://www.wecc.org/Reliability/Approved%20Dynamic%20Models%20May%202022.pdf.

[50]   V. Vittal et.al., *Power System Control and Stability*, 3rd ed. Wiley-IEEE Press, 2019.

[51]   "IEEE Recommended Practice for Excitation System Models for Power System Stability Studies," in IEEE Std 421.5-1992, vol., no., pp.1-56, 10 Aug. 1992, doi: 10.1109/IEEESTD.1992.106975.

[52]   Siemens PSS®E version 35.2 (2020). *Program Application Guide Volume 2*.

[53]   Siemens PSS®E version 35.2 (2020). *Model Library*.

[54]   Mojdeh Khorsand Hedman, "Analytical approaches for identification and representation of critical protection systems in transient stability studies", Ph.D Dissertation, Arizona State Univesrity, 2017.

[55]   North American Electric Reliability Corporation, *PRC-006-3*. [Online]. Available: Programs and Departments: Standards: PRC-006-3.

[56]   A. M. Abed, "WSCC voltage stability criteria, undervoltage load shedding strategy, and reactive power reserve monitoring methodology," 1999 IEEE Power Engineering Society Summer Meeting. Conference Proceedings (Cat. No.99CH36364), 1999, pp. 191-197 vol.1, doi: 10.1109/PESS.1999.784345.

[57]   North American Electric Reliability Corporation, PRC-024-3—Frequency and Voltage Protection Settings for Generating Resources.

[58]   Wildfire in Southern Washington is Caused by Wind Turbine that Caught Fire [Online]. Available: https://www.oregonlive.com/news/2019/07/wildfire-in-southern-washington-reportedly-caused-by-burning-wind-turbine.html.

[59]   Siemens PSS®E version 35.2 (2020). *Application Program Interface Manual.*

[60]   T. Zhao, H. Zhang, X. Liu, S. Yao and P. Wang, "Resilient Unit Commitment for Day-Ahead Market Considering Probabilistic Impacts of Hurricanes," in IEEE Transactions on Power Systems, vol. 36, no. 2, pp. 1082-1094, March 2021, doi: 10.1109/TPWRS.2020.3025185.

APPENDIX A

PARAMETERS FOR PSS®E DYNAMIC MODELS

A.1 Wound Rotor Synchronous Machine (GENROU)

τ'_{d0}	τ''_{d0}	τ'_{q0}	τ''_{q0}	H	D	x_d	x_q
7.00	0.025	0.75	0.05	4.83	0.00	2.20	2.10
x'_d	x'_q	x''_d	x''_q	x_l	$S(1.0)$	$S(1.2)$	
0.22	0.416	0.32	0.32	0.147	0.109	0.300	

A.2 IEEE ST1 (1980) Exciter (EXST1)

T_R	V_{IMAX}	V_{IMIN}	T_C	T_B	K_A
0.00	0.10	-0.10	1.00	10.00	100.00
T_A	V_{RMAX}	V_{RMIN}	K_C	K_F	T_F
0.02	5.00	-5.00	0.05	0.00	1.00

A.3 Steam Turbine Governor (TGOV1)

R	T_1	V_{MAX}	V_{MIN}	T_2	T_3	D_t
0.05	0.50	1.00	0.00	3.00	10.00	0.00

A.4 Gas Turbine Governor (GGOV1)

R	T_{pelec}	$maxerr$	$minerr$	K_{pgov}	K_{Igov}	K_{dgov}	T_{dgov}	V_{MAX}
0.04	1.0	0.05	-0.05	10.0	2.0	0.0	1.0	1.0
V_{MIN}	T_{act}	$Kturb$	$Wfnl$	T_b	T_c	$Teng$	T_{fload}	K_{pload}
0.15	0.5	1.5	0.2	0.1	0.1	0.0	3.0	2.0
K_{Iload}	$Ldref$	Dm	$Ropen$	$Rclose$	K_imw	$Aset$	Ka	T_a
0.67	1.0	0.0	0.10	-0.10	0.002	0.01	10.0	0.01
T_{rate}	db	T_{sa}	T_{sb}	Rup	$Rdown$			
$1.25P_{rate}$	0.0	4.0	5.0	99.0	-99.0			

A.5 Hydro Turbine Governor (HYGOV)

R	r	T_r	T_f	T_g	V_{ELM}
0.04	0.30	5.00	0.05	0.50	0.20
G_{MAX}	G_{MIN}	T_w	A_t	D_{turb}	q_{NL}
1.00	0.00	1.00	1.20	0.50	0.08

A.6   Wind Plant Model

Second Generation Type 3 WTG (WT3G2)

T_{Iqcmd}	T_{Iqcmd}	K_{PLL}	K_{iPLL}	PLL_{MAX}	P_{rated}	V_{LVPL1}
0.02	0.00	0.00	0.00	0.10	1.5	0.5
V_{LVPL2}	G_{LVPL}	V_{HVRCR}	CUR_{HVRCR}	R_{Ip_LVPL}	$T_{\_LVPL}$	N_{WTG}
0.90	1.22	1.20	2.00	10.00	0.02	500

Electric Converter (WT3E1)

T_{fv}	K_{pv}	K_{iv}	X_C	T_{fp}	K_{pp}	K_{ip}	PMX
0.15	18	5	0	0.05	3.00	0.6	1.12
PMN	QMX	QMN	IP_{MAX}	T_{RV}	RP_{MX}	RP_{MN}	$T_{\_Power}$
0.04	0.436	-0.436	1.12	0.02	0.45	-0.45	5.00
K_{qi}	V_{MINCL}	V_{MAXCL}	K_{qv}	XIQ_{min}	XIQ_{max}	T_v	T_p
0.10	0.90	1.10	40.0	0.50	1.45	0.05	0.05
Fn	ωP_{min}	ωP_{20}	ωP_{40}	ωP_{60}	P_{min}	ωP_{100}	
1.00	0.69	0.78	0.98	1.12	0.74	1.2	

Mechanical System Model (WT3T1)

V_w	H	$DAMP$	K_{aero}	$Theta2$	H_{tfrac}	$Freq1$	D_{shaft}
1.25	4.95	0.00	0.007	21.98	0.875	1.800	1.500

Pitch Controller Model (WT3P1)

T_p	K_{pp}	K_{ip}	K_{pp}	K_{ip}	$TetaMin$	$TetaMax$	$RTetaMax$	PMX
0.30	150	25	3	30	0	27	10	1.15